Isolation of fibroblast derived extracellular vesicles using magnetic beads and click chemistry

Jorinde Scholten

Chair: Associate prof.dr. R. Bansal
Daily supervisor: R. Booijink
External member: prof.dr.ir. P. Jonkheijm

Bachelor Biomedical Engineering
University of Twente

July 4, 2023

Abstract

English: Hepatocellular carcinoma (HCC) is one of the most common types of cancer worldwide. Early diagnosis of HCC leads to higher survival rates. However, a sensitive method to detect HCC in early stages is not yet available. HCC often develops via liver fibrosis and cirrhosis. Activated fibroblasts play a role in this process. Extracellular vesicles (EVs) are vesicles released by all cells in the body; also by activated fibroblasts. They can provide useful information about disease progression. Immunoaffinity-based capturing techniques, such as using magnetic beads and click chemistry with an antibody, enable the isolation of specific types of EVs. The aim of this research was to isolate fibroblast derived EVs using magnetic beads and click chemistry, to detect liver fibrosis in early stages. In order to achieve this, a fibroblast specific surface marker needed to be identified. This was done by cell stainings and Dot blot. Also, the EVs were characterised by Calcein stainings and Dynamic Light Scattering (DLS) measurements. Finally, the conjugation with magnetic beads was performed. The Dot blots showed aspecific binding, most likely caused by the tertiary antibody. For LX-2 cells, representing hepatic stellate cells, no fibroblast specific surface marker was identified. Therefore, cell lines were switched to human primary prostate fibroblasts (hPrFs), which were found to express Fibroblast activation protein-α (FAP). For both cell lines EVs were confirmed to be present in the EV samples. Conjugation for hPrF EVs with FAP antibody showed the ability of the system to isolate fibroblast derived EVs using magnetic beads and click chemistry. However, as efficiency was low, further research is needed to improve the conjugation.

Nederlands: Hepatocellulair carcinoom (HCC) is wereldwijd een van de meest voorkomende soorten kanker. Vroegtijdig diagnosticeren van HCC verhoogt de overlevingskansen. Echter, een sensitieve methode om HCC in een vroeg stadium te detecteren is nog niet beschikbaar. HCC ontwikkelt zich vaak via leverfibrose en -cirrose. Geactiveerde fibroblasten spelen een rol in dit proces. Extracellulaire vesikels (EVs) zijn blaasjes afkomstig van alle cellen in het lichaam. Ze kunnen bruikbare informatie geven over ziekteverloop. Technieken gebaseerd op immunoaffiniteit, zoals het gebruik van magnetische beads en klikchemie met een antilichaam, maken de isolatie van een specifiek type EV mogelijk. Het doel van dit onderzoek was het isoleren van extracellulaire vesikels van fibroblasten met magnetische beads en klikchemie, om zo leverfibrose in een vroeg stadium te kunnen detecteren. Hiervoor moest een specifiek antilichaam voor fibroblasten worden gevonden. Dit is gedaan met cell kleuringen en *Dot blot*. Ook zijn de EVs gekarakteriseerd met een *Calcein* kleuring en door *Dynamic Light Scattering* (DLS) metingen. Uiteindelijk is de conjugatie uitgevoerd. De *Dot blot* liet aspecifieke binding zien, waarschijnlijk veroorzaakt door het tertiare antilichaam. Voor LX-2 cellen, welke stellaatcellen representeren, is geen fibroblast-specifiek antilichaam gevonden. Daarom is er van cellijn gewisseld en zijn menselijke primaire prostaat fibroblasten gebruikt, welke *Fibroblast activation protein-α* (FAP) tot expressie bleken te brengen. Voor beide cellijnen was bevestigd dat EVs aanwezig waren in de EV samples. De conjugatie voor EVs van prostaat fibroblasten met FAP antilichaam liet zien dat het systeem om EVs van fibroblasten te isoleren met magnetische beads en klikchemie werkt. Echter, aangezien de efficiëntie laag was, is verder onderzoek nodig om de conjugatie te verbeteren.

Contents

1 Introduction

1.1 Liver diseases

Hepatocellular carcinoma (HCC) is one of the most common cancer types worldwide. The survival rate for patients having HCC is relatively low; it accounts for more than 800.000 new deaths per year [1]. A curative treatment, for example by resection or transplantation of the liver or radiofrequency ablation (RFA), can currently only be performed in early stages [2–4]. Early diagnosis thus leads to higher survival rates [2–4]. However, a sensitive method to detect HCC in early stages is not yet available.
Different factors are known to contribute to the risk of developing HCC, including (viral) Hepatitis B and C and non-alcoholic fatty liver disease (NAFLD) [5,6]. These can cause chronic injury to the liver, which can lead to fibrosis and cirrhosis (figure 1) [7].
Liver fibrosis is characterised as the replacement of liver tissue with scar tissue. On a cellular level, liver fibrosis is characterised by the presence of activated fibroblasts. These produce an excessive amount of extracellular matrix components [8]. Liver cirrhosis, next, is one of the major risk factors for developing HCC. Up to 80% of the people with HCC have a cirrhotic liver [9]. In the process of liver injury, shortening of telomeres takes place. This causes chromosomal instability, which in turn contributes to the onset of HCC [10].
Liver cirrhosis not only is a risk factor for the development of HCC, but it can also leads to other complications, such as loss of liver function due to the replacement of functional tissue by scar tissue. Also, portal hypertension can occur as a consequence of increased liver stiffness [7].

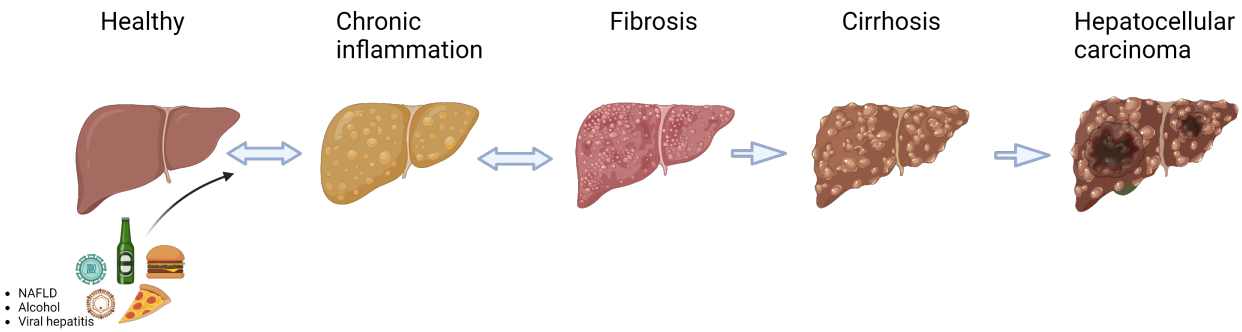

Figure 1: *Development of Hepatocellular carcinoma (HCC). A major risk factor of HCC is liver cirrhosis. Injury of the liver can be caused by different aetiologies, such as viral hepatitis or non-alcoholic fatty liver disease (NAFLD). Under influence of chronic injury, liver fibrosis and eventually cirrhosis can develop. (Created with Biorender)*

1.1.1 Activated fibroblasts

As described before, activated fibroblasts play a role in the development of liver fibrosis and cirrhosis. Activated fibroblasts normally function in tissue repair throughout the whole body [11].
Activated fibroblasts in the liver originate from the activation of hepatic stellate cells (HSCs) [8]. In the healthy liver, HSCs are quiescent and one of their main functions is to store vitamin A in lipid droplets. If they are influenced by, for example, chronic injury, their shape and activity changes; they transdifferentiate into activated fibroblasts (or myofibroblasts) [8, 12, 13], seen in figure 2. The morphology of the cell changes towards a more extended shape and the HSCs loose their spines [8]. Also, adherens junctions of HSCs with hepatocytes are lost in the process [14]. This happens in combination with increased YAP/TAZ expression [14]. The process of activation is mediated by multiple compounds, such as cytokines and growth factors, for example Transforming Growth Factor β (TGFβ), Platelet Derived Growth Factor (PDGF) and Vascular Endothelial Growth Factor (VEGF) [15–19]. The activated fibroblasts form an altered combination of components for the extracellular matrix (ECM), including an enhanced production of collagens [20]. The process of chronic HSC activation leads to liver fibrosis and, eventually, cirrhosis [8].

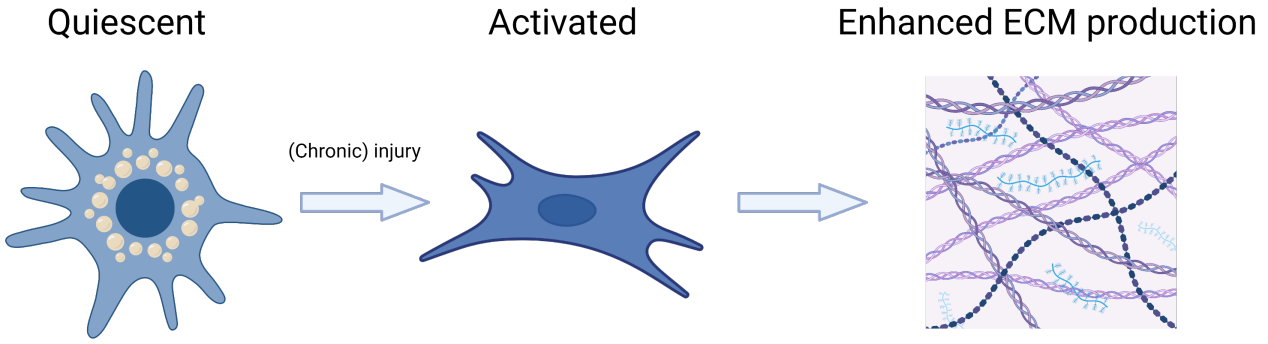

Figure 2: *The activation of hepatic stellate cells (HSCs). HSCs change under influence of chronic injury from a quiescent type into an activated fibroblast with altered functioning, including enhanced production of extracellular matrix (ECM) components. (Created with Biorender)*

1.1.2 Cancer-associated fibroblasts

Apart from being a risk factor for the development of HCC, activated fibroblasts also play a role in the progression of HCC. Cancer-associated fibroblasts (CAFs) are activated fibroblasts [21]. They can originate from various types of cells [22]. CAFs interact with tumor cells, by creating the tumor microenvironment (TME) and releasing cytokines [23]. In this way, they can stimulate tumor-growth, angiogenesis and proliferation [24–26]. However, not all CAFs are tumor-supportive. There is also evidence that certain types of CAFs can inhibit tumor growth [23].
CAFs are, in general, defined by the expression of αSMA, FAP and Thy-1 (or CD90) [22]. However, not all CAFs express the same surface markers, as different subpopulations are found with different expression patterns [23]. The expression of CAFs can give information about the prognosis for a patient in various types of cancer, for example in HCC [27] or brain metastasis [28]. Examples of how the expression of surface markers of CAFs is related to prognosis in different types of cancer are listed in table 1.

Table 1: *Examples of the effect of CAFs with specific markers in various types of cancers. Lo=Low, Med=Medium, Hi=High; Ref=Reference.*

Cancer type	Origin CAF	Associated marker	Effect	Ref
Colorectal	Unknown	Endoglin	Cancer progression and metastasis	[29]
Brain metastasis	Pericytes blood vessels, endothelial progenitor cells, astrocytes	PDGF, αSMA	Poor prognosis and recurrence	[28]
Breast	Unknown	FAP, Podoplanin (PDPN)	Decreased T cell proliferation	[30]
Breast	Pericytes lymph node	αSMA (Hi), FAP (Hi), CD29 (Med-Hi), PDPN (Hi), PDGFRβ (Hi)	Lymph node metastasis	[31]
Breast	Pericytes lymph node	FAP (Lo-Med), CD29 (Hi), αSMA (Hi), PDPN (Lo), PDGFRβ (Med)	Lymph node metastasis	[31]
Breast	Multiple	CD29 (Med), FAP (Hi), FSP1 (Med), αSMA (Hi), PDGFRβ (Med-Hi), CAV1 (Lo)	T cell attraction	[32]
Breast	BM-derived progenitor cells, pericytes, preadipocytes, etc.	Integrin α11	Tumor progression	[33]
Colorectal	Pericryptal Lepr-lineage cels	MCAM/CD146	Poor prognosis	[34]
Liver	Hepatic stellate cell	CD36	Immunosuppressive	[35]

1.1.3 Current diagnosing methods

Current methods to detect liver fibrosis and cirrhosis include biopsy, ultrasound-based techniques and serological tests. A liver biopsy is the main diagnosing tool for liver fibrosis and cirrhosis and it is also used to diagnose HCC [36]. However, it is an invasive method, which is unpleasant for the patient, and it can lead to side-effects, such as bleeding. Furthermore, the sensitivity of a biopsy is relatively low, due to unequal distribution of the degree of fibrosis throughout the liver [37, 38].
Over the last years, ultrasound techniques are developed to examine the stage of fibrosis in the patient. Examples of these techniques are Fibroscan or Transient Elastography (TE), and ElastPQ [39, 40]. Ultrasound based techniques measure the stiffness of the liver. In this way, the degree of fibrosis can be determined in a non-invasive manner. This technique is less sensitive for lower degrees of fibrosis [39]. Also, factors such as obesity, to which NAFLD can be related, influence the performances of ultrasound-based techniques [41].
Moreover, multiple serological tests exist to determine the degree of fibrosis. Examples of these are APRI (aspartate aminotransferase (AST) to platelet ratio index), the PRTA-score, based on PDGFRβ expression, and Fibrotest [42–44]. However, these mainly show a difference between no or mild fibrosis and severe fibrosis or cirrhosis. Between no fibrosis and mild fibrosis cannot clearly be distinguished. Therefore, these tests are less useful for early detection of liver fibrosis [45, 46].
In table 2, the described methods are listed with their advantages and limitations and sensitivity and specificity are compared.

Table 2: *Methods to diagnose liver fibrosis and cirrhosis. Methods are listed with their advantages, limitations, sensitivity and specificity. Ref=Reference.*

Method	Principle	Advantages	Limitations	Sensitivity	Specificity	Ref
Biopsy	Histological analysis of liver tissue	Direct analysis of the liver tissue	Invasive; risk for bleeding; unpleasant for patient	Low	High	[38]
Fibroscan	Ultrasound; based on transient elastograpy	Non-invasive	Less functional in obese patients	Medium; lower for lower degrees of fibrosis	High	[41]
ElastPQ	Ultrasound; based on ultrasound shear wave elastography point quantification	Non-invasive	High standard deviations	Medium; lower for lower degrees of fibrosis	Medium-high	[40]
APRI	Serological test; aspartate aminotransferase to platelet ratio index	Simple procedure for patient	Not suitable for early stages of fibrosis	Low	Very high	[43]
PRTA-score	Serological test; based on PDGFRβ expression	Simple procedure for patient	Not tested for earliest stage of fibrosis	Medium-high	Medium-high	[43]
Fibrotest	Serological test; based on six different markers	Simple procedure for patient	Not suitable for early stages of fibrosis	Medium	Medium	[44]

So, there is a need for a novel method that can detect liver fibrosis in early stages. Analysis of extracellular vesicles from blood circulation could be such a diagnostic method.

1.2 Extracellular vesicles

CAFs and activated fibroblasts secrete extracellular vesicles (EVs), similar to all cells in the body [47].
EVs can circulate in body fluids, for example blood, urine, saliva and cerebrospinal fluid and can be classified in different subtypes (figure 3). Microvesicles have a size of about 100 to 1000 nm and are formed by the outward budding of the plasma membrane of the cell. Exosomes have a size of about 30-100 nm and are released from the cell via a multivesicular body (MVB). Apoptotic bodies (1000-5000 nm) are a different type of EV. These EVs originate from cells that have undergone apoptosis [48].

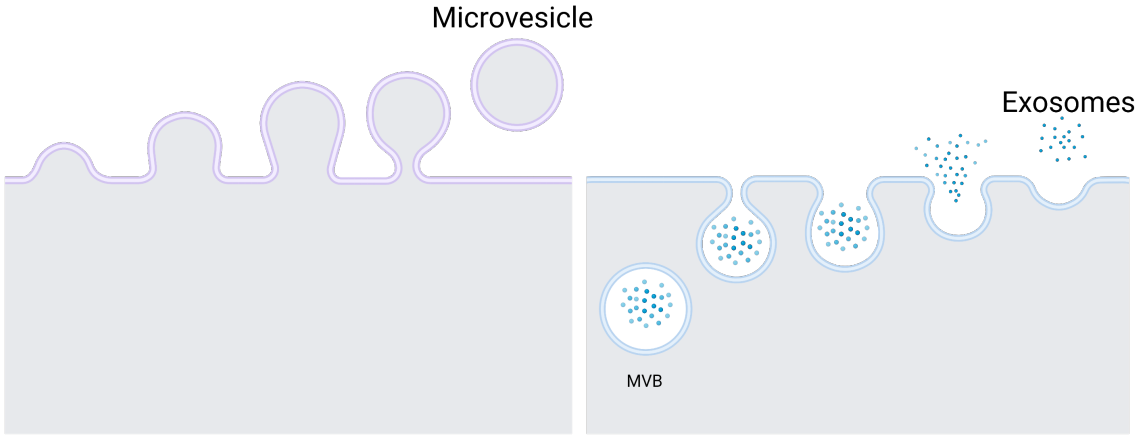

Figure 3: *Formation of exosomes and microvesicles. Exosomes are released from a cell via a multivesicular body (MVB). Microvesicles are formed by outward budding of the plasma membrane. (Created with Biorender)*

EVs can contain various biomolecular cargo, depending on cellular origin and states, including proteins, lipids and nucleic acids. These biomolecules result in stimulatory or inhibitory signals, leading to proliferation, apoptosis or cytokine production of the target cell [48]. EVs are found to function as a communication mechanism between cells in for example the brain [49], kidneys [50] and bones [51]. They also contribute to inflammation processes [52]. Furthermore, extracellular vesicles can promote cancer progression [53].
As they give information about the cells they originate from, EVs could be useful as a diagnostic tool. An example of this is the number of EVs present: upon activation of HSCs, production of EVs is upregulated [54]. Also, as EVs influence cellular behaviour, they could be useful as a therapeutic tool [55,56]. Exosomal miRNA, for example, was found to play a role in the inhibition of cancer proliferation and metastasis [53, 57–60].

1.2.1 Fibroblast derived extracellular vesicles

As discussed, EVs function as communication mechanisms between cells and they are seen to mediate in diseases. Specifically, EVs of activated fibroblast can have an influence on the course of a disease too [61–69].
As mentioned before, CAFs can contribute to tumour progression, possibly via EVs. These are, for example, found to promote metastasis of lung cancer [61], proliferation and angiogenesis in colorectal cancer [62] and aggressiveness of pancreatic cancer [63]. EVs of corneal myofibroblasts have an influence on migration of corneal epithelial cells [70]. Moreover, EVs of synovial fibroblasts are found to play a role in osteoarthritis [71]. The influence of EVs on liver diseases is seen too: HSC derived EVs are found to mediate liver fibrosis [64]. Furthermore, they play a role in the metabolic switch of non-parenchymal liver cells [65]. EVs of HSCs can also promote HCC progression [66–68] and they induce cytokine release and macrophage migration [69]. This also works the other way around as EVs of hepatocytes can activate HSCs [53, 72–75] and the secretion of EVs of mouse HSCs is upregulated after activation of these cells [76].

1.2.2 Extracellular vesicle isolation techniques

Multiple methods can be used to isolate EVs; for example ultracentrifugation, size-exclusion chromatography, ultrafiltration and immunoaffinity capture-based technique [77].

1.2.2.1 Ultracentrifugation- and filtration Ultracentrifugation- and filtration are EV isolation techniques that are mainly based on differences in size (and density for ultracentrifugation) between the particles in the sample. In ultracentrifugation, larger particles sediment faster or with less centrifugal force than smaller particles. In ultrafiltration, larger particles cannot pass the filter, while smaller particles can [77].

1.2.2.2 Size-exclusion chromatography Another method to isolate EVs based on size is size-exclusion chromatography. Here, the sample is diluted and the larger particles will move faster through the fluid than the smaller particles [77]. The advantage of ultracentrifugation, size-exclusion chromatography and ultrafiltration is that they are relatively simple. However, they do not allow for isolation of specific types of EVs.

1.2.2.3 Immunoaffinity-based techniques In immunoaffinity-based techniques EVs are captured by binding to an antibody. In this way there can be distinguished between different types of EVs by selecting a specific antibody [77]. Immunoaffinity capture-based technique provides the selection of EVs by their surface markers using antibodies, thereby making it possible to distinguish between different types of EVs.
The EV isolation techniques discussed here are listed with their advantages and limitations in table 3.

Table 3: *Techniques to isolate extracellular vesicles. Main advantages and limitations of each techniques are listed [77].*

Isolation technique	Main advantages	Limitations
Ultracentrifugation	Fast	No separation of EVs from other particles of the same size
Ultrafiltration	Simple	Possibly deformation of EVs; no separation of EVs from other particles of the same size
Size-exclusion chromatography	Simple	No separation of EVs from other particles of the same size
Immuno-affinity based	Separation of different subgroups of EVs possible	Relatively complicated method

To isolate EVs using immunoaffinity-based techniques, surface markers are used. EVs generally express the same surface markers as the cells they originate from [78]. General EV markers are tetraspanins. Tetraspanins, like CD9, CD63 and CD81 are transmembrane proteins [79], highly present on EVs [80].
For fibroblasts, various relatively specific surface markers can be identified, as seen for the CAFs in section 1.1.2. The expression of activated fibroblasts is thus different from the expression of quiescent fibroblasts or quiescent HSCs. Surface markers of activated fibroblast will therefore be discussed shortly.

Surface markers of activated fibroblasts Activated fibroblasts express Fibroblast activation protein-α (FAP) [81–83]. Fibroblast activation protein-α (FAP), also known as Seprase, is a transmembrane protein. It is expressed by activated fibroblasts, including CAFs; FAP is not expressed by healthy fibroblasts. Increased expression of FAP is seen for various types of cancer and in other conditions, such as fibrosis and arthritis [84,85]. For liver cirrhosis specifically, increased expression of FAP is also seen [83]. Other surface markers that are related to activated fibroblasts are αSMA, Vimentin, PDGFR-α [86–90]. CD90 is a cell surface marker that is expressed by CAFs. Expression of CD90 is also increased in patients with cirrhosis and in patients with HCC [25, 91].
In vitro, LX-2 cells are relevant in the context of activated fibroblasts in liver fibrosis. LX-2 cells are HSCs with features of activated HSCs considering their expression [92–94]. They are found to be positive for various HSC surface markers, such as αSMA and Vimentin and they also have characteristics of bone marrow-derived mesenchymal stem cells (BM-MSCs) and express for example CD13 and CD146 [93]. A more extensive list of LX-2 cell surface markers and which type of cell this marker is an indication for can be found in table 4.

Table 4: *Various surface markers described to be expressed by LX-2 cells. [92, 94–96]*

Surface marker	**Type of marker**
CD9	Tetraspanin
CD13	Mesenchymal
CD29	Mesenchymal
CD44	Mesenchymal
CD49e	Mesenchymal
CD63	Tetraspanin
CD73	Mesenchymal
CD90	Mesenchymal; CAF
CD105 (Endoglin)	Mesenchymal
CD146	Mesenchymal
CD166	Mesenchymal
CD271	Activated HSC
HLA class-I	Mesenchymal
αSMA	Activated fibroblast; CAF
Vimentin	Mesenchymal; activated fibroblast
PDGFRβ (CD140b)	Mesenchymal; pro-fibrogenic
Fibronectin	Pro-fibrogenic
TGFβ receptor type I	Pro-fibrogenic
TGFβ receptor type II	Pro-fibrogenic
Desmin	Hepatic stellate cell
FAP	Activated fibroblast

1.2.2.4 Click chemistry Click chemistry provides a process to join small units together by a click reaction. Certain features apply to click reactions, such as simple reaction conditions and no formation of byproducts or only formation of byproducts that can easily be removed [97]. Click chemistry can thus be used to link two compounds in a simple manner. In combination with magnetic beads, it can therefore play a role in EV isolation [98–101].

2 Aim & objectives

To detect liver fibrosis in early stages in order to have more treatment options, the EVs of activated fibroblasts need to be isolated. It is known that EVs of hepatocytes can be captured using magnetic beads and click chemistry [98–100]. However, for fibroblasts, it is not yet known whether the same technique can be applied. Therefore, the aim of this research is to isolate fibroblast derived EVs using magnetic beads and click chemistry. To achieve this, first fibroblast specific surface antibodies, that can eventually be used to capture the EVs, need to be identified. Furthermore, the fibroblast derived EVs need to be characterized. This is necessary as the characteristics of these EVs could have an influence on, for example, the capturing efficiency. Finally, magnetic enrichment of the EVs will be performed.

EVs will be derived from the supernatant of cultured LX-2 cells, which represent activated human hepatic stellate cells, and human prostate fibroblasts (HPrF). The EVs will be concentrated and characterised using Tangential Flow Filtration (TFF) and Dynamic Light Scattering (DLS) respectively. Identification of fibroblast specific surface marker will be done using cell stainings and Dot blot. Since FAP is expressed by activated fibroblasts, including cultured fibroblasts, but not by healthy fibroblasts, it is hypothesized that FAP antibody will bind to the fibroblast derived EVs. This enables specific capturing of the activated fibroblast derived EVs using magnetic beads and click chemistry. To test the hypothesis, a magnetic bead will be bound to FAP antibody. This will be done via click chemistry using Tetrazine (Tz) and trans-Cyclooctene (TCO). FAP antibody is then expected to bind to the EVs, thereby enabling the isolation of these EVs. In this process, a magnet will be used to isolate the conjugated beads. To determine whether the fibroblast derived EVs are captured, fluorescent labelling and flow cytometry will be used.

3 Method

3.1 Cell culture and staining - LX-2 cells

For the first experiments, human hepatic stellate cells, LX-2 cells (provided by Prof. Scott Friedman, Mound Sinai Hospital, NY, USA) were seeded in a T175 flask (5000 cells/cm^2) in medium containing DMEM -Glutamax, 10% fetal bovine serum (FBS), antibiotics (penicillin 50 U/ml and streptomycin 50 µg/ml, Sigma, St. Louis, USA). Compared to using 1% FBS, the cells are activated more in 10% FBS [102]. After 24 hours of incubation at 37 °C, 5% CO_2, the medium was removed and a total of 30 ml starvation medium (0% FBS) was added. After 90 hours, the starvation medium was removed and collected and the cells were washed twice using phosphate buffered saline (PBS). To detach the cells, the cells were incubated in 3 ml 0.05% Trypsin-EDTA (Sigma), after which 17 ml of medium was added to the cells and the cells were counted. After centrifugation at 300xg for 5 minutes, the medium was collected for EV extraction and 10 ml PBS was added to the cells. The cells were centrifuged for another 5 minutes at 300xg, PBS was removed and the cells were fixed in 2 ml 4% formaldehyde in PBS for 15 minutes at room temperature. Thereafter, the cells were centrifuged at 300xg for 5 minutes, PBS with 1% bovine serum albumin (BSA) was added and the cells were stored at 4 °C. To stain the cells, an antibody conjugated to the fluorophores Alexa Fluor 647 (AF-647), Alexa Fluor 405 (AF-405), Phycoerythrin (Pe), Allophycocyanin (APC) or Fluorescein isothiocyanate (FITC) was used. 2 µl FAP-AF647 antibody (R&D systems, 0.2 mg/ml, FAB3715R, Minneapolis, USA) was added to 100 µl fixed cells and incubated for 1 hour. The Eppendorf was covered in aluminium foil to prevent photobleaching of the staining. The cells were then centrifuged at 300xG and resuspended in PBS with 1% BSA twice. The FAP-AF647 stained cells were analysed using fluorescence activated cell sorting (FACS; BD FACSAria II), where an unstained sample was used as a control. Here, one channel showing forward scatter (FSC) against side scatter (SSC), related to the size and complexity of the measured particles respectively, and one channel to observe the fluorophore was chosen. The excitation and emission values were set at 633 and 660/20 nm and 10.000 events were measured. The gate was set for the unstained cells. The staining was also visualized using an inverted microscope (Nikon eclipse Ti) with brightfield and APC settings.

LX-2 cells (P47) were, a second time, cultured as described above. This time, the cells were divided for staining with fixation and without fixation. One part of the LX-2 cells were then fixed using 2 ml of 4% formaldehyde in PBS. 100 µl cells were stained using FAP-AF647 and CD90-FITC (Invitrogen, 0.2 mg/ml, 11-0909-42, Carlsbad, USA) antibodies (1:50); this was incubated for 1 hour at room temperature. The cells were centrifuged at 300xg and washed twice in 1% BSA in PBS. The non-fixed LX-2 cells were also stained with FAP-AF647 and CD90-FITC antibodies (1:50). After incubation for 1 hour, they were washed twice in 2% FBS in PBS. FACS was used to analyse the stained cells similarly to the first staining. The FITC channel was added (excitation-emission: 488-530/30 nm). The gates were set for the fixed and non-fixed unstained cells separately.

LX-2 cells were cultured again; this time including treatment with TGFβ (10 ng/ml). The cells were split and both halves were kept in starvation medium (0% FBS). After 24 hours, one of the two flasks was treated with TGFβ (30 µl). After again 24 hours, the EVs of both the treated and the untreated LX-2 cells were harvest as described above (section 3.1). The EVs were then stored at 4 °C. After 3,5 hours, the EVs were concentrated using TFF as described in section 3.2. The sample was diluted in PBS (1:1) for analysis by DLS. The untreated and the treated cells were stained for 1 hour at 4 °C with 6 antibodies with fluorophore (1 million cells per staining): CD9-Pe (Invitrogen, 1.2 mg/ml, 12-0098-42, Carlsbad, USA), CD13-Pe (BD Biosciences, 555394, USA), CD63-FITC (R&D systems, 0.2 mg/ml, IC5048G-100UG, Minneapolis, USA), CD90-FITC (Invitrogen, 0.2 mg/ml, 11-0909-42, Carlsbad, USA), Vimentin-AF405 (R&D systems, 0.2 mg/ml, IC2105V-100UG, Minneapolis, USA) and FAP-AF647. Again, the unstained cells were stored at 4 °C for the same time. The cells were then fixed with 4% formaldehyde in PBS and analysis was done by FACS. Extra channels with excitation emission 488-585/42 nm for Pe and 375-450/40 nm for AF405 were added.

Moreover, one week later, fixed LX-2 cells and fixed TGFβ treated LX-2 cells, both stored at 4°C, were stained with CD146-Pe (BD Biosciences, 0.05 mg/ml, 562135). Unstained LX-2 cells and unstained TGFβ treated LX-2 cells were used as a control and analysis was done using FACS.

The experiment described above was hereafter once repeated, where Lx-2 cells were again cultured and treated with TGFβ as described before and 8.14 million LX-2 cells and 9.9 million TGFβ treated LX-2 cells were present. The antibodies used to stain the cells are listed in table 5.

Table 5: *Antibodies with conjugated fluorophore used for staining of the cells and analysis with FACS. For each antibody, concentration, manufacturer, catalog number, city and country are given.*

Antibody	Fluorophore	Concentration	Manufacturer	Cat. No.	City	Country
CD9	Pe	1.2 mg/ml	Invitrogen	12-0098-42	Carlsbad	USA
CD9	APC	0.2 mg/ml	Molecular Probes	A15698	unknown	Czech Republic
CD13	Pe	unknown	BD Biosciences	555394	Franklin Lakes	USA
CD63	FITC	0.2 mg/ml	R&D systems	IC5048G-100UG	Minneapolis	USA
CD90	FITC	0.2 mg/ml	Invitrogen	11-0909-42	Carlsbad	USA
CD146	Pe	0.05 mg/ml	BD Biosciences	562135	Franklin Lakes	USA
FAP	AF647	0.2 mg/ml	R&D systems	FAB3715R	Minneapolis	USA
Vimentin	AF405	0.2 mg/ml	R&D systems	IC2105V-100UG	Minneapolis	USA

3.2 Extracellular vesicle concentration and characterisation - LX-2 cells

The medium obtained from the cells, described above, was centrifuged at 300xg for 10 minutes to remove remaining cells. The supernatant was collected in another tube. This was centrifuged at 2800xg for 10 minutes to remove dead cells and debris. The supernatant was then transferred to another tube. This sample was concentrated by TFF using TFF-easy (Hansa BioMed, HBM-TFF). The volume was reduced to about 2 ml. 1 ml concentrated EVs was used for the DLS measurement (Zetasizer Nanoseries Nano-Zs from Malvern Instruments).

3.3 Extracellular vesicle staining - LX-2 cells

100 µl concentrated EVs was stained using 2 µl FAP-AF647 antibody (R&D systems). Another 100 µl concentrated EVs was stained using 2 µl Calcein AM solution (Invitrogen, 65-0853-81, Carlsbad, USA; dissolved in 1 mM DMSO and then dissolved 10 times in PBS to create a working concentration of 2 µM). The tubes were covered in aluminium foil to prevent photobleaching of the stainings. This was incubated for 1 hour.
The stainings were visualized using an inverted microscope (Nikon eclipse Ti). Brightfield, FITC and APC filters were used and the images were processed using ImageJ.

3.4 Dot Blot - LX-2 cells

Dot blot was performed using CD9, CD63, CD90-FITC, FAP-AF647 and αSMA antibodies. Concentrated EVs, stored overnight at 4 °C, were used. First, dilutions of the EV samples with medium (0 % FBS) were made in ratios 1:0, 1:1, 2:1, 5:1, 10:1 and 0:1. For all antibodies, 2 µl of the sample was spotted on a nitrocellulose blotting membrane (Amersham Protran 0.45; GE Healthcare Life Science, 10600093, Germany). The membranes, added to 15 ml tubes, were blocked using 5% Blotting grade blocker non-fat Dry milk (BioRad) in TBST (1x Tris buffered saline (TBS) with 0.1% Tween-20). This was incubated for 1 hour on a roller. The membranes were washed 3 times using TBST for 5 minutes. 0.5 µg antibody was added per ml TBS, with a total of 3 ml solution per membrane. The primary antibodies used were CD9, CD63, CD90-FITC, FAP-AF647 and αSMA. This was incubated overnight on a roller at 4 °C. Next day, the membranes were washed 3 times using 5 ml TBST for 5 minutes on a roller, after which the secondary antibody, goat-anti-mouse HRP (Dako; in TBS 1:100), was added. After incubation for 1 hour on a roller, the membranes were washed again 3 times with TBST for 5 minutes on a roller. The tertiary antibody, mouse-anti-goat HRP (Dako; in TBS 1:100), was then added and incubated for 1 hour on a roller. Again, the membranes were washed 3 times with TBST for 5 minutes on a roller. After removing the TBST, 3 ml TBS was added per membrane and the membranes were placed on the roller until further use. Pierce ECL Western Blotting Substrate (Thermo Scientific) was prepared following the manufacturer's instructions in ratio 1:40. The membranes were removed from the tubes and covered with ECL for 5 minutes. Analysis was done using a Blot and Gel Imager (Cell Source) and images were processed using ImageJ.

Thereafter, a second Dot blot was performed as described above, now using 8 different primary antibodies and a control without primary antibody. CD9 (Hansa BioMed), CD13-Pe (BD Biosciences), CD63 (Hansa BioMed), CD90-FITC (Invitrogen), CD146-Pe (Invitrogen), FAP-AF647 (R&D systems), αSMA (Sigma) and Vimentin-AF405 (R&D systems) were used as primary antibodies (0.5 µg/ml). For all primary antibodies and the control -except Vimentin- a goat-anti-mouse HRP secondary antibody (1:100) was added and a rabbit-anti-goat HRP tertiary antibody (1:100). For Vimentin, a rabbit-anti-rat HRP secondary antibody (Southern Biotech) was used and a goat-anti-rabbit HRP tertiary antibody (Dako). The Dot blot was performed on fixed LX-2 cells, fixed LX-2 cells treated with TGFβ, EVs from LX-2 cells and EVs from LX-2 cells treated with TGFβ. These had all been stored for 5 days at 4 °C. Instead of tubes, the membranes were placed in Petri dishes for blocking and incubating. To fully cover the membranes, 6 ml primary antibody solution was added and 5 ml secondary and tertiary antibody solution. The Petri dishes were placed on a shaker. Pierce ECL Western Blotting Substrate was prepared here following the manufacturer's instructions in ratio 1:1.

A third Dot blot was performed, with a similar procedure as described for the second Dot blot and a fifth sample consisting of HepG2 EVs was included. The primary antibodies added here were CD9 (Hansa Biomed), FAP-AF647 (R&D systems) and αSMA (Sigma) (5 ml antibody solution per membrane). To improve blocking, this was diluted in TBST + 5% non-fat dry milk. Also, the secondary antibody and tertiary antibody were diluted in TBST, both in concentration 1:1000.

A fourth Dot blot was performed to find out the cause for the aspecific binding observed in the previous experiments. This was done using 3 PVDF membranes (Thermo Scientific, 88520, Ireland). Two, similar to the control as described before, without a primary antibody and one without a primary and a tertiary antibody. The membranes were activated by covering them with methanol for 1 minute. Then they were covered with MilliQ for 10 seconds and finally in TBS for 5 minutes. After drying partially, the samples were spotted and the membranes were blocked and processed further as described before. The primary antibody incubation step was done for one hour at room temperature instead of overnight at 4°C. Serial dilutions of the samples were made in TBS instead of PBS + 2% FBS or medium. Samples were the same as used for experiment 3 and they were stored for 5 days before use.

A fifth Dot blot was performed, without the use of a tertiary antibody. Procedure was equal to the procedure as described for the fourth experiment. However, all membranes, except for the control, were treated with a primary and a secondary antibody. 9 primary antibodies were used in total: CD9, CD13, CD63, CD90, CD146, FAP, αSMA and Vimentin. The control did not contain a primary antibody. The sample was the same as used for experiments 3 and 4. It was stored for one week before use. The primary antibody was incubated overnight at 4 °C on a shaker.

All antibodies used for the Dot blot are listed in tables 6 (primary) and 7 (secondary and tertiary).

Table 6: *Antibodies used as primary antibodies in the Dot blots. For each antibody, fluorophore (if conjugated), host, concentration, manufacturer, catalog number, city and country are given.*

Antibody	Fluorophore	Host	Concentration	Manufacturer	Cat. No.	City	Country
CD9	-	Mouse	1 mg/ml	Hansa BioMed	HBM-CD9-100	Tallinn	Estonia
CD13	Pe	Mouse	unknown	BD Biosciences	555394	Franklin Lakes	USA
CD63	-	Mouse	1 mg/ml	Hansa BioMed	HBM-CD63-100	Tallinn	Estonia
CD90	FITC	Mouse	0.2 mg/ml	Invitrogen	11-0909-42	Carlsbad	USA
CD146	Pe	Mouse	0.05 mg/ml	BD Biosciences	562135	Franklin Lakes	USA
FAP	AF647	Mouse	0.2 mg/ml	R&D systems	FAB3715R	Minneapolis	USA
Vimentin	AF405	Rat	0.2 mg/ml	R&D systems	IC2105V-100UG	Minneapolis	USA
αSMA	-	Mouse	2 mg/ml	Sigma	A2547	Jerusalem	Israel

Table 7: *Antibodies, horseradish-peroxidase-conjugated (HRP), used as secondary and tertiary antibodies in the Dot blots. For each antibody, manufacturer, catalog number, city and country are given.*

Host	Reactivity	Manufacturer	Cat. No.	City	Country
Goat	Mouse	Dako	P0447	Santa Clara	USA
Goat	Rabbit	Dako	P0448	Santa Clara	USA
Rabbit	Goat	Dako	P0449	Santa Clara	USA
Rabbit	Rat	Southern Biotech	6130-05	Birmingham	USA

The similarities and differences between the five performed Dot blots are presented in table 8.

Table 8: *Overview of the procedures for the five performed Dot blots. The control includes the secondary and tertiary antibody, but not the primary.*

Dot blot	Membrane type	Incubation in	Primary antibody solution	Secondary antibody solution	Tertiary antibody solution	Control
1	Nitrocellulose	Tube	0.5 µg/ml in TBS	1:100 in TBS	1:100 in TBS	No
2	Nitrocellulose	Petri dish	0.5 µg/ml in TBS	1:100 in TBS	1:100 in TBS	Yes
3	Nitrocellulose	Petri dish	0.5 µg/ml in TBST + 5% non-fat dry milk	1:1000 in TBST	1:1000 in TBST	Yes
4	PVDF	Petri dish	0.5 µg/ml in TBST + 5% non-fat dry milk	1:1000 in TBST	-	Yes
5	PVDF	Petri dish	0.5 µg/ml in TBST + 5% non-fat dry milk	1:1000 in TBST	-	Yes

3.5 Conjugation - LX-2 cells

100 µl of Thiol magnetic beads (Bioneer, T5-1019-1, Republic of Korea; Accubeads 1-5 µm) dissolved in PBS (10 mg/ml) were used. 7.2 µl of OPSS-PEG5-NH2 (R&D systems, PG2-Amos-5k; 30 mg/ml) and 92.8 µl of PBS was added and placed on a roller mixer (Grant-bio, PTR-60, speed 7) at room temperature for 2 hours (pH=7).The beads were then washed 5 times using 200 µl of PBS by the use of a magnet. Finally, the beads were resuspended in 100 µl of PBS (pH=8.5). Then, 7.9 µl of 6-methyl-tetrazine(Tz)-PEG5-NHS (Conju-Probe,

CP-6062; in DMSO 30 mg/ml) was added to 92.1 µl of PBS (pH=8.5). This was added to 100 µl of OPSS-beads. It was then placed on a roller mixer to react. After 2 hours, the beads were washed again 5 times using PBS and they were then stored in 100 µl PBS with 1% BSA at 4 °C for later use. A CD9-APC (Molecular probes, 0.2 mg/ml A15698, Czech Republic) antibody solution was made in 100 µl of PBS (1:100). 91.4 µl PBS and 8.6 µl of TCO-PEG4-NHS ester (Jena bioscience, CLK-A137-10; in DMSO 3 mg/ml) was added to this solution. After incubation at a roller mixer for 1 hour at room temperature (packed in aluminium foil to prevent bleaching), the solution was purified using Amicon ultra 0.5 ml filter (Millipore, UFC501024) and centrifuging at 5000 rpm for 20 minutes. This was repeated 3 times, adding 100 µl PBS every time. Finally, the column was centrifuged reversed at 5000 rpm for 5 minutes. 100 µl PBS with 1% BSA was added and the antibody solution was stored overnight at 4 °C. 800.000 fixed LX-2 cells (4% formaldehyde in PBS) were resuspended in 100 µl PBS + 2% FBS. 20 µl of TCO-CD9 was added and this was incubated at the roller bank for 1 hour. 5 µl of conjugated beads were added to 10 µl of antibody-TCO. This was washed 3 times in PBS with 1% BSA. PBS with 1% BSA was added to reach a total volume of 250 µl for all samples and the samples were analysed by FACS. Gates were set for the empty beads. Channels with excitation-emission 488-530/30 nm and 488-585/42 nm were added to analyse the presence of CD9-APC and Tz respectively. Also, FSC against SSC was added.

The conjugation was performed a second time in a similar way. Instead of CD9-APC, CD63 without fluorophore (Hansa BioMed, 1 mg/ml, HBM-CD63-100) was used as antibody and EVs were used instead of cells. The EVs were stored at 4 °C for 2 weeks before use. To visualize the EVs, they were stained with Calcein (1:500).

3.6 Cell culture and staining - prostate fibroblasts

Prostate fibroblasts (ATCC) were seeded in a T175 flask in medium containing DMEM -Glutamax, containing 10% fetal bovine serum (FBS) and antibiotics (penicillin 50 U/ml and streptomycin 50 µg/ml, Sigma). Human prostate fibroblasts are activated fibroblasts. The feature they have similar to in vivo activated HSCs is that they express FAP. [103]. After reaching confluence, the medium was removed and starvation medium (0% FBS) was added. After 72 hours of incubation (37°C, 5% CO_2), the starvation medium was removed and collected. This was then further processed as described for the LX-2 cells. Also, the cells were incubated with Trypsin-EDTA, centrifuged, washed and fixed as described above. They were then stained with FAP-AF647 antibody and this was again analysed using FACS.

3.7 Extracellular vesicle characterisation - prostate fibroblasts

The sample containing EVs was characterised by DLS in the same way as described for the LX-2 cells in section 3.2. However, this experiment was done 24 hours after harvesting of the EVs.

3.8 Extracellular vesicle staining - prostate fibroblasts

The sample containing EVs was stained in the same way as described for the LX-2 cells in section 3.3. Analysis with an inverted microscope was done at 40x magnification. In addition a FACS measurement was performed with the stained and unstained EVs.

3.9 Conjugation - prostate fibroblasts

The conjugation was performed using FAP antibody and EVs of prostate fibroblasts. The EVs had been stored for 24 hours before use. The procedure was similar to the conjugation procedure described for the LX-2 cells in section 3.5. Here, the gate to analyse the Calcein staining was set on the unstained EVs.

A second conjugation was performed similarly as decribed above, but the added concentration of FAP was increased from 0.5 µg/ml to 5 µg/ml. Also, 3 times as much sample was made for beads-OPSS-Tz+TCO-FAP and beads-OPSS-Tz+TCO-FAP-EV to improve the FACS measurement. Concentrations for these samples were constant.

4 Results & discussion

4.1 Cell staining - LX-2 cells

To analyse the expression of FAP on hepatic stellate cells (LX-2), a FACS measurement with FAP-AF647 antibody stained cells was done. The results of this measurement can be seen in figure 4. The gate is set for the unstained cells. A slight shift to the right of the FAP stained cells is visible compared to the unstained cells. However, less than 1% of the FAP stained cells is considered positive.

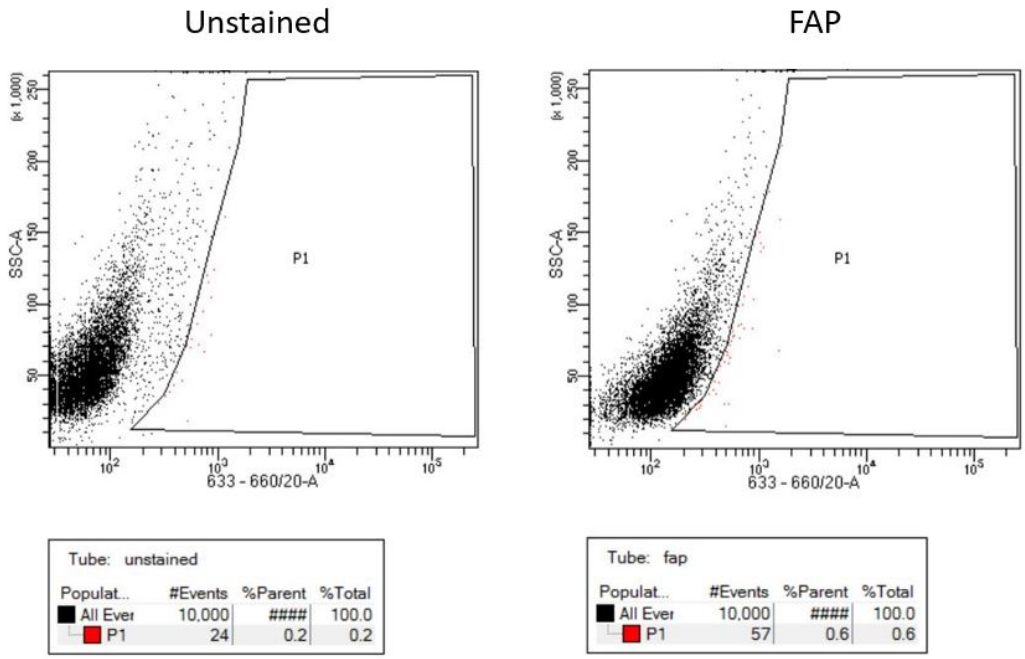

Figure 4: *FACS analysis of FAP-AF647 stained fixed LX-2 cells. The gate is set for the unstained cells. Less than 1% is considered FAP-positive.*

Given the low positivity in figure 4, next step was to study the influence of fixation on cell staining by comparing non-fixed and fixed, unstained and stained, LX-2 cells in a FACS measurement (figure 5). Here, a difference is observed between the fixed and the non-fixed cells. Compared to the non-fixed cells (figures 5A and B), the fixed cells show a small shift to the left with excitation at 488 nm (figure 5C) and a small shift to the right with excitation at 633 nm (figure 5D).

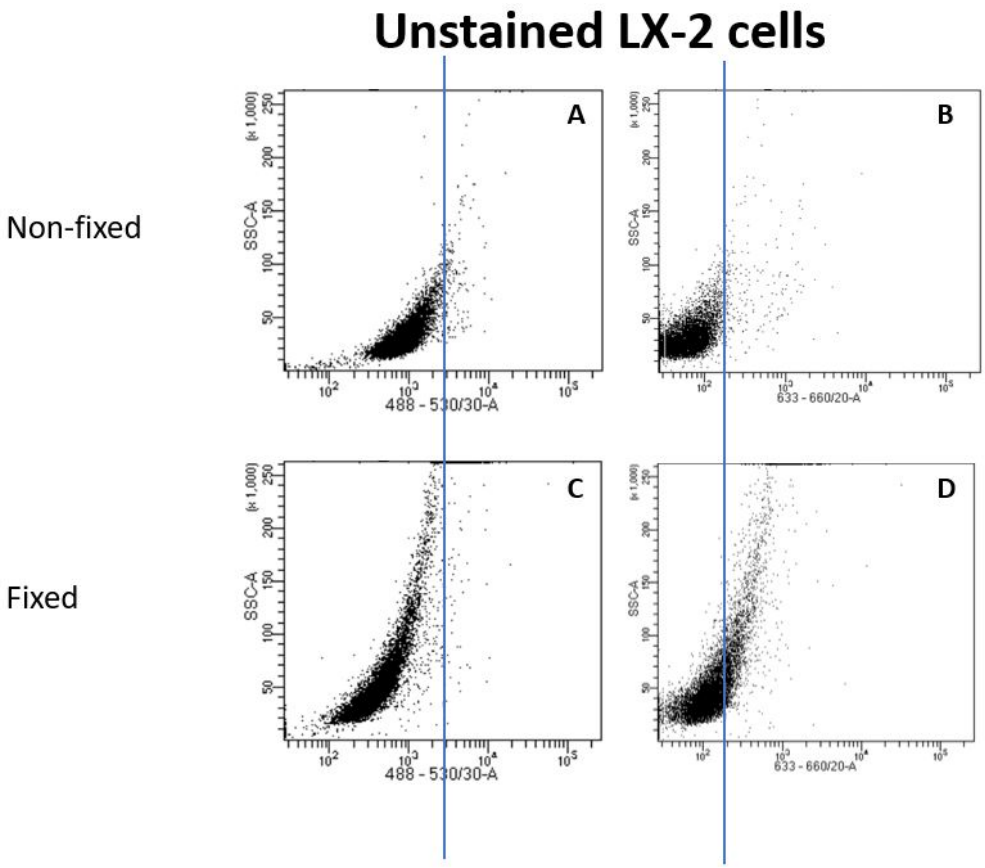

Figure 5: *Difference between non-fixed and fixed, unstained LX-2 cells in FACS analysis. A) Non-fixed cells at excitation-emission 488-530/30 nm; B) Non-fixed cells at excitation-emission 633-660/20 nm; C) Fixed cells at excitation-emission 488-530/30 nm; D) Fixed cells at excitation-emission 633-660/20 nm. At excitation-emission 488-530/30 nm there is a shift of the fixed cells to the left compared to the non-fixed cells; at excitation-emission 633-660/20 nm there is a shift of the fixed cells to the right compared to the non-fixed cells.*

Furthermore, non-fixed and fixed cells were stained with FAP-AF647 and CD90-FITC antibodies. Gates were again set for the unstained cells. For the FAP stained cells, both fixed and non-fixed, there is a slight shift. However, only 3% and 4% of the non-fixed and fixed cells respectively is considered positive compared to the unstained cells (figure 6). For CD90 stained fixed cells a shift is visible compared to the unstained cells; 53% of the cells is considered positive (figure 7). For the non-fixed cells this effect is considerably less, about 3%.

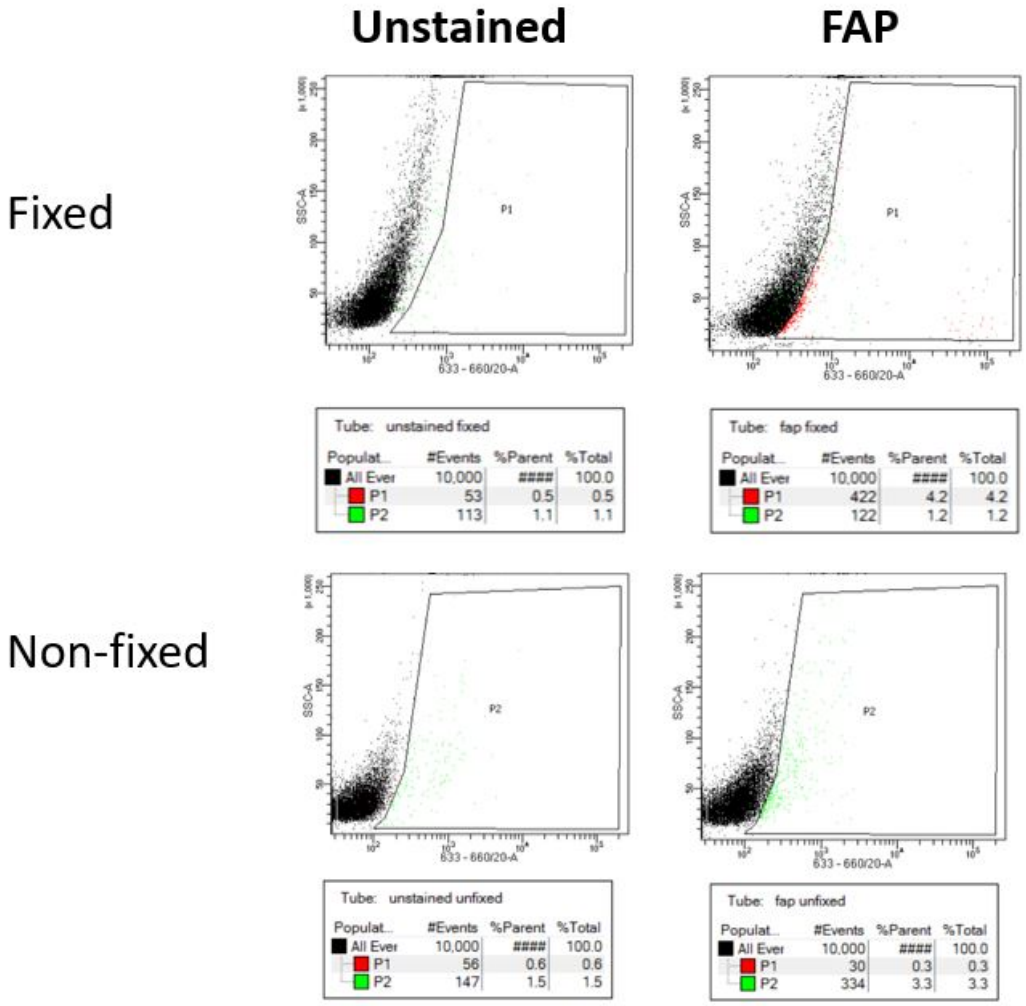

Figure 6: *FACS analysis of FAP-AF647 stained, fixed and non-fixed LX-2 cells. The gate is set for the unstained cells. 4% is positive for the fixed FAP stained cells; 3% is positive for the non-fixed FAP stained cells. For the fixed cells, events considered positive are red; for the non-fixed cells, events considered positive are green.*

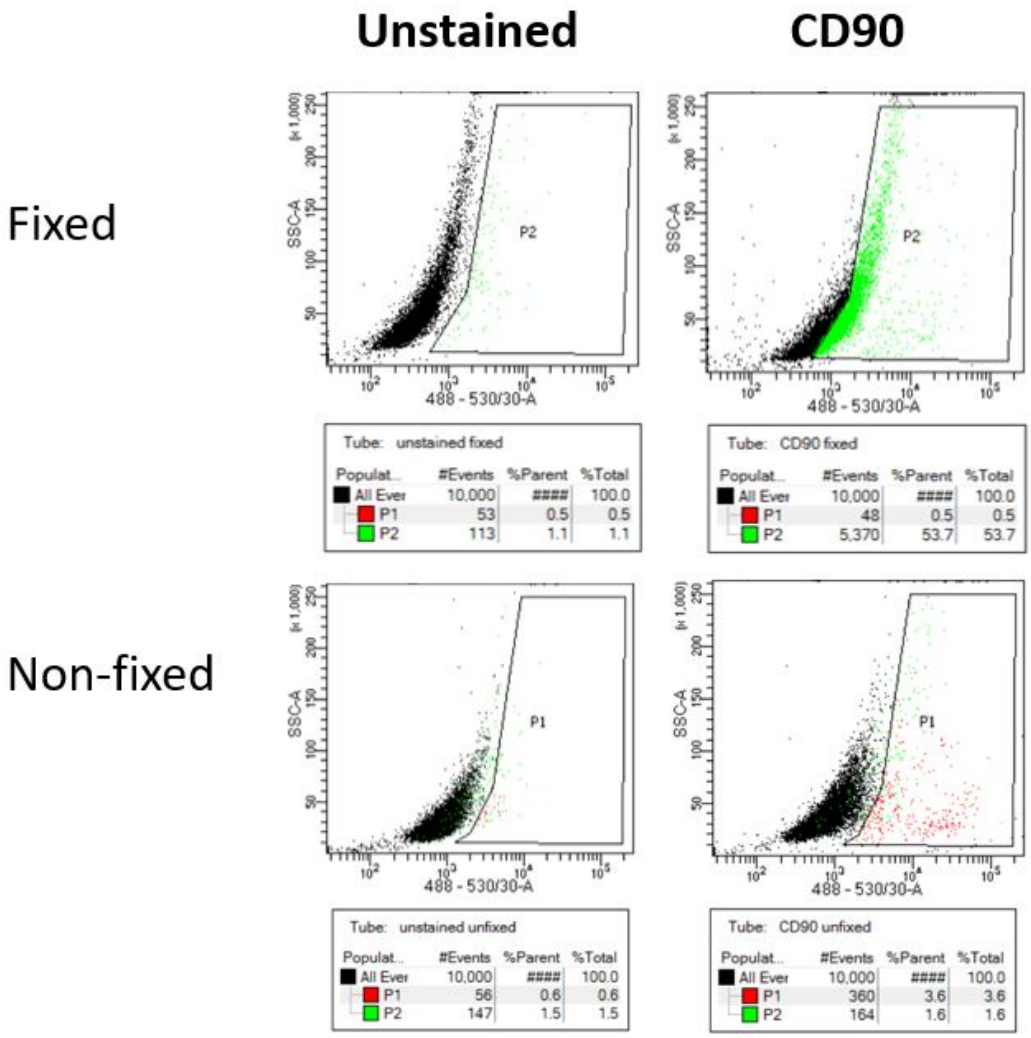

Figure 7: *FACS analysis of CD90-FITC stained, fixed and non-fixed LX-2 cells. The gate is set for the unstained cells. 53% is positive for the fixed CD90 stained cells; 3% is positive for the non-fixed CD90 stained cells. For the fixed cells, events considered positive are green; for the non-fixed cells, events considered positive are red.*

Fixation thus led to shifts in the measurement. However, whether it was a shift to the left or a shift to the right depended on the excitation-emission values (figure 5). This was not as expected. It was hypothesized that fixation would prevent an antibody from binding, as fixation causes crosslinking between proteins [104], and that it would therefore lead to a decrease in fluorescent signal in FACS analysis. A possible explanation for the found results could be the influence of auto-fluorescence. Changes in auto-fluorescence after fixation are described for leukocytes [105]. A similar effect could be the case for LX-2 cells. Furthermore, an increase of fluorescence intensity of FITC conjugated antibodies after fixation is described for platelets [106].

So far, an optimal surface antibody positive for all LX-2 cells was not found. Moreover, it was not known if activation of LX-2 cells influences their surface antibody expression. Therefore, next, the expression of CD9 (Pe), CD13(Pe), CD63 (FITC), CD90 (FITC), CD146 (PE), FAP (AF647) and Vimentin (AF405) on normal LX-2 cells (control) and TGFβ treated LX-2 cells was tested. The results per antibody can be seen in figures 8-14. Gates were set for the unstained non-treated cells. As no significant difference was observed between the unstained control and the unstained TGFβ treated cells, the same gates were used for the TGFβ treated cells. For both the TGFβ treated cells and the control, CD9 has the highest percentage (93 percent) of positive cells relative to the unstained cells. The stainings with the other antibodies are mainly negative compared to the unstained cells. Also, no clear difference is observed in expression of the control and the TGFβ treated LX-2 cells.

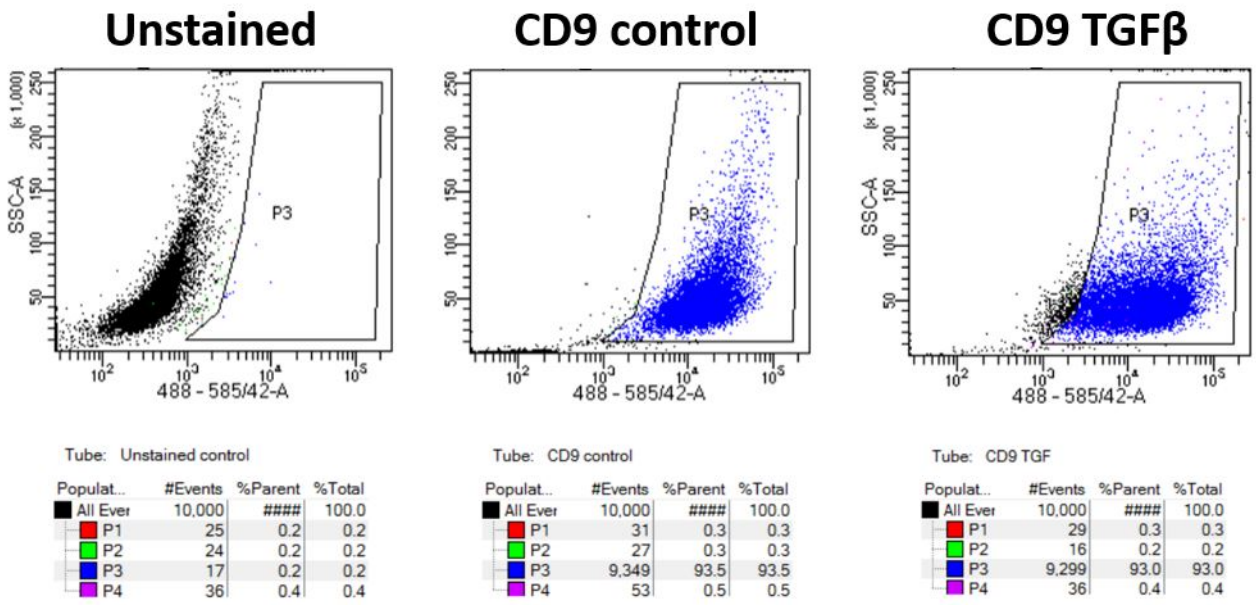

Figure 8: *FACS analysis of CD9-Pe stained (fixed) LX-2 cells (control) and TGFβ treated LX-2 cells. The gate is set for the unstained control. For both the control and the TGFβ treated cells, 93% is positive.*

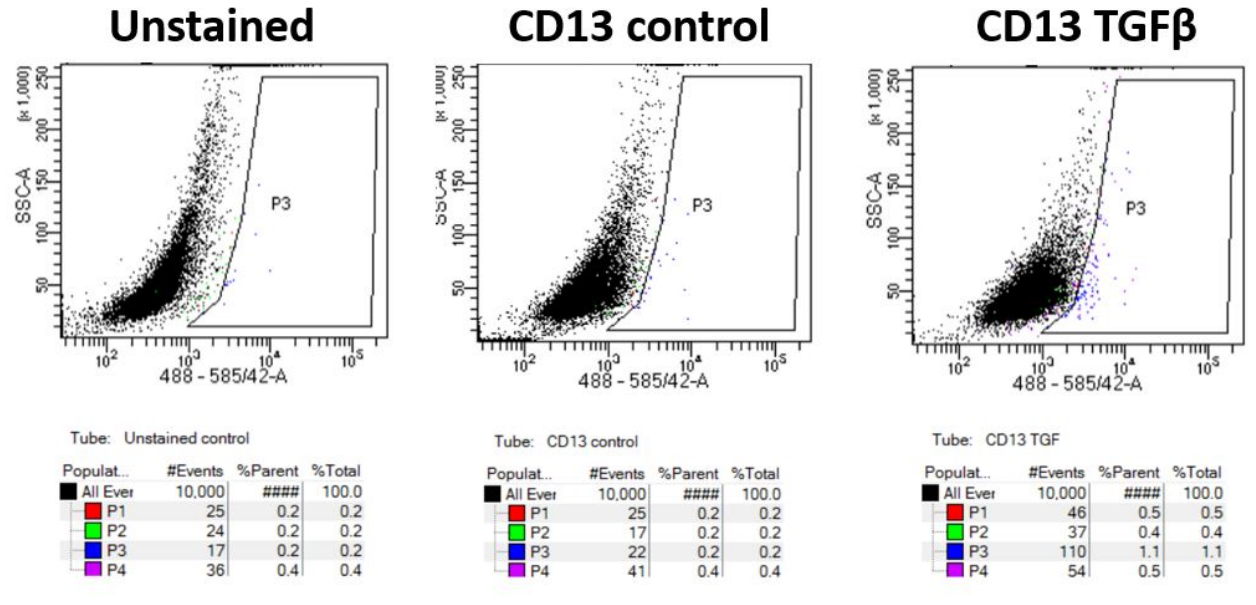

Figure 9: *FACS analysis of CD13-Pe stained (fixed) LX-2 cells (control) and TGFβ treated LX-2 cells. The gate is set for the unstained control. For the control, 0% is positive; for the TGFβ treated cells, 1% is positive.*

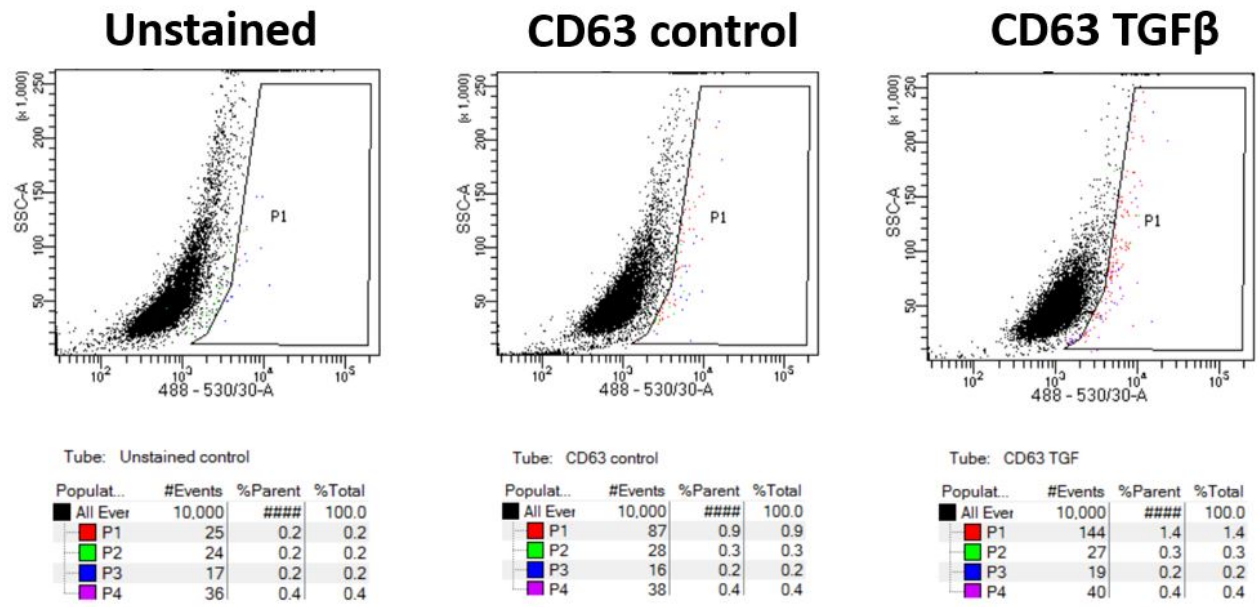

Figure 10: *FACS analysis of CD63-FITC stained (fixed) LX-2 cells (control) and TGFβ treated LX-2 cells. The gate is set for the unstained control. For both the control and the TGFβ treated cells, about 1% is positive.*

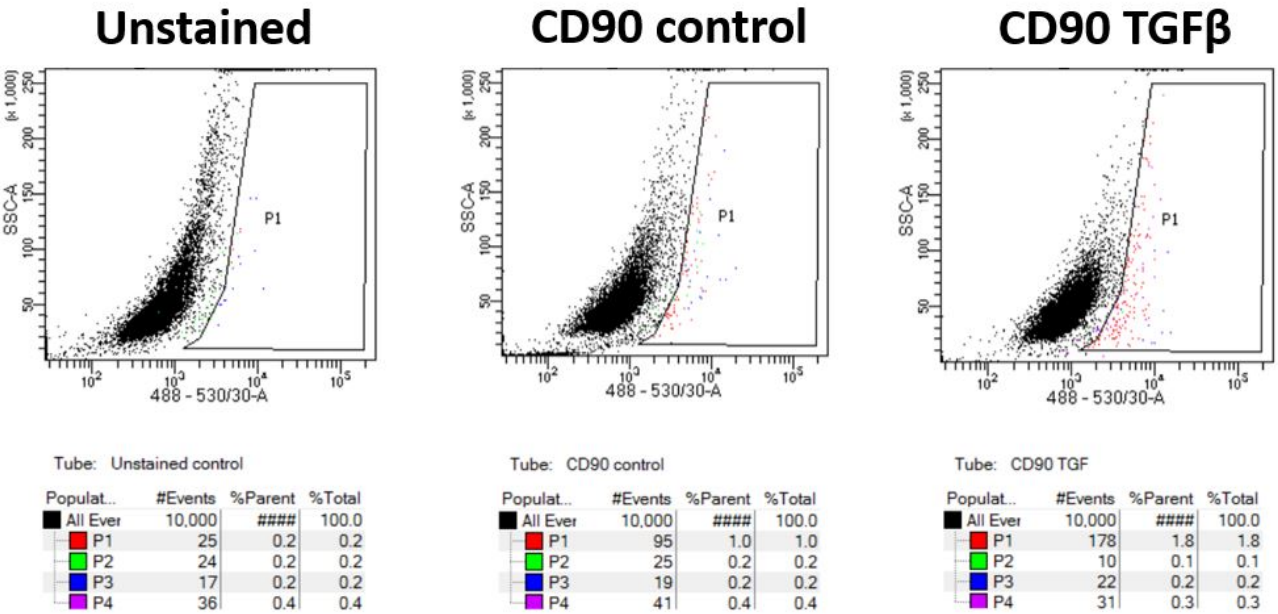

Figure 11: *FACS analysis of CD90-FITC stained (fixed) LX-2 cells (control) and TGFβ treated LX-2 cells. The gate is set for the unstained control. For the control, 1% is positive; for the TGFβ treated cells, almost 2% is positive.*

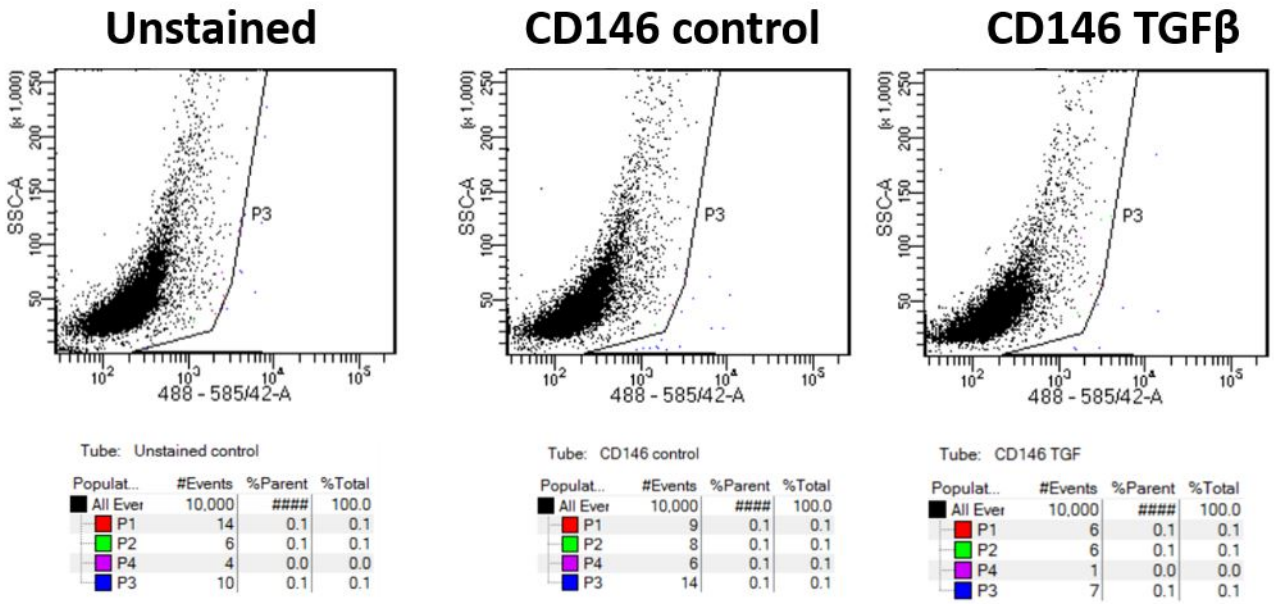

Figure 12: *FACS analysis of CD146-Pe stained (fixed) LX-2 cells (control) and TGFβ treated LX-2 cells. The gate is set for the unstained control. For both the control and the TGFβ treated cells, 0% is positive.*

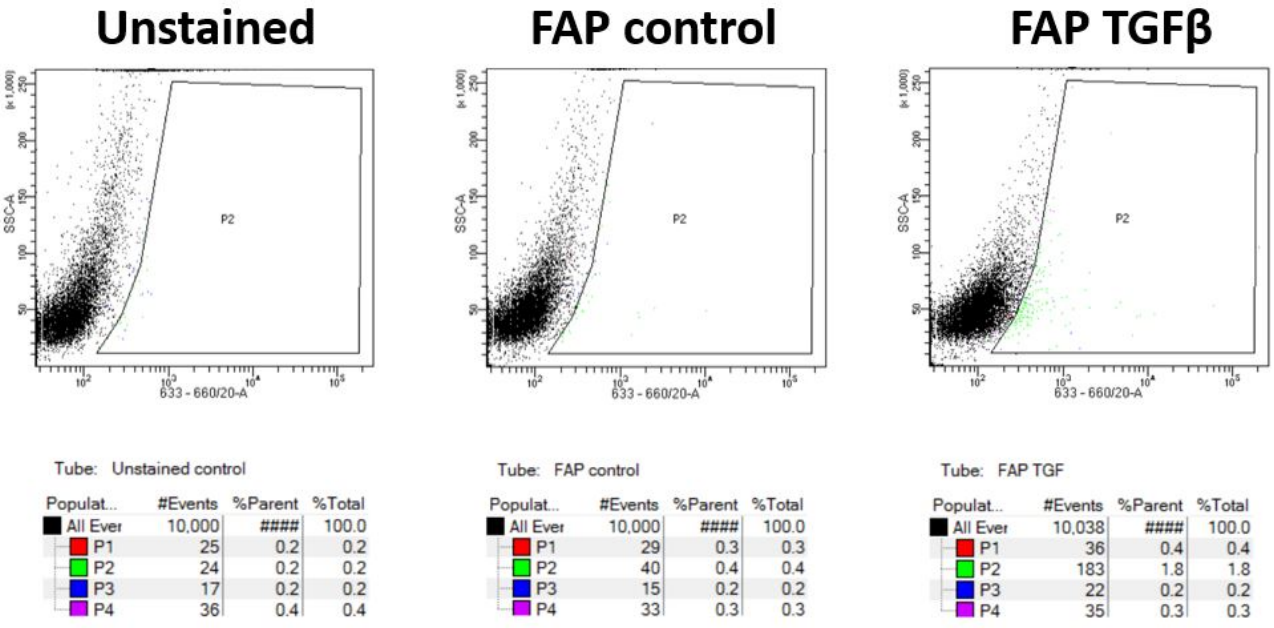

Figure 13: *FACS analysis of FAP-AF647 stained (fixed) LX-2 cells (control) and TGFβ treated LX-2 cells. The gate is set for the unstained control. For the control, 0% is positive; for the TGFβ treated cells, almost 2% is positive.*

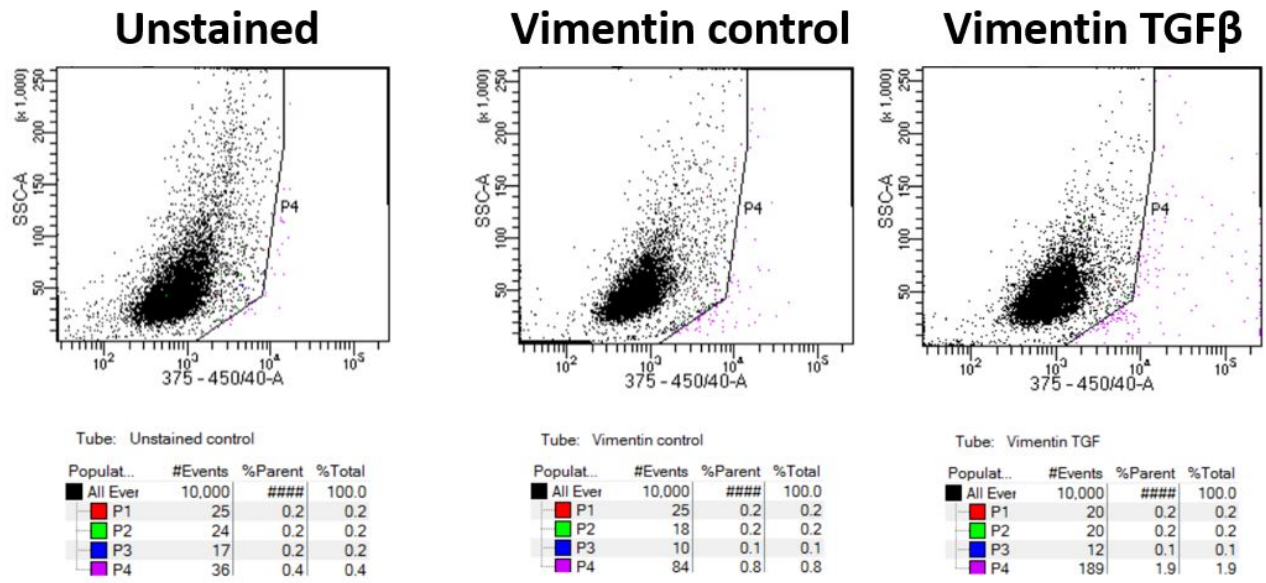

Figure 14: *FACS analysis of Vimentin-AF405 stained (fixed) LX-2 cells (control) and TGFβ treated LX-2 cells. The gate is set for the unstained control. For the control, 0% is positive; for the TGFβ treated cells, almost 2% is positive.*

As seen above, results were still not as expected, since no surface marker - except for CD9 - was found to be positive for all LX-2 cells. To confirm these findings, the same experiment was repeated (figures 15-21). As before, gates were set for the unstained control. Here, the normal LX-2 cells were found to be positive for CD90 (74%; figure 18). However, this was measured at excitation-emission 488-585/42, which is the Pe channel, while the cells were stained with CD90-FITC. Similar to the previous staining, CD9 was positive for both the control (73%) and the TGFβ treated LX-2 cells (91%), as can be seen in figure 15. The other antibody stainings resulted mainly in negative events. The findings of these cell stainings are not in line with literature, as it is described that LX-2 cells express CD9 [95], CD13 [93], CD63 [96], CD90 [93], CD146 [93], FAP [107] and Vimentin [94] and that there is upregulation of, for example, FAP after treatment with TGFβ [107].

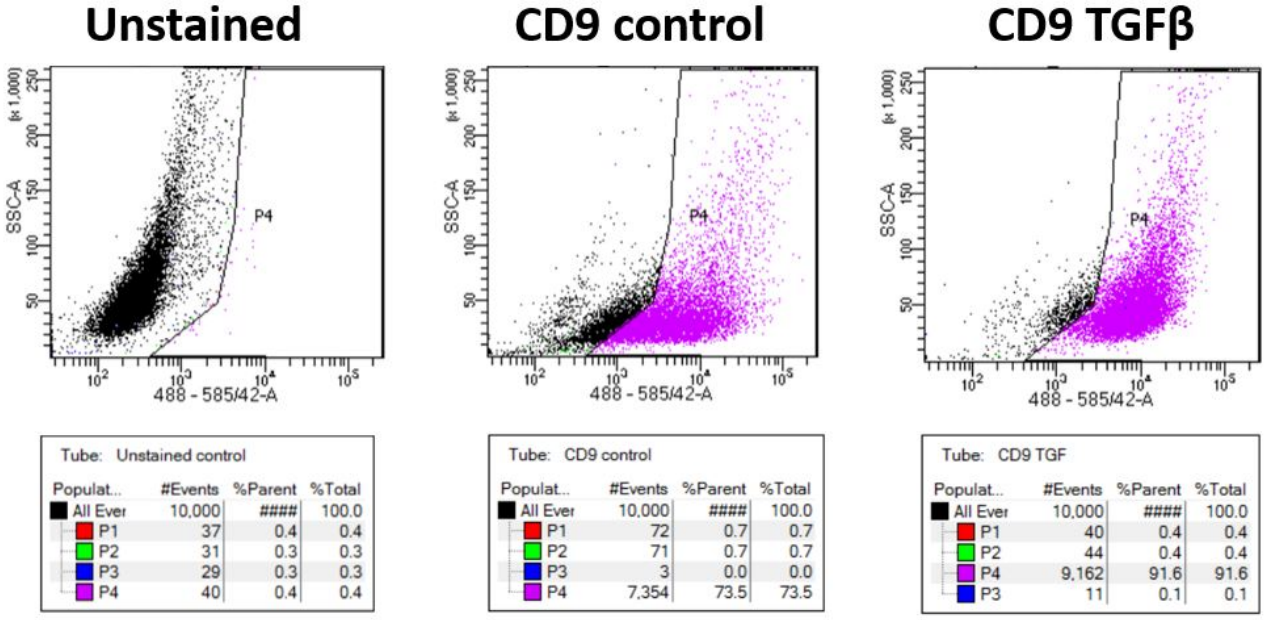

Figure 15: *FACS analysis of CD9-Pe stained (fixed) LX-2 cells (control) and TGFβ treated LX-2 cells. The gate is set for the unstained control. For the control, 73% is positive; for the TGFβ treated cells, 91% is positive.*

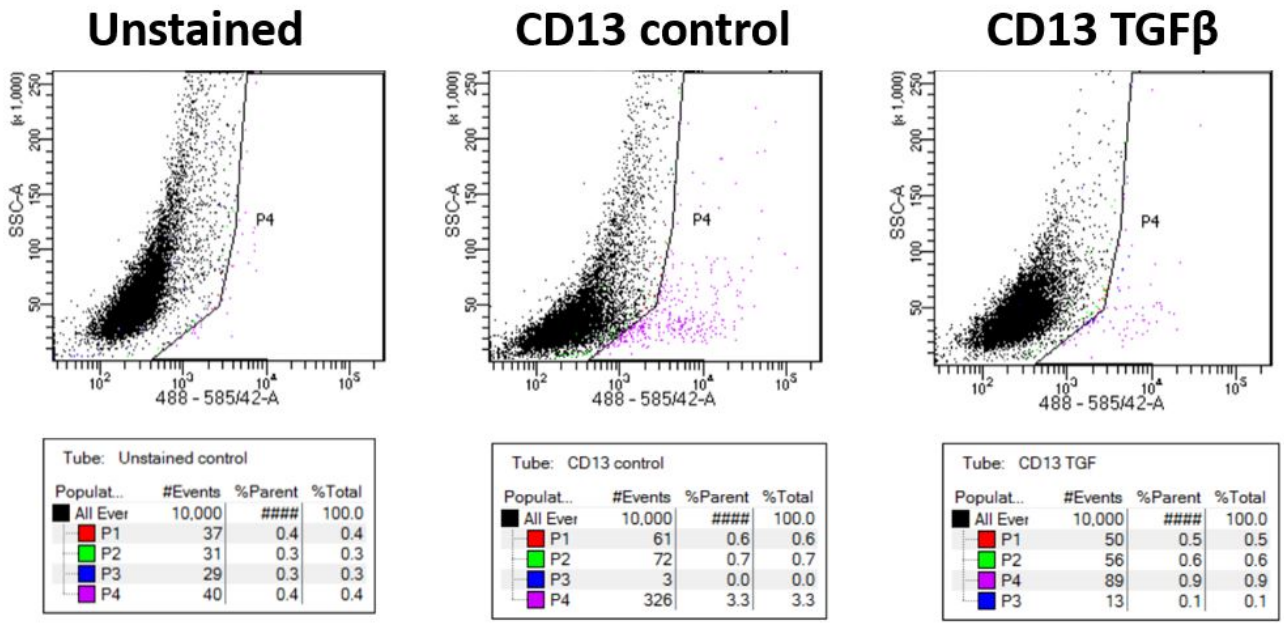

Figure 16: *FACS analysis of CD13-Pe stained (fixed) LX-2 cells (control) and TGFβ treated LX-2 cells. The gate is set for the unstained control. For the control, 3% is positive; for the TGFβ treated cells, almost 1% is positive.*

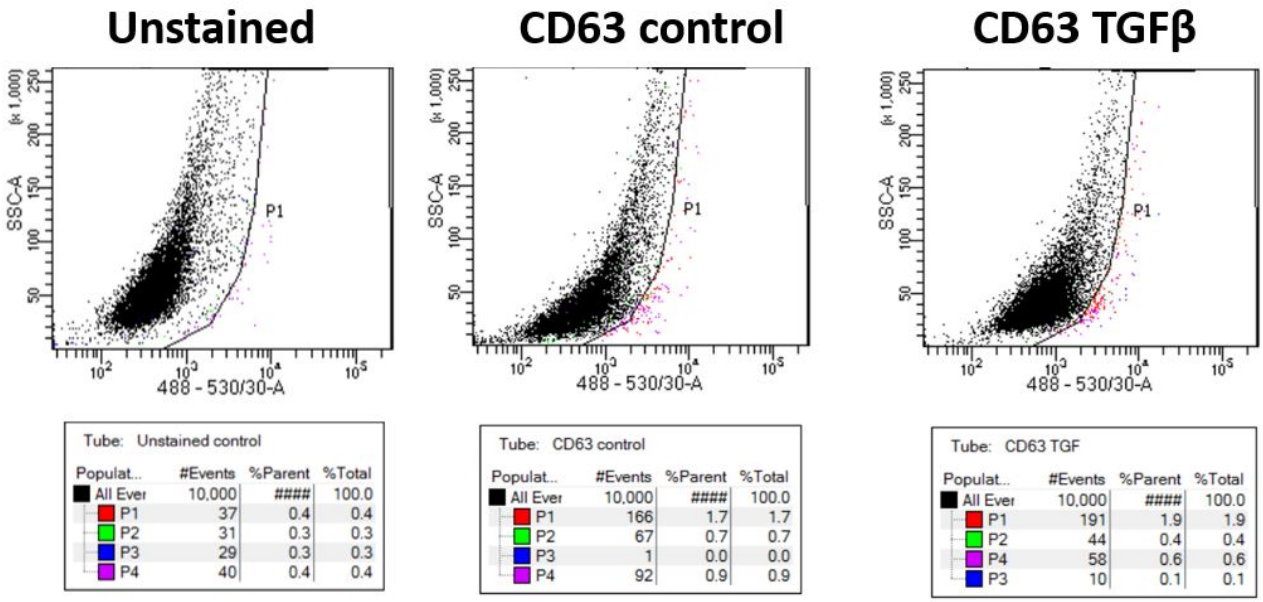

Figure 17: *FACS analysis of CD63-FITC stained (fixed) LX-2 cells (control) and TGFβ treated LX-2 cells. The gate is set for the unstained control. For both the control and the TGFβ treated cells, about 1% is positive.*

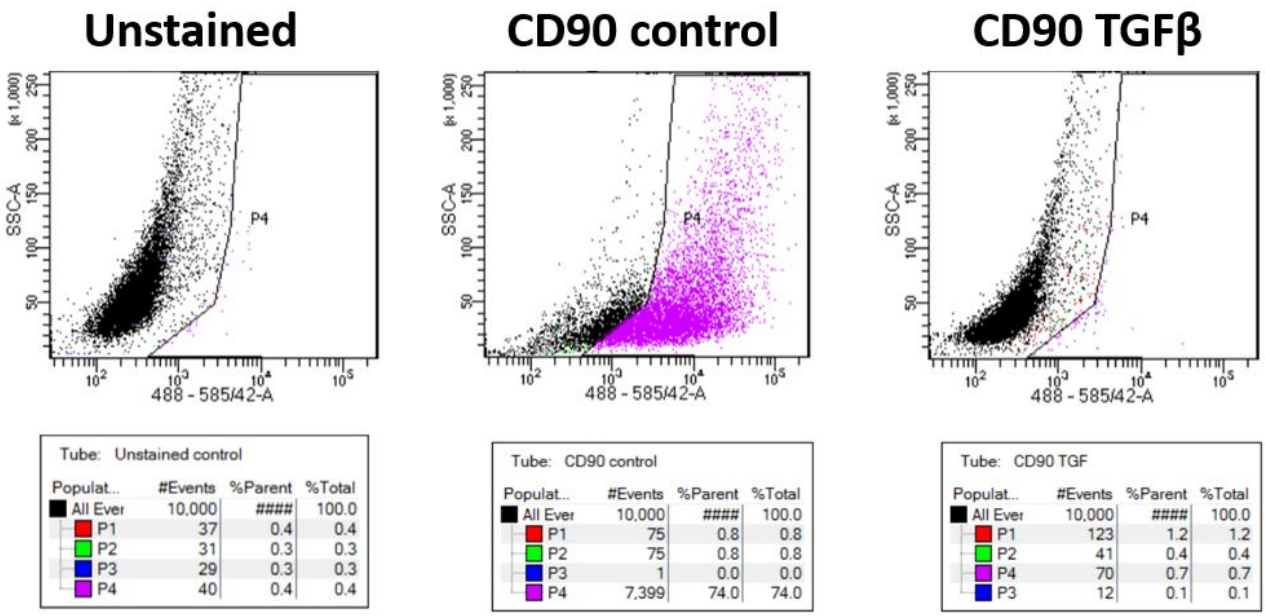

Figure 18: *FACS analysis of CD90-FITC stained (fixed) LX-2 cells (control) and TGFβ treated LX-2 cells. The gate is set for the unstained control. For the control, 74% is positive in Pe and 0% in FITC; for the TGFβ treated cells, 0% is positive in Pe and 1% in FITC.*

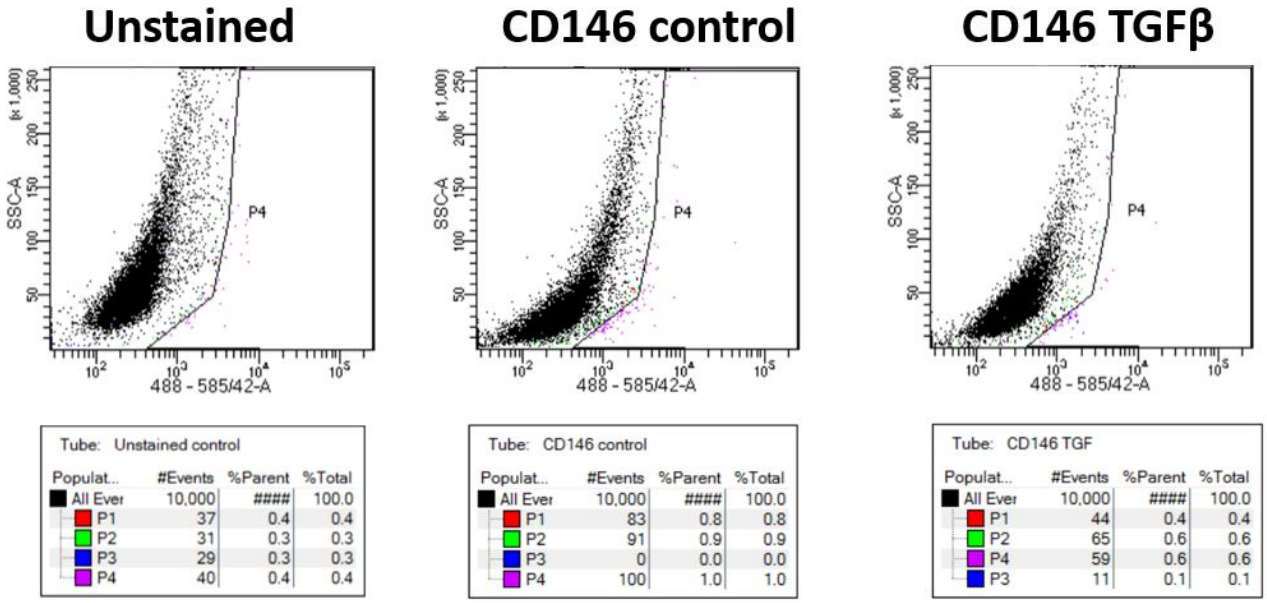

Figure 19: *FACS analysis of CD146-Pe stained (fixed) LX-2 cells (control) and TGFβ treated LX-2 cells. The gate is set for the unstained control. For the control, 1% is positive; for the TGFβ treated cells, 0% is positive.*

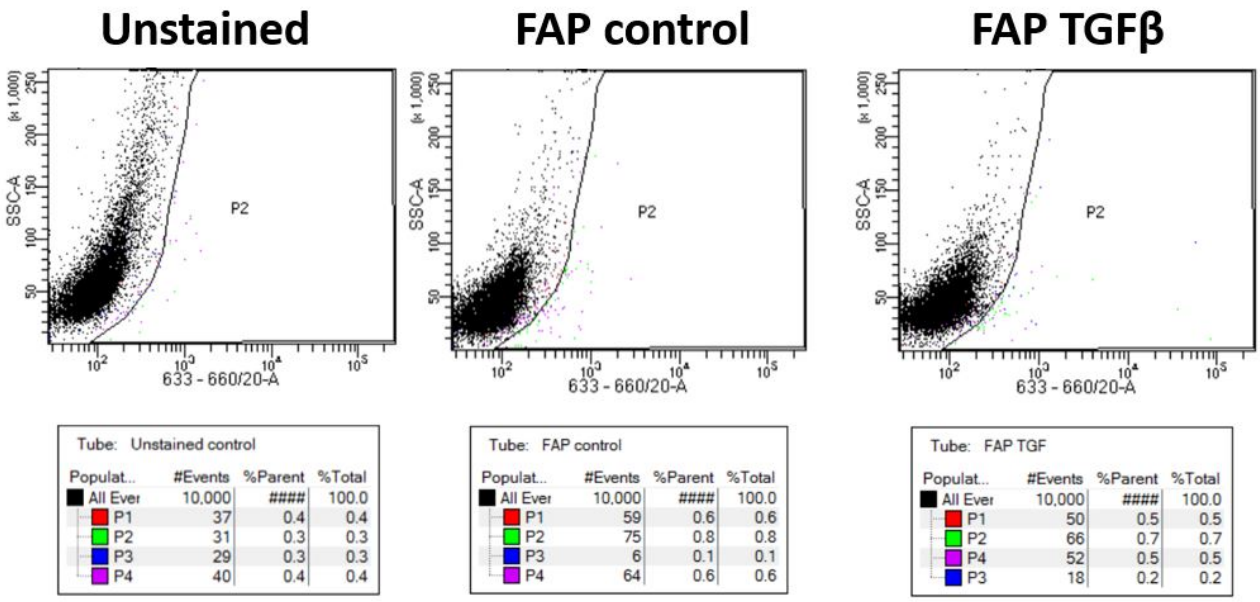

Figure 20: *FACS analysis of FAP-AF647 stained (fixed) LX-2 cells (control) and TGFβ treated LX-2 cells. The gate is set for the unstained control. For both the control and the TGFβ treated cells, almost 1% is positive.*

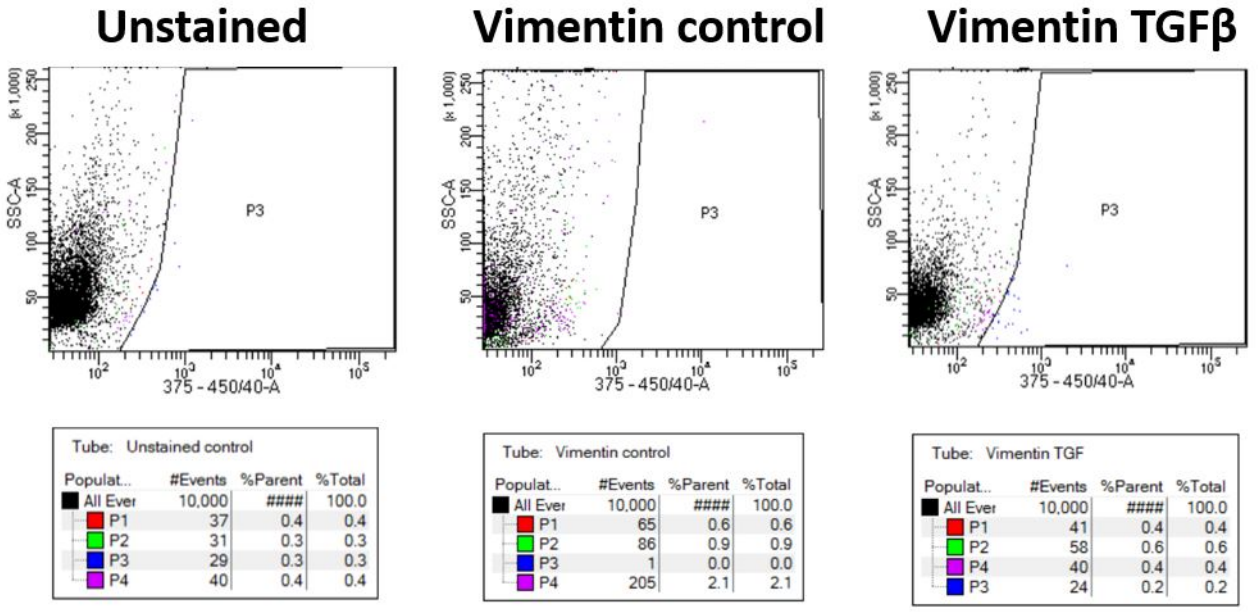

Figure 21: *FACS analysis of Vimentin-AF405 stained (fixed) LX-2 cells (control) and TGFβ treated LX-2 cells. The gate is set for the unstained control. For both the control and the TGFβ treated cells, 0% is positive.*

An overview of the cell stainings is given in table 9. For all antibodies, the percentage of positive events (percentages positive for the unstained cells subtracted) is averaged over the number of stainings for both the normal LX-2 cells and the TGFβ treated LX-2 cells. This clearly shows that the LX-2 cells here were only strongly positive for CD9. The results of CD90 were inconsistent and therefore, the average percentage does not give an actual representation of the result for this antibody.

Table 9: *Overview of the cell stainings. Percentages are averaged over all performed stainings. Percentages positive for the unstained cells are subtracted per measurement. n = number of stainings.*

Antibody	n (control)	LX-2 control [%]	n (TGFβ)	LX-2 TGFβ [%]
CD9	2	83.2 ± 14.2	2	92.0 ± 1.1
CD13	2	1.5 ± 2.1	2	0.7 ± 0.28
CD63	2	1 ± 0.4	2	1.4 ± 0.2
CD90	4	32.5 ± 36.4	2	1.0 ± 0.9
CD146	2	0.3 ± 0.4	2	0.1 ± 0.1
FAP	5	1.3 ± 1.5	2	1.0 ± 0.8
Vimentin	2	0.2 ± 0.3	2	0.8 ± 1.1

4.2 Extracellular vesicle staining - LX-2 cells

To confirm the presence of EVs in the sample and test the presence of FAP on the cells and EVs, FAP stained cells and EV samples and a Calcein stained EV sample were visualized using an inverted microscope. This can be seen in figure 22.
In figure 22A, containing the FAP-AF647 stained cells, a cell can be observed in the brightfield channel. However, in the APC channel (figure 22D), no signal is visible. The brightfield channel shows the presence of spots in the EV samples (figures 22B and C; indicated by blue arrows). The Calcein stained EV samples, visualized at the FITC channel, can be seen in figure 22E. Spots were observed (indicated by a blue arrow). However, these were only visible for a few seconds before disappearing. For the FAP stained EV sample in the APC channel (figure 22F), no signal was detected.

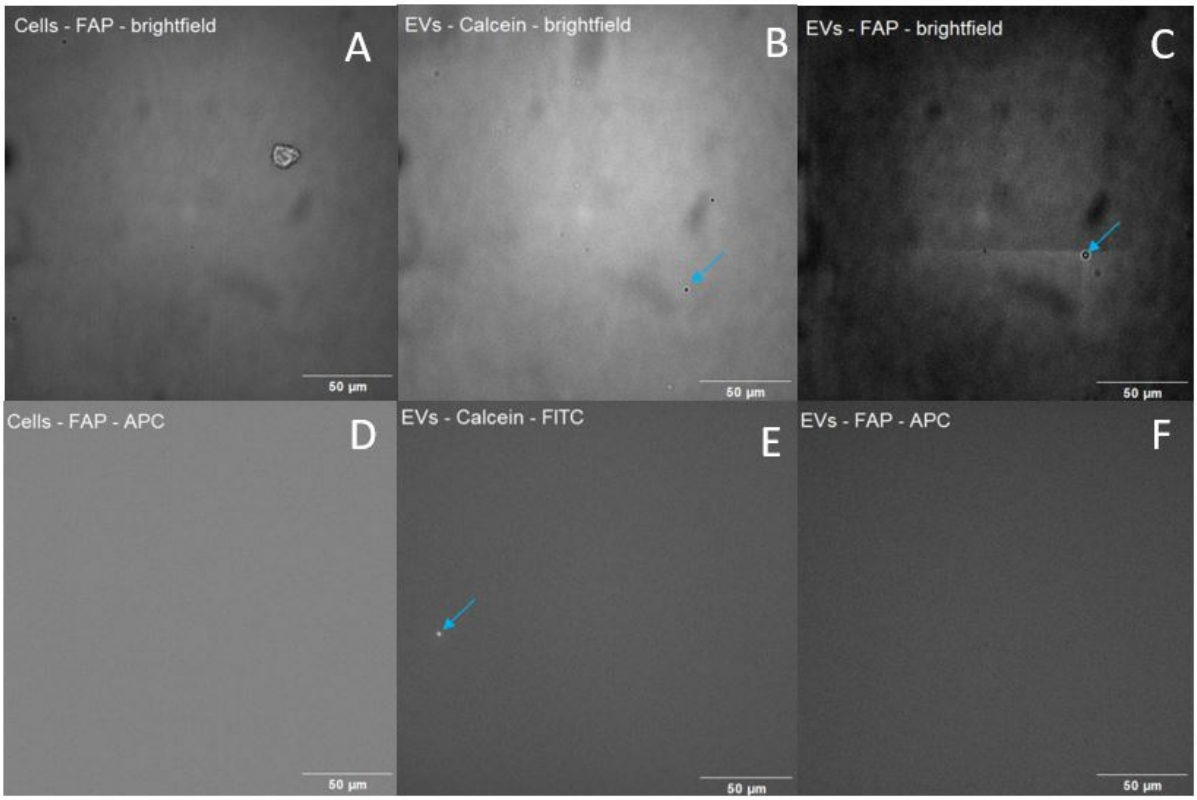

Figure 22: *Staining of LX-2 cells and EVs, visualized using an inverted microscope. Scalebar is 50 micrometers. A) FAP-AF647 stained cells, brightfield; B) Calcein stained EVs, brightfield; C) FAP-AF647 stained EVs, brightfield; D) FAP-AF647 stained cells, APC; E) Calcein stained EVs, FITC; F) FAP-AF647 stained EVs, APC. EVs are indicated by blue arrows.*

Cells were thus observed as mentioned before. As there was no signal from the FAP-AF647 staining, it could be concluded that the cells did not express FAP. This confirms the results found with the FACS measurements. The analysis of the extracellular vesicle staining using an inverted microscope showed the presence of particles in the sample, in the brightfield channel. In the FITC channel, it was confirmed that these particles were stained with the Calcein staining, despite rapid photobleaching. From these results, it can be concluded that EVs were present in the sample, as Calcein stains EVs [108]. For the FAP-AF647 stained EVs, similar particles were

observed in brightfield, however, in the APC channel no signal was observed. Therefore, FAP-AF647 either did not bind to the EVs or its fluorescence was too weak to observe here. In this case, since the cells did not express FAP and EVs generally express the same surface markers as the cells they originate from [78], it is most likely FAP-AF647 did not bind to the EVs.

4.3 Extracellular vesicle characterisation - Dynamic Light Scattering - LX-2 cells

The size of particles in the LX-2 EV sample was determined by DLS measurements. The results can be seen in table 10. Z-average and PdI are given as the average value over 3 measurements. The obtained Z-average is 850 ± 433 nm; the PdI is 0.835 ± 0.163. Differences in size and PdI between the 3 measurements were relatively large. Therefore, these values are not considered fully accurate. Since all measurements gave sizes in the range of 100-1000 nm, it can be said that there were particles present with the size of EVs [48]. This was in line with the expectation. Whether or not these particles indeed were EVs, cannot directly be concluded; the presence of other particles, such as proteins, was not excluded. In literature EVs of LX-2 cells with sizes in the range of 50 to 420 nm were described [109].

Table 10: *Size and PdI, represented by Z-average, of the particles in EV samples of LX-2 cells. Size and PdI per sample are averaged over 3 measurements.*

Days after EV harvesting	Sample	Z-average [nm]	PdI
0	EVs LX-2	850 ± 433	0.835 ± 0.163

In a following experiment, DLS was performed on EV samples of the LX-2 cells and the TGFβ treated LX-2 cells. One measurement was done at the day of EV harvesting; one measurement was done 7 days after EV harvesting. The results can be seen in table 11. Z-average and PdI are averaged over 3 measurements. The average measured size is 488 ± 63 nm for the EVs of the LX-2 cells without TGFβ and 512 ± 58 nm for the EVs of the LX-2 cells with TGFβ treatment. Research shows EVs of TGFβtreated LX-2 cells with size varying between 100 and 600 nm [66], which is similar to the results found here. The PdI for both samples is similar. However, it should be noticed that the measured Z-averages and PdIs varied considerably over the 3 measurements. It can be observed that the measured Z-averages increased strongly after storage of the EVs at 4 °C for 7 days. Also, this effect is more present for the EVs of the LX-2 cells without TGFβ treatment than for the EVs of the LX-2 cells with TGFβ treatment (11107 ± 3027 nm for the control and 4383 ± 1823 nm for the TGFβ treated).

Table 11: *Size and PdI, represented by Z-average, of the particles in EV samples of LX-2 cells and TGFβ treated LX-2 cells (1:1 in PBS). Size and PdI per sample are averaged over 3 measurements.*

Days after EV harvesting	Sample	Z-average [nm]	PdI
0	EVs LX-2 control (1:1 in PBS)	488 ± 63	0.693 ± 0.039
0	EVs LX-2 TGFβ (1:1 in PBS)	512 ± 58	0.619 ± 0.099
7	EVs LX-2 control (1:1 in PBS)	11107 ± 3027	0.412 ± 0.365
7	EVs LX-2 TGFβ (1:1 in PBS)	4383 ± 1823	0.853 ± 0.365

It was expected to find similar values at day 0 for the control sample as found with the first DLS measurement. However, this was not the case. The measured Z-average of the EV sample of the LX-2 cells without TGFβ treatment in the second DLS measurement is about half the value measured with the first DLS measurement. Also, the measured PdI is higher in the first measurement. Variation between the measurements was lower for the second measurement than for the first DLS measurement. A possible cause for the difference between the first and the second DLS measurement could be the difference in sample preparation: before the second DLS measurement, PBS was added to the samples (1:1). The samples of the first measurement did not contain PBS. Storage of the EVs in PBS, even for short periods, can influence the features of the EVs [110]. It was expected that the particles in the samples would aggregate and that, because of that, measured sizes would increase. This was indeed the case. Again values varied strongly between the measurements. However, measured sizes were all in the range of thousands of nanometers. Therefore, it is important to conclude that the sample changes over time, as this can influence results of other experiments. It should also be noticed that the increase in measured size was less for the TGFβ treated LX-2 EVs than for the non-treated LX-2 EVs. It was found in research that the size of LX-2 EVs changed with change of treatment [111]. TGF treated LX-2 cells were also found to release smaller EVs than non-treated LX-2 cells [111], which is different from the results found here.

4.4 Dot Blot - LX-2 cells

To find a suitable surface antibody for EV binding to fibroblasts, Dot Blot was performed on the LX-2 derived EV samples with FAP, αSMA, CD9, CD63 and CD90 antibodies. The result can be seen in figure 23. Ratios of the serial dilutions are given as EV:medium. For every used antibody, spots are visible. It can also be seen that the spots on the left, which originate from higher concentrations of EV sample, are brighter than the spots on the right. Also, the sixth spot of every membrane, originating from 100% medium and 0% EVs, is not visible.

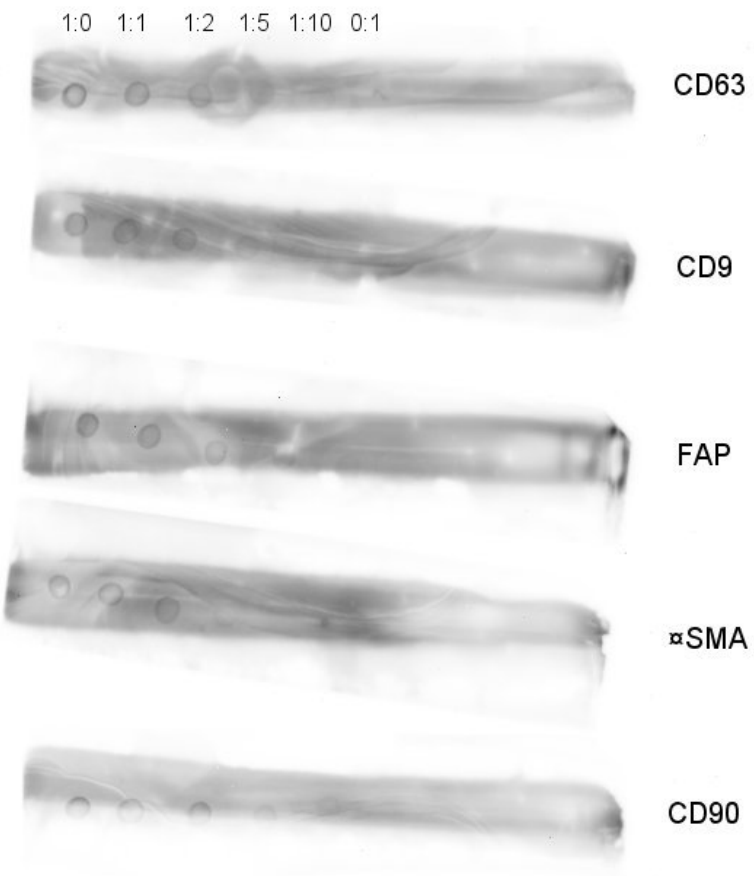

Figure 23: *Dot blot of LX-2 derived EVs using FAP, αSMA CD9, CD63 and CD90 antibodies. Ratios of the serial dilutions are given as EV:medium. Spots are visible for all used antibodies.*

As mentioned, spots were thus visible for all used antibodies and intensity dependent differences were observed for the different concentrations of EVs. Also, for medium only no spot was observed. This was in line with literature, as LX-2 cells, and thus LX-2 derived EVs, are described to be positive for these surface markers [92, 95, 96, 107]. However, the results obtained with the cell staining as described in section 4.1 indicated otherwise. As no control without primary antibody was included, aspecific binding of the secondary and tertiary antibodies was not excluded. Furthermore, quality of the images of the membranes was relatively low and stripes were present. This was thought to be caused mainly by the procedure, i.e. incubation of the membranes in tubes.

Therefore, a second dot blot was performed where more antibodies were included: CD9, CD13, CD63, CD90, CD146, FAP, Vimentin and αSMA. Also, a negative control of only secondary and tertiary antibody was included. Here, LX-2 derived EVs with and without TGFβ treatment were spotted, as well as LX2 cells with and without TGFβ treatment, all in a serial dilution. The results can be seen in figure 24.

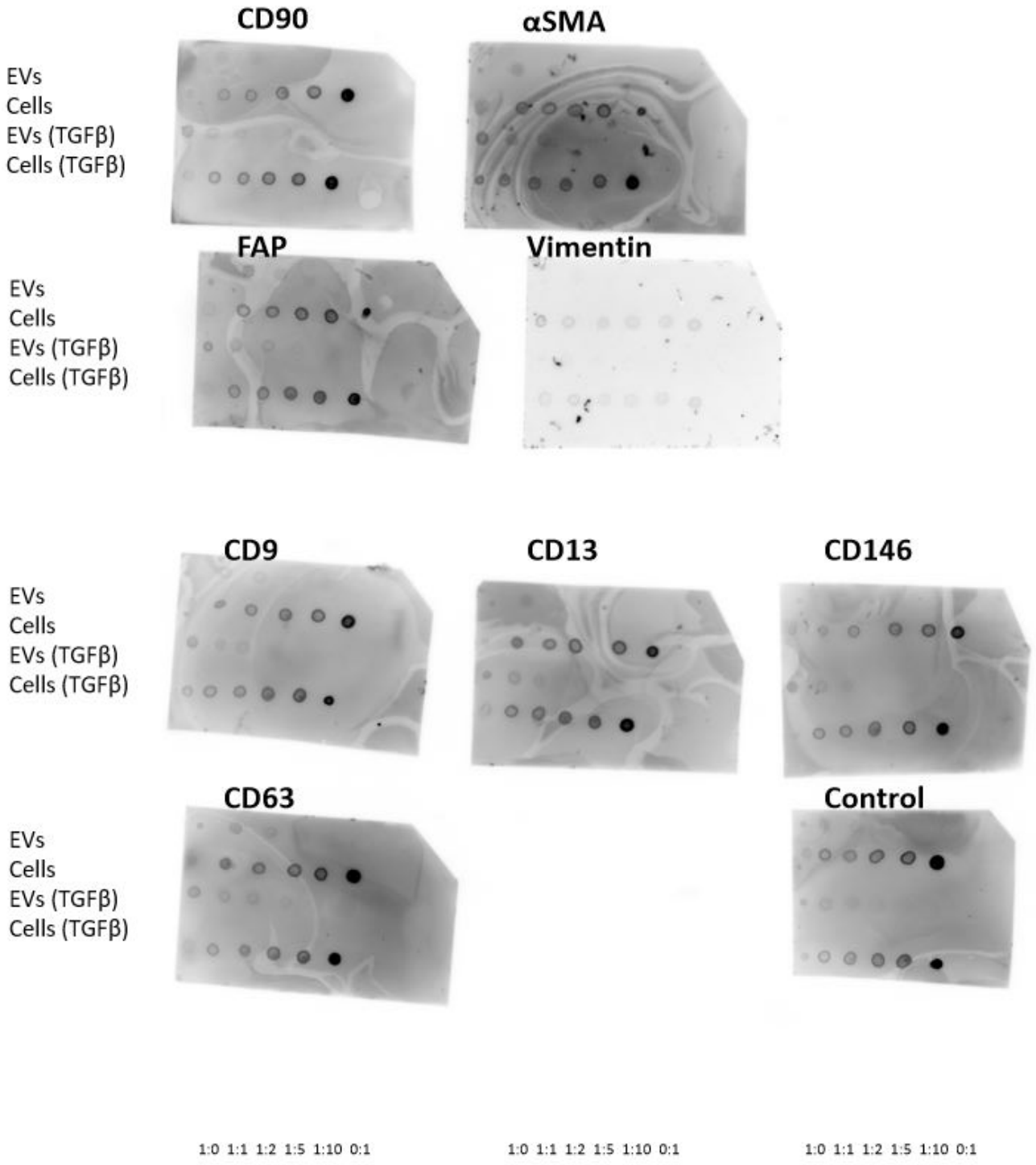

Figure 24: *Dot blot for LX-2 cells, LX-2 cell derived EVs, TGFβ treated LX-2 cells and TGFβ treated LX-2 cell derived EVs using CD9, CD13, CD63, CD90, CD146, FAP, Vimentin and αSMA. Ratios of the serial dilutions are given as (EV:medium) and (cells:PBS+2%FBS). For all antibodies, spots are visible. However, the control is positive too. Remarkably, for the cells the spots are brighter for lower concentrations.*

To increase quality of the images after the first Dot blot, the membranes were processed in Petri dishes instead of tubes. Background signal was reduced strongly compared to the first Dot blot in this way. As can be seen in figure 24, the control was positive for all four samples. This means that there was aspecific binding

of the secondary or tertiary antibody. Therefore, no conclusions can be drawn from the other membranes. It should be noticed here that the membrane with the primary antibody Vimentin had different secondary and tertiary antibodies and it can therefore not be determined whether or not there was aspecific binding for this membrane. Possible cause for aspecific binding is limited blocking of the membranes [112, 113]. Also, high concentrations of secondary and tertiary antibody can lead to high background signal [114].

In the next experiment, an attempt has been made to prevent aspecific binding by diluting the primary antibody in TBST + 5% non-fat dry milk instead of in TBS. Also, the secondary and tertiary antibody were diluted in TBST, both with a concentration of 1:1000. It was expected that these adjustments in the protocol would cause the control to be negative. However, as can be seen in figure 25, this was not the case. From this experiment no conclusions could thus be drawn.

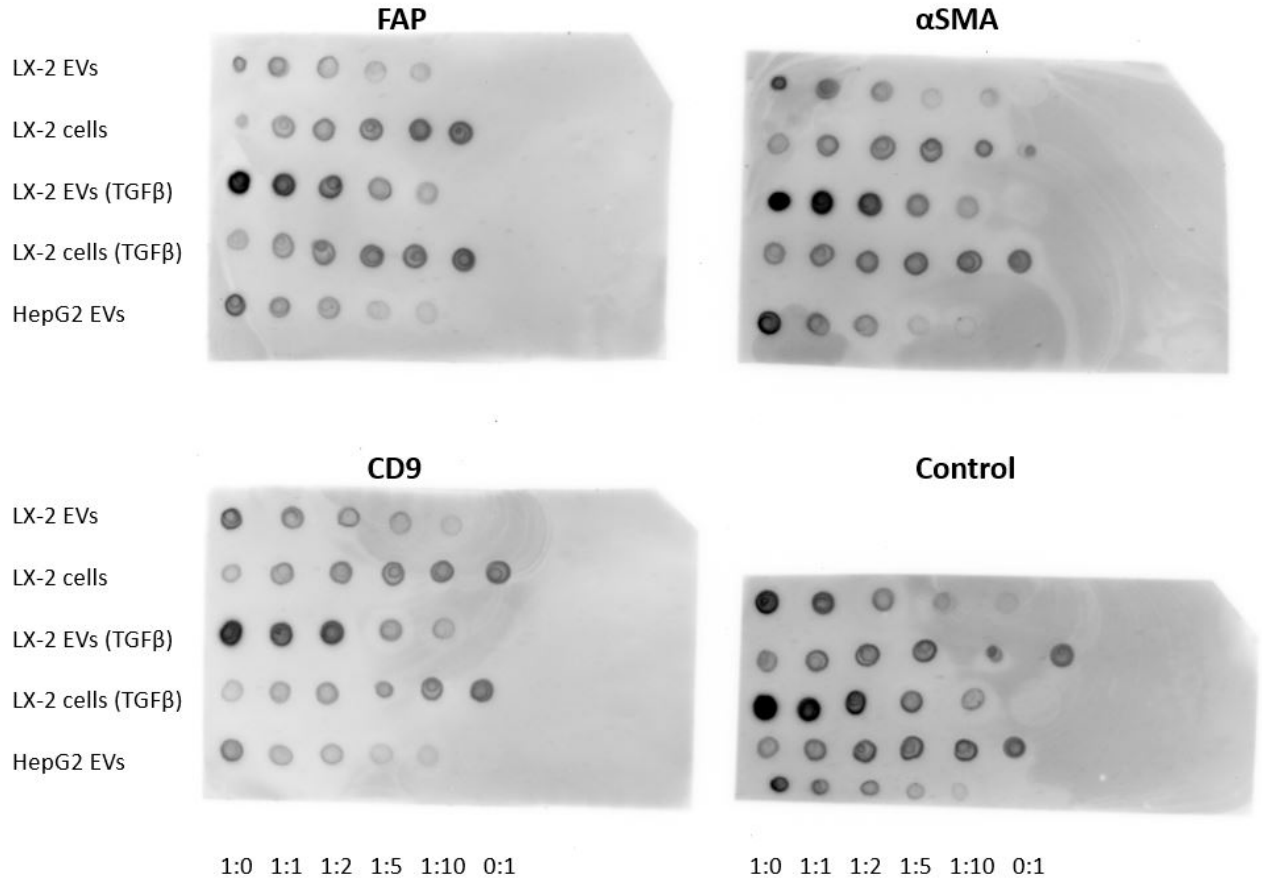

Figure 25: *Dot blot for LX-2 cells, LX-2 cell derived EVs, TGFβ treated LX-2 cells, TGFβ treated LX-2 cell derived EVs and HepG2 cell derived EVs. The primary antibodies used here are FAP, αSMA and CD9. Ratios are given as (EV:medium) and (cell:PBS+2%FBS). It can be seen that the control is positive.*

To examine the influence of the secondary and the tertiary antibody in the negative control being positive in the previous experiments, a fourth Dot blot was performed. The results can be seen in figure 26. Ratios are given as EV:TBS or cell:TBS. No incubation with primary antibodies was done. One membrane was only treated with a secondary antibody; two membranes were treated with both a secondary and a tertiary antibody. The two membranes on the right, with both a secondary and tertiary antibody, showed spots, similarly to the controls in the previous experiments. Furthermore, the intensity of the dots of the cells decreases for lower concentrations. The membrane with only the secondary antibody, on the left (position indicated by the rectangle), was not visible. These results indicate that the tertiary antibody bound aspecifically. It was also seen that the intensity of the spots originating from the cells did not increase for lower concentrations here as was the case for the previous experiments. This suggests that PBS with FBS, in which the cells were diluted, contains particles to which the antibodies can bind.

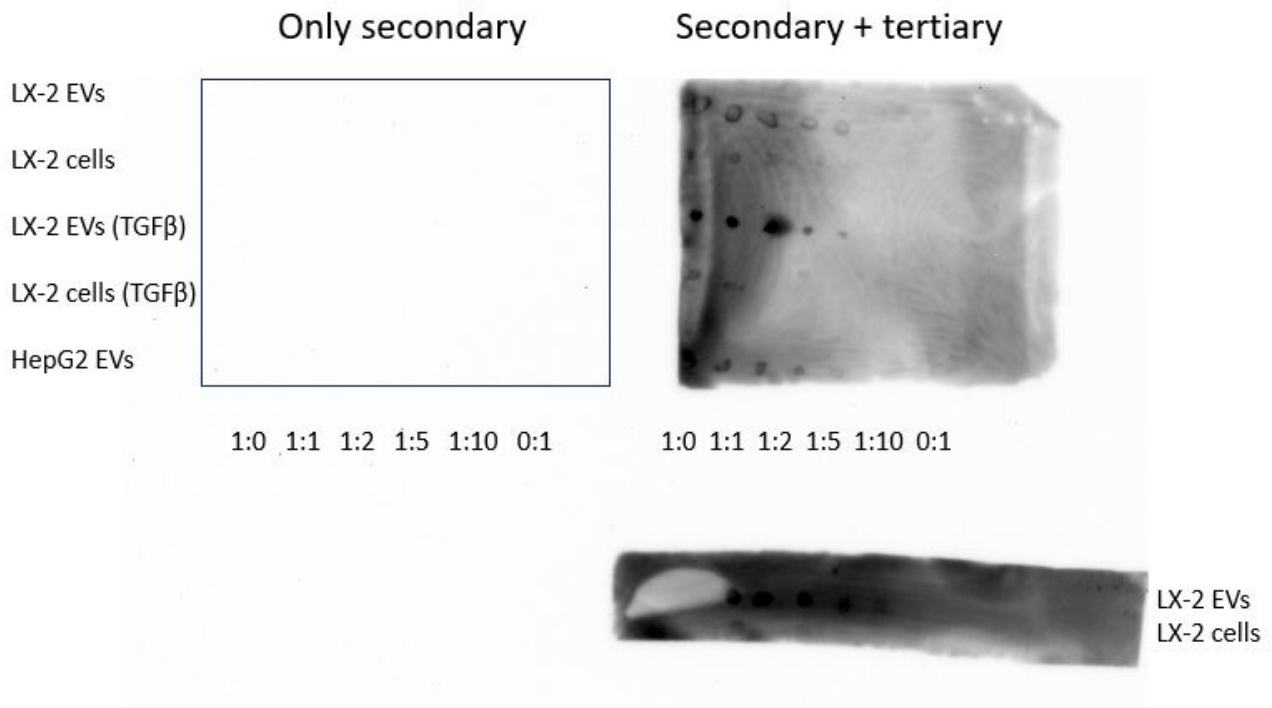

Figure 26: *Dot blot for LX-2 cells, LX-2 cell derived EVs, TGFβ treated LX-2 cells, TGFβ treated LX-2 cell derived EVs and HepG2 cell derived EVs. Ratios are given as EV:TBS or cell:TBS. No primary antibodies were used. For the left membrane (location indicated by the rectangle), also no tertiary antibody was used. The two membranes at the right were treated similar to the controls in the previous experiments, including a secondary and a tertiary antibody. The membrane without the tertiary antibody did not give a signal. At the membranes with both the secondary and tertiary antibodies, spots were visible.*

Since it was found that the tertiary antibody caused aspecific binding, a fifth Dot blot was performed without a tertiary antibody (figure 27). Although it was expected that this would cause a decrease of intensity of the obtained signal, this would lead to more reliable results. Here, again, LX2 cells and EVs derived from LX2 cells (with or without TGFβ), as well as HepG2 derived EVs, were spotted on the membranes in a serial dilution. The resolution was low, partially as a consequence of the camera of the imaging device being overheated due to use for a large amount of time. Decrease in signal strength from excluding the tertiary antibody could also have had an influence on the resolution. The control shows no clear spots, indicating that aspecific binding is prevented here and that the tertiary antibody indeed caused the negative control to be positive. However, the experiment needs to be repeated to increase reliability of the results. In case the control is negative, the other membranes can be analysed. For CD90, αSMA and FAP no signal is detected. This would mean that the EVs and cells used here were not positive for these antibodies. However, the position of the membranes next to the membrane with Vimentin could have caused the imaging device to stop the measurement early as the signal of Vimentin was very strong. The difference in signal strength between Vimentin and the other antibodies is likely caused by using a different secondary antibody as discussed before. Furthermore, for CD63 spots are visible. Although this is in line with literature [96], this result is not consistent with the results found with FACS analysis.

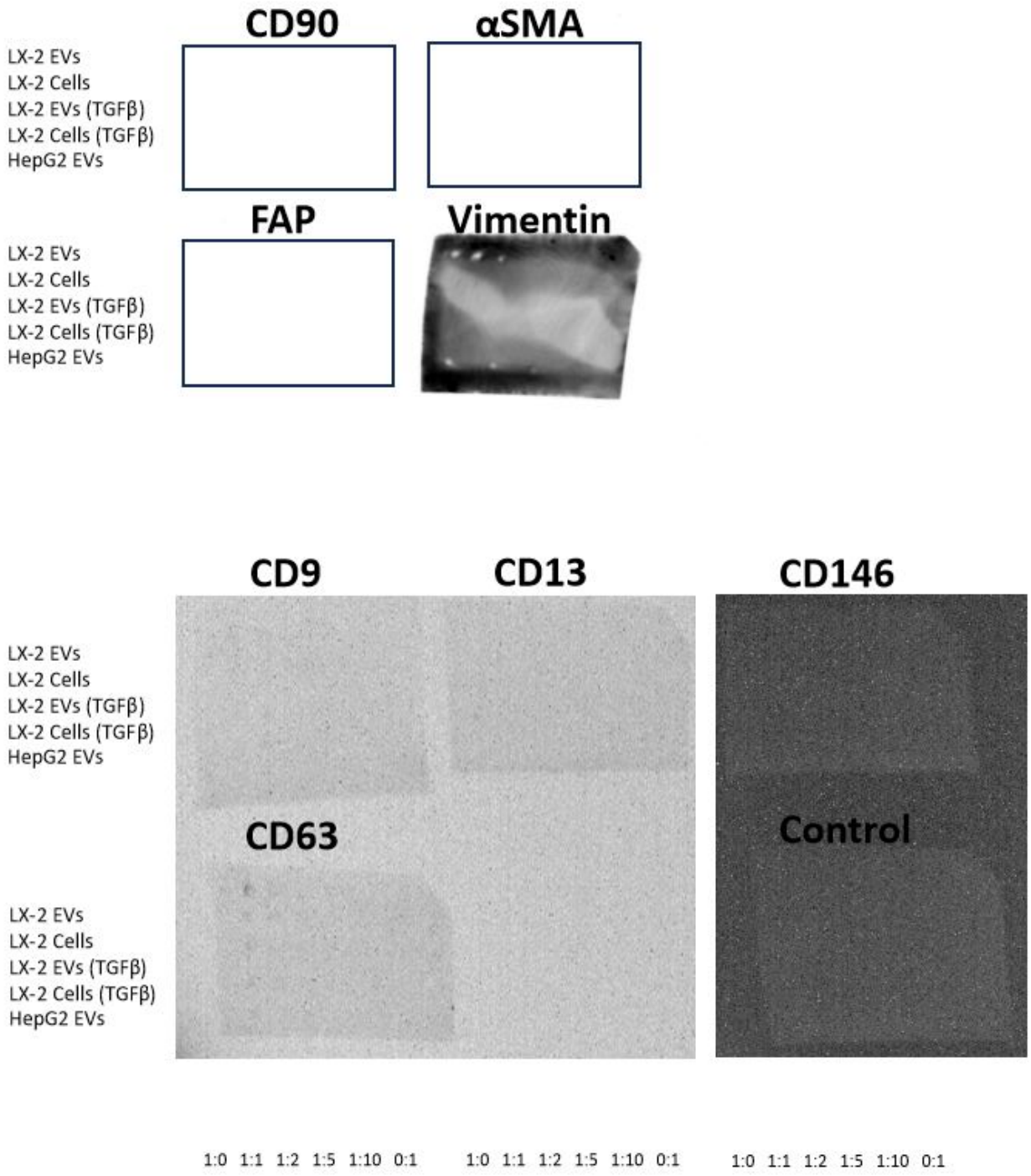

Figure 27: *Dot blot for LX-2 cells, LX-2 cell derived EVs, TGFβ treated LX-2 cells, TGFβ treated LX-2 cell derived EVs and HepG2 cell derived EVs. Ratios are given as EV:TBS or cell:TBS. CD9, CD13, CD63, CD90, CD146, Vimentin, aSMA and FAP primary antibodies were used. CD63 and Vimentin were considered positive*

4.5 Magnetic enrichment - LX-2 cells

For the first conjugation, CD9-APC (633-660/20 nm) was used in combination with LX-2 cells. In figure 28, the FACS results of this can be seen. A gate is set for the empty beads (P1; 488-585/42 nm). Beads are present in all samples in figure 28a and a positive signal for P1, originating from adding Tz, can be observed (36%). It can therefore be concluded that Tz has bound to the beads-OPSS (partially). Almost no events were measured for the TCO-CD9 sample in 28b. This is most likely caused by the small size of TCO-CD9. Furthermore, it can be seen that cells were present in the TCO-CD9-LX2 sample. However, since no control using LX-2 cells without CD9-APC was measured, no gate could be set, as the influence of factors, such as auto-fluorescence, in the sample was not clear. Hence, no conclusions can be drawn about whether or not the cells here were bound to CD9-APC. In the last two samples, which can be seen in 28c, very few beads were present. Although the volume of beads-OPSS-Tz added to these samples was relatively small - only 5 µl for both - the beads

were visible in the sample. It is therefore unclear what exactly caused the small number of events in the FACS measurement. The beads will most likely have been at the bottom of the sample, which could not be measured with the FACS. However, the low number of measured events thus leads to decreased reliability of the results, as the measured events may not have been representative for the whole sample.
The sample containing the full system shows two populations, one of which is positive for P1. This indicates the presence of beads-OPSS-Tz. The other population is negative for P1 and as it is different from the population assumed to be beads (considering the FSC-SSC plot), this population most likely consists of the LX-2 cells. This means that, as expected, both the beads and the cells are present in the sample. However, as the two populations are visible, the cells and the beads seem to be present separately in the sample and not bound. It cannot directly be concluded which two compounds in this case did not attach, because only the beads and the cells can be observed from the FACS results and only Tz and CD9-APC are fluorescently labeled. It is thus possible that TCO did not bind to either Tz or CD9, but, also, whether CD9 has bound to TCO cannot be concluded, as mentioned earlier. Moreover, although the results indicate the presence of two different populations, one being the cells and one being the beads, looking at the procedure in which the sample is washed multiple times, only compounds that were bound to the beads should have been present in the sample. Furthermore, it is important to note that capturing cells with this procedure has not been tried before and it is thus not a proven technique for cells.

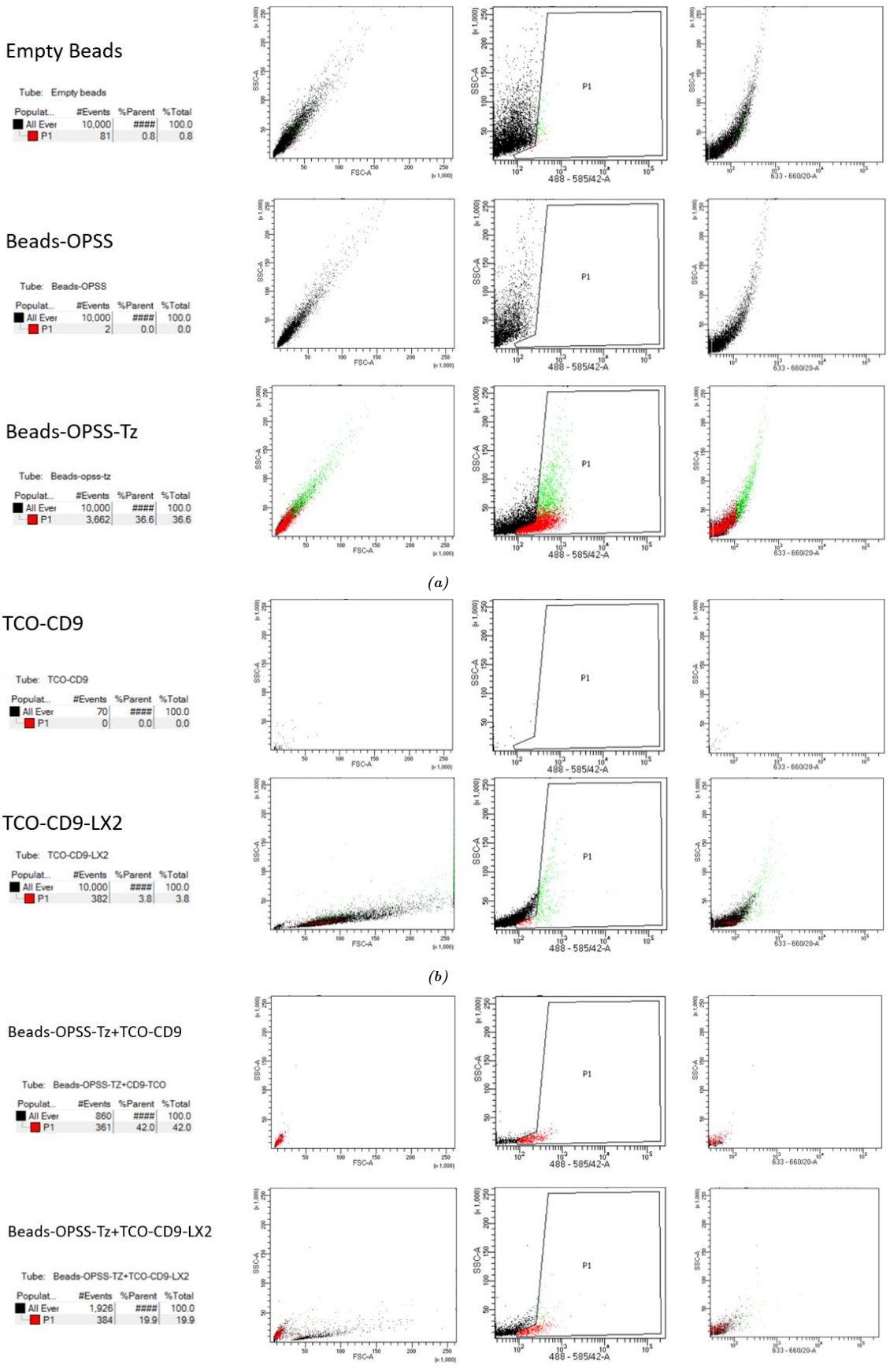

Figure 28: *FACS analysis of the conjugation with LX-2 cells and CD9-APC antibody. The gate (P1) is set for the empty beads. Tz is fluorescent in Pe: 488-585/42 nm; APC: 633-660/20 nm. a) Samples with empty beads, beads-OPSS and beads-OPSS-Tz. Beads are present in all samples. In the beads-OPSS-Tz sample, positive events in P1, originating from adding Tz, can be observed. b) Samples with TCO-CD9 and TCO-CD9-LX2. Almost no events were measured in the TCO-CD9 sample. Cells can be observed in the TCO-CD9-LX-2 sample; fluorescence from CD9-APC cannot directly be observed. c) Samples with beads-OPSS-Tz+TCO-CD9 and beads-OPSS-Tz+TCO-CD9-LX2S. Very few beads were present in these samples. The sample with the full system consists of two populations.*

As no clear positive results were obtained with the first conjugation, a second conjugation using Calcein stained LX-2 EVs and CD63 antibody was performed. As the system was not tested for usage with cells, EVs were chosen here. In this way, the potential influence of using cells instead of EVs could be examined. CD63 antibody was chosen instead of CD9 antibody, as no fluorescent signal originating from CD9-APC antibody seemed to be present in the first conjugation, although this was not confirmed with a control, as mentioned before, and cells stainings showed positive results for CD9. Although CD63 is a general EV marker [82], the cells seemed not to express CD63 and it cannot be concluded whether the EVs did. Therefore, it cannot be determined whether the obtained results are a consequence of the conjugation itself or the absence of binding affinity of these EVs for CD63 antibody. The results of the conjugation with LX-2 derived EVs and CD63 antibody are shown in figure 29. Gates (P1 and P2) were set for the empty beads. The results of the first part of the conjugation were similar to the results described for the first conjugation, with 32% positive for Tz (P1). Similar to the staining of the cells with CD9-APC in the first conjugation, it cannot be concluded here whether or not the EVs were positive for the Calcein staining, as no unstained EVs were measured. However, the measured events of TCO-CD63-EV mainly appeared at the right side of the plot. It is therefore assumed that the EVs were indeed stained with Calcein and that the gate (P2), set here, gives an indication whether EVs were present in the sample. From the TCO-CD63-EV sample, it can be concluded that there is a fluorescent signal measured in Pe, the channel in which Tz is measured too. This needs to be taken into account while evaluating the full system, as the presence of TCO-CD63-EV thus already leads to positive events for both P1 and P2. It should be noticed that, again, the numbers of measured events for the samples without the beads were very low. Therefore, results are less reliable. For both the last two samples, about 3.000 events were measured, which is also considerably less than the goal of 10.000 measured events. For the full system, one population can be observed in contrast with the first conjugation. 35% of the events was positive for P1 and 1.5% was positive for P2. Positive events for P2 indicate the presence of TCO-CD63-EV as mentioned before. Assuming all components that were not bound to the beads were removed in the procedure, some EVs seem to have bound to the beads via OPSS, Tz, TCO and CD63. However, in this case, efficiency of binding was very low. Except for the need of a higher efficiency in the conjugation to achieve successful isolation of the EVs, an antibody specific for (activated) fibroblasts is required. As CD63 is a general EV surface marker [80], it could, hypothetically, capture most types of EVs. For the purpose of this research described in section 2, this is undesirable.

Empty Beads

Tube: Empty beads			
Populat...	#Events	%Parent	%Total
All Ever	10,000	####	100.0
P2	5	0.0	0.0
P1	5	0.0	0.0

Beads-OPSS

Tube: Beads-OPSS			
Populat...	#Events	%Parent	%Total
All Ever	10,000	####	100.0
P2	17	0.2	0.2
P1	17	0.2	0.2

Beads-OPSS-Tz

Tube: Beads-opss-tz			
Populat...	#Events	%Parent	%Total
All Ever	10,000	####	100.0
P2	9	0.1	0.1
P1	3,291	32.9	32.9

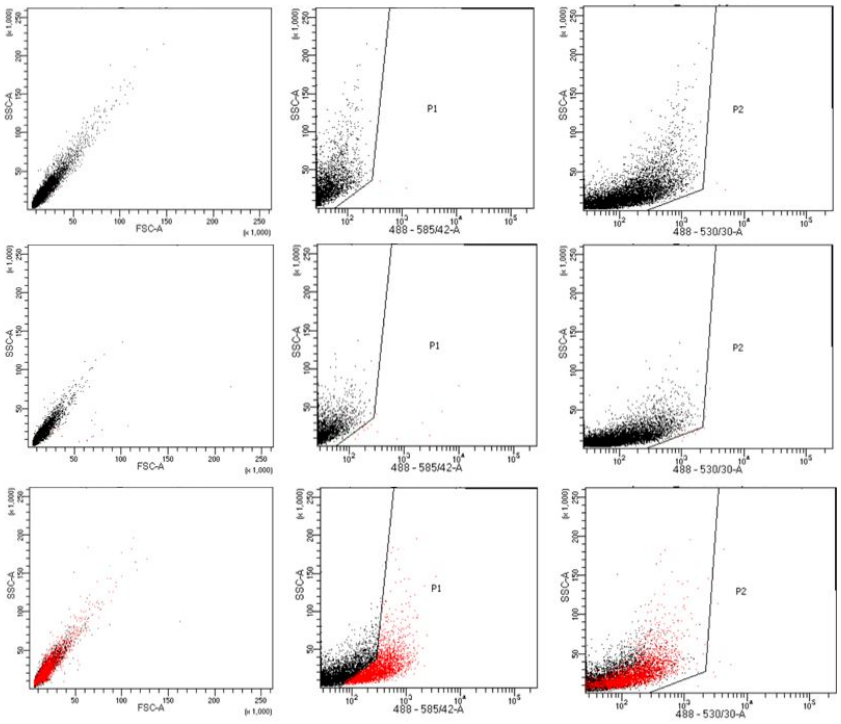

(a)

TCO-CD63

Tube: TCO-CD63			
Populat...	#Events	%Parent	%Total
All Ever	152	####	100.0
P2	3	2.0	2.0
P1	4	2.6	2.6

TCO-CD63-EV

Tube: TCO-CD63-EV			
Populat...	#Events	%Parent	%Total
All Ever	430	####	100.0
P2	267	62.1	62.1
P1	227	52.8	52.8

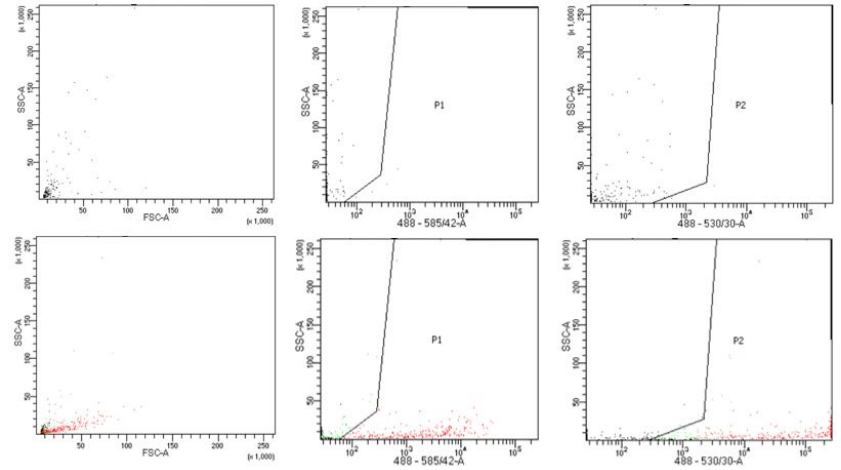

(b)

Beads-OPSS-Tz + TCO-CD63

Tube: Beads-OPSS-TZ+TCO-CD63			
Populat...	#Events	%Parent	%Total
All Ever	3,025	####	100.0
P2	11	0.4	0.4
P1	801	26.5	26.5

Beads-OPSS-Tz + TCO-CD63-EV

Tube: Beads-OPSS-TZ+TCO-CD63-EV			
Populat...	#Events	%Parent	%Total
All Ever	3,061	####	100.0
P2	47	1.5	1.5
P1	1,088	35.5	35.5

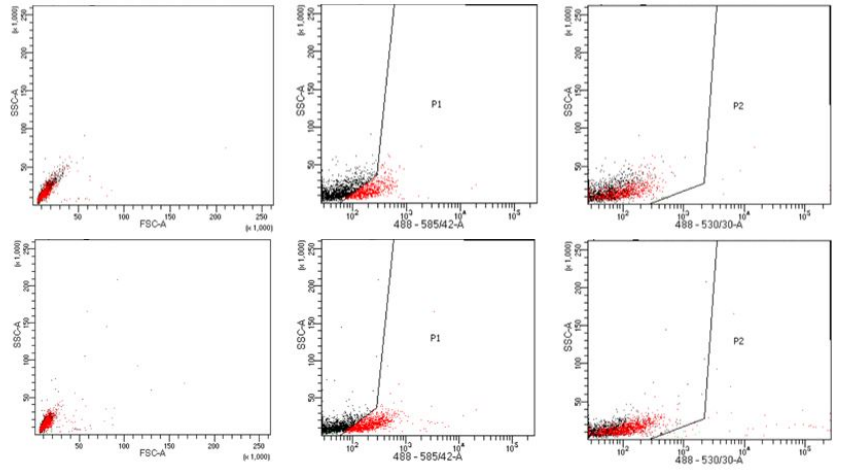

(c)

Figure 29: *FACS analysis of the conjugation for Calcein stained LX-2 EVs with CD63. Gates are set for the empty beads. Tz is fluorescent in Pe (488-585/42 nm), Calcein in FITC (488-530/30 nm). a) FACS analysis of the samples containing empty beads, beads-OPSS and beads-OPSS-Tz are shown. Beads are present in all samples. Adding Tz led to a percentage of 32% of the events that were positive for P1. b) FACS analysis of the samples containing TCO-CD63 and TCO-CD63-EV. Very few events were measured for both samples. However, TCO-CD63-EV is, partially, positive for both P1 and P2. c) FACS analysis of the samples containing beads-OPSS-Tz+TCO-CD63 and beads-OPSS-Tz+TCO-CD63-EV. About 3.000 events were measured for both samples. 1.5% was positive for P2, indicating the presence of EVs in the sample.*

4.6 Cell staining - prostate fibroblasts

As no suitable, fibroblast specific surface marker was found for the used LX-2 cells, it was decided to switch cell lines. Instead of hepatic stellate cells, human primary prostate fibroblasts (hPrF) were used. These cells, despite not being hepatocyte related, are known to express high levels of FAP antibody [103]. So, they were hypothesized to serve as a suitable model to test the immunocapturing system.
To test the expression of the human prostate fibroblasts for FAP, these cells were stained with FAP-AF647 antibody. The FACS results can be seen in figure 30. 88% of the cells is positive for FAP.

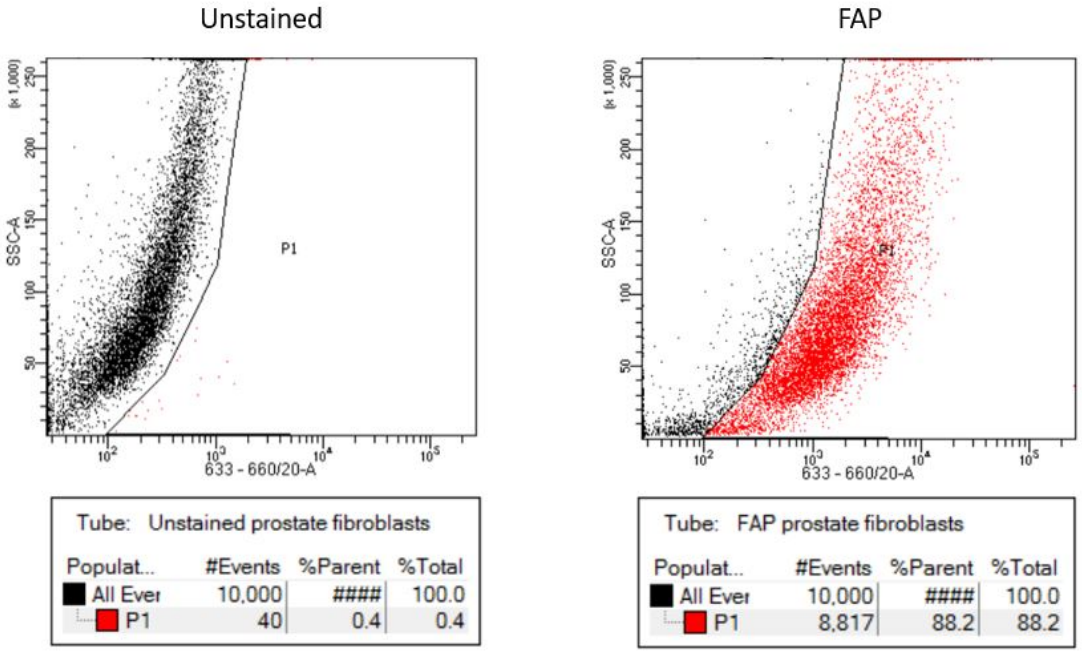

Figure 30: *FACS analysis of FAP-AF647 stained human prostate fibroblasts. The gate is set for the unstained cells. Compared to the unstained cells, 88% of the stained cells is positive for FAP.*

4.7 Extracellular vesicle staining - prostate fibroblasts

The presence of EVs in the hPrF EV sample was studied by a Calcein staining. Also, to examine further whether the EVs and cells expressed FAP, they were stained with FAP-AF647 antibody and visualized using an inverted microscope. The results can be seen in figure 31. The brightfield channel shows the presence of cells (figure 31A). Also, particles, similar to those confirmed to be EVs for the LX-2 samples, were observed in the EV samples (figures 31B and C). For the Calcein staining a signal was seen with the microscope, which confirms the presence of EVs. However, due to rapid bleaching this could not be imaged clearly. Nevertheless, dark spots are present in the image (figure 31E). It is not clear whether these are originating from Calcein stained EVs. It can be seen that in both the cell and EV sample stained with FAP a signal is obtained (figures 31D and F), confirming the binding of FAP-AF647 antibody to the prostate fibroblasts and to the prostate fibroblast derived EVs.

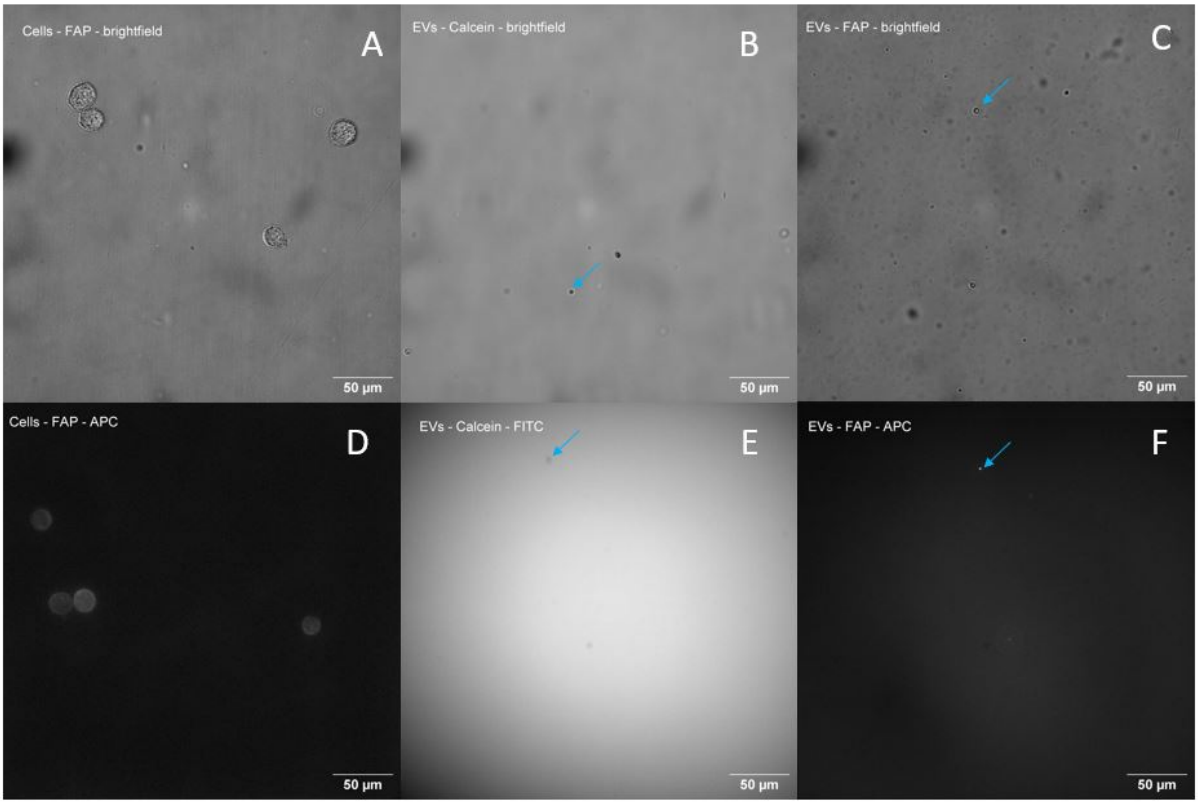

Figure 31: *Staining of human prostate fibroblasts (hPrF) and hPrF derived EVs, visualized using an inverted microscope. Scalebar is 50 micrometers. A) FAP-AF647 stained cells, brightfield; B) Calcein stained EVs, brightfield; C) FAP-AF647 stained EVs, brightfield; D) FAP-AF647 stained cells, APC; E) Calcein stained EVs, FITC; F) FAP-AF647 stained EVs, APC. EVs are indicated by blue arrows.*

Moreover, a FACS analysis of the EVs was done. The unstained EVs, Calcein (visible in FITC: 488-530/30 nm) stained EVs and FAP-AF647 (visible in APC: 633-660/20) stained EVs were examined (figure 32). The gates are set based on the unstained EVs. The results show that 95% of the Calcein stained EVs were indeed positive in the FITC channel compared to the unstained EVs. This thus shows that almost all the particles that were measured from this sample with the FACS were indeed EVs, as Calcein stains intact EVs [108]. For the FAP-stained EVs 47% percent is positive compared to the unstained EVs. The signal originating from the FAP-AF647 staining is thus weaker than from the Calcein staining. This can have multiple causes. One possibility is the fluorophore giving a weak signal or having bleached partially. Another possibility is decreased binding affinity of the antibody to the EVs, possibly caused by the presence of the fluorophore. However, it should be noticed that, different from the cell stainings where washing is included in the process, positive events here do not directly mean that FAP-AF647 is bound to the EVs. FAP-AF647 could also be present solely or bound to other components in the EV sample.

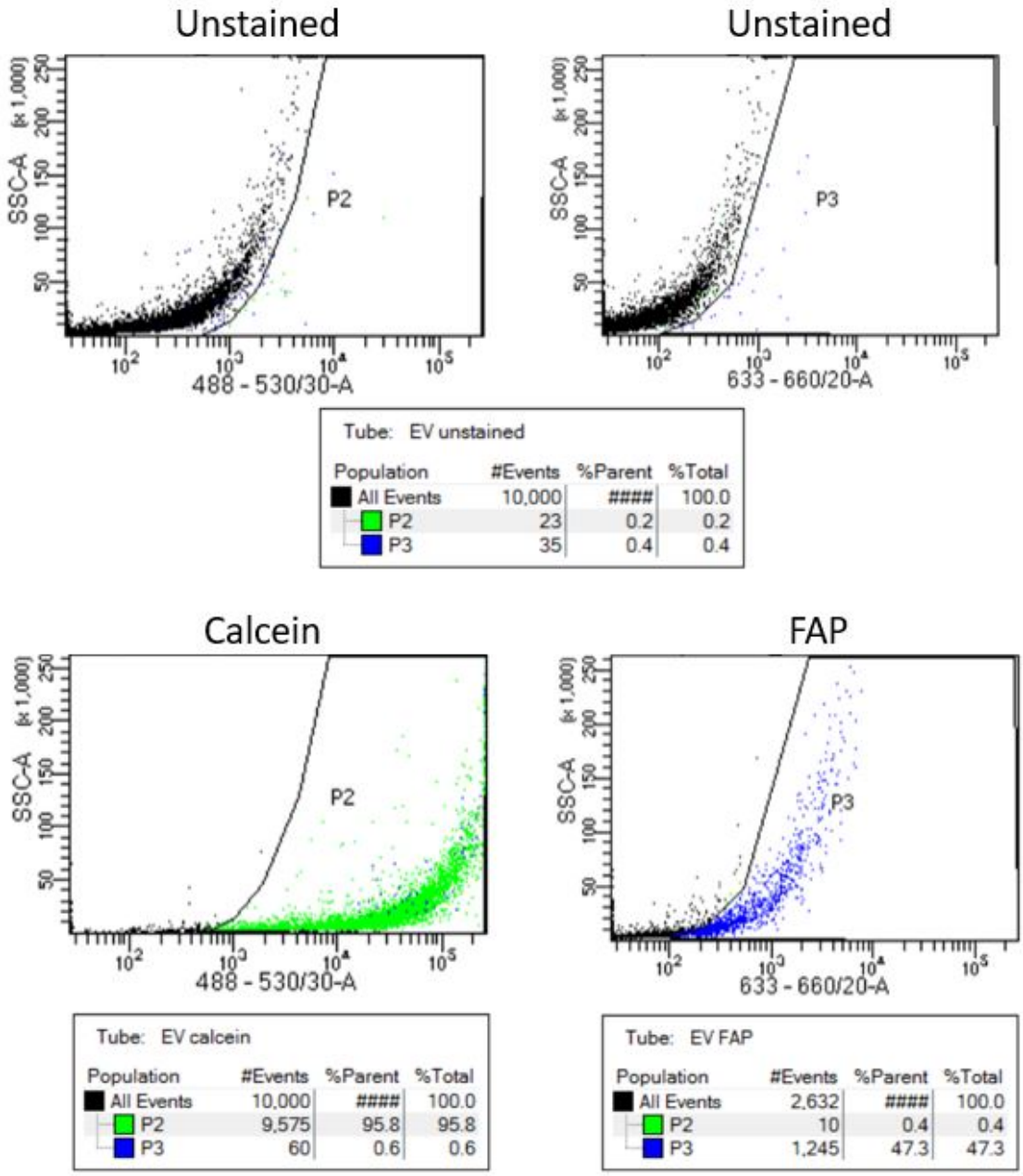

Figure 32: *FACS analysis of Calcein and FAP-AF647 stained human prostate fibroblast derived EVs. Gates (P2 and P3) are set for the unstained EVs. Calcein is visible in FITC: 488-530/30 nm; FAP-AF647 is visible in APC: 633-660/20. 95% of the Calcein stained EVs was positive for P2. 47% of the FAP-AF647 stained EVs was positive for P3.*

4.8 Extracellular vesicle characterisation - Dynamic Light Scattering - prostate fibroblasts

The size of the HPrF EVs was measured using DLS 1 day after EV harvesting (table 12). The found average size of the particles in the sample was 1975 ± 462 nm and the PdI was 1.000 ± 0.

Table 12: *Size and PdI, represented by Z-average, of the particles in EV samples of human prostate fibroblasts (HPrF). Size and PdI per sample are averaged over 3 measurements.*

Days after EV harvesting	Sample	Z-average [nm]	PdI
1	EVs HPrF	1975 ± 462	1.000 ± 0

The found size is much larger than the size of the LX-2 EVs. Here, the time between EV harvesting and the DLS measurement could have caused this difference. To be able to compare the two types of EVs, a DLS measurement should be performed at the day of harvesting for the HPrF EVs. In literature, EVs of prostate CAFs with a size of 30 to 150 nm are described [115].

4.9 Conjugation - prostate fibroblasts

To isolate fibroblast derived EVs using a fibroblast specific antibody, the conjugation was performed using EVs of prostate fibroblasts and FAP-AF647 antibody. However, due to a very low number of measured events for the last 3 samples, no conclusions can be drawn from this conjugation. Results of this can be seen in the Appendix, section 7.1.

The conjugation, using EVs of human prostate fibroblasts and FAP-AF647 antibody, was thereafter repeated. Concentration of FAP-AF647 was increased here compared to the previous experiment and the EVs had been stored for 1 day. Results can be seen in figure 33. P1 is set for the empty beads again.
The results of the empty beads, beads-OPSS and beads-OPSS-Tz (figure 33b) are similar as described before. This is as expected, because neither the antibody nor the EVs influence these steps. Here, 28% is positive for Tz. To visualize the Calcein staining of the EVs and the binding of FAP-AF647 to the EVs, the other gates (P2 and P3 respectively) are set to the unstained EVs (figure 33a). It should be noticed that, in this way, the unstained EVs are positive for P1 too.
For TCO-FAP, very few events were measured (figure 33c), similarly to earlier measurements of TCO-antibody. However, 62% is positive for P3, indicating the signal of FAP-AF647 can be observed here. Also, 10% is positive for P1 and 2% for P2 (although this means 6 events in this case due to the low total number of events), which could influence the interpretation of the results when combining with beads-OPSS-Tz and the EVs. Furthermore, whether or not FAP was bound to TCO here cannot be determined, as, considering the procedure, the sample certainly contained both components. For the TCO-FAP-EV sample, positive events for P1, P2 and P3 are observed. For both P2 and P3, 5% is positive. 13% is positive for P1. Compared to the unstained EVs, this indicates the presence of FAP and Calcein stained EVs. Again, it cannot be concluded from this whether or not the components in the sample were bound. In addition, no sample containing Calcein stained EVs only was measured here. Therefore, if the EVs were stained with Calcein succesfully cannot be said for sure. However, the percentage of P2-positive events was similar to those measured in the first conjugation, where a Calcein stained EV sample was measured too. This indicates that the EVs were stained. Moreover, the low percentages of EVs possibly stained with Calcein and bound to FAP-AF647 can be caused by different scenarios. Firstly, it is possible that the procedure was not very efficient and led to a low number of stained or bound EVs. Another possibility is the presence of other larger particles in the EV sample. If these particles were not influenced by the Calcein staining and not bound to FAP-AF647, but they were large enough to be measured by the FACS, they could have influenced the result. A third option is a relatively low fluorescence intensity compared to, for example, the beads.
The sample with Beads-OPSS-Tz+TCO-FAP is strongly positive for P3 (83%; figure 33d). As the sample is washed after incubation of Beads-OPSS-Tz with TCO-FAP, it is assumed that all components that were not bound to the beads were washed away. Therefore, the sample being positive for P3, indicates binding of TCO to both FAP and Tz and formation of Beads-OPSS-Tz-TCO-FAP. It is remarkable that the percentage of positive events for P3 is this high, as it was seen that about 28% of the beads was bound, via OPSS, to Tz. Therefore, it was expected that 28% would be the maximal percentage that could possibly be achieved. This outcome could be caused by the manner the binding of the components is quantified here. If the fluorescent signal of Tz is decreased, for example by prolonged exposure to light, the signal measured with FACS may not be labeled as a positive event, although Tz would still have the capacity to bind to TCO. Another option would be aspecific binding of FAP-AF647 to either the beads or OPSS.
For the full system, beads-OPSS-Tz+TCO-FAP-EV, positivity is only observed for P1 (17%). The full system clearly shows two populations. One similar to the Beads-OPSS-Tz and one similar to the unstained EVs. The presence of both beads and EV sample could have led to this. This seems to be confirmed by one population being positive for P1 and thus consisting of Beads-OPSS-Tz. However, as discussed before, due to the gates for Tz being based on the empty beads, the EVs are positive for P1 too. Therefore, this does not directly explain the second population. As said before, washing is meant to remove all the components not bound to the beads. The two populations could therefore also be explained by the presence of both conjugated beads (e.g. Beads-OPSS-Tz-TCO-FAP-EV) and unconjugated beads (e.g. empty beads). Nevertheless, the events are hardly positive for P2 and P3. This can be caused by a low efficiency of the conjugation process. This could have led to a very small number of events originating of the full system compared to events originating from only Beads-OPSS-Tz or even empty beads. This is in agreement with the low percentages measured for TCO-FAP-EV. It should be taken into account that the beads used here were stored for 24 hours, which could have led to this possible decrease in binding efficiency. As mentioned before, there is some evidence that the features of EVs can change over time [110].

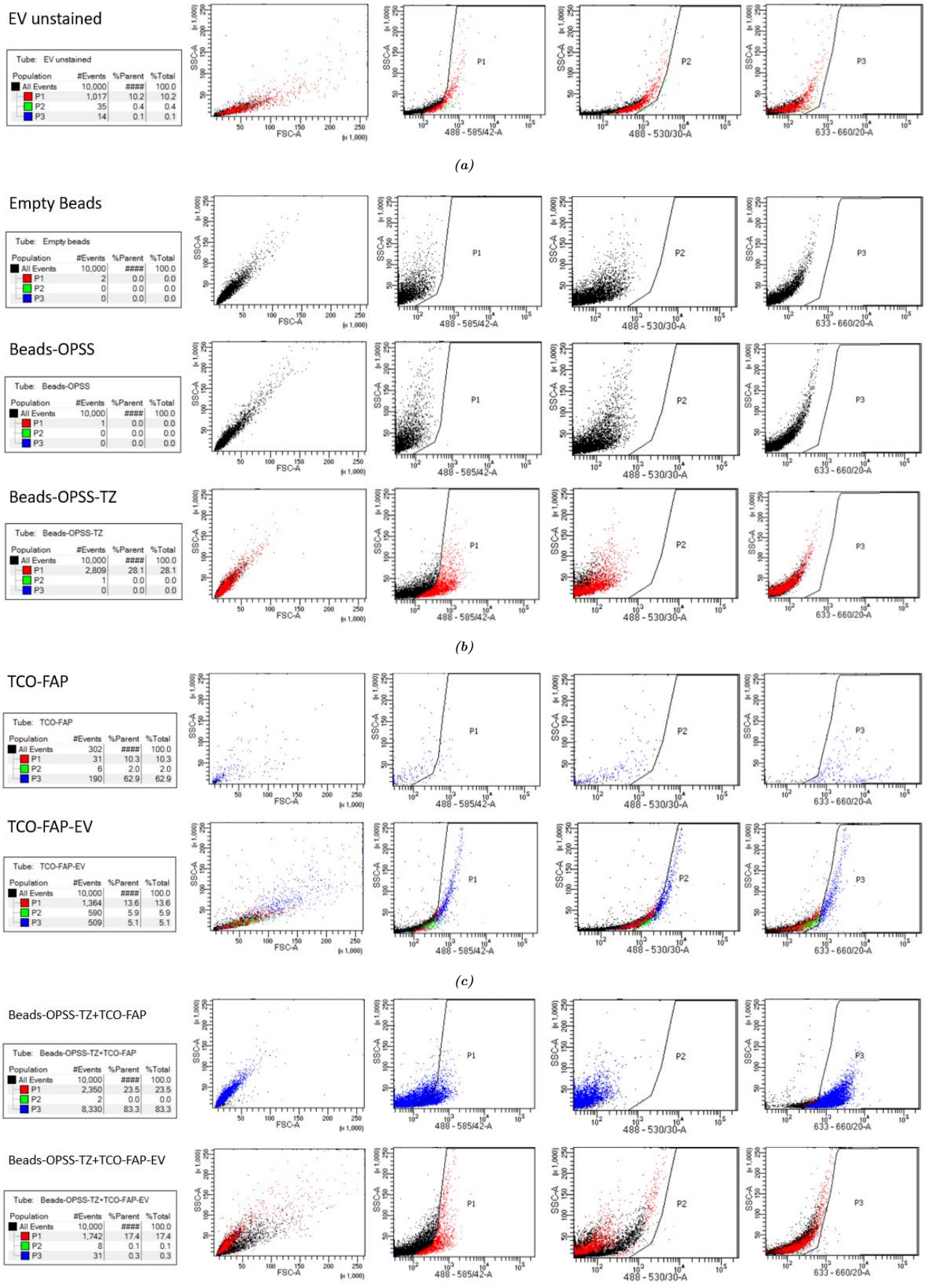

Figure 33: *FACS analysis of the conjugation for Calcein stained human prostate fibroblast derived EVs with FAP antibody. The first gate (P1), to visualize Tz, is set for the empty beads. The other gates (P2 and P3), to visualize Calcein and FAP-AF647 respectively, are set for the unstained EVs. Note that, in this way, the EVs are positive for P1 too. a) Unstained EVs; b) Empty beads, beads-OPSS and beads-OPSS-Tz are shown. 28% of Beads-OPSS-Tz is positive for P1; c) TCO-FAP and TCO-FAP-EV. For both P2 and P3, 5% of TCO-FAP-EV is positive; d) Beads-OPSS-Tz+TCO-FAP and beads-OPSS-Tz+TCO-FAP-EV. Beads-OPSS-Tz+TCO-FAP shows positivity for P1 (23%) and P3 (83%), but not P2. The full system, consisting of Beads-OPSS-Tz+TCO-FAP-EV is mainly positive for P1, but not for P2 and P3. However, 2 populations can be observed in this sample.*

5 General discussion & recommendations

5.1 General discussion

5.1.1 Cell staining - LX-2 cells

In this research, the surface markers expressed by LX-2 cells were studied in order to find a suitable antibody for immunocapturing of the EVs. As shown in figures 4 and 6-21 and summarized in table 9, only CD9 was consistently positive. As this is a general EV marker [79, 80], no fibroblast specific surface marker was found for the LX-2 cells. The procedure of fixation of the cells had an influence on the FACS results as shown in figure 5. A similar effect was seen for other cell types in literature [105, 106]. Fixation could have possibly led to retainment of structure of the cells in comparison to the living cells during the FACS measurement. Also, it can cause background fluorescence [116]. However, in a staining, it could have hindered the antibodies from binding to the surface proteins via crosslinking [104, 116]. Although this should be taken into account, especially in quantitative analysis of the FACS results, and adjustments needed to be done in setting the gate, it seemed not to have a significant effect on the analysis of the stainings here. Nevertheless, the varying results for staining with CD90 antibody shows that stainings need to be repeated multiple times to obtain reliable results and, possibly, that the cells can change in their expression over time. Also, the effect of TGFβ treatment on the expression of the LX-2 cells was studied. No significant differences between the TGFβ treated cells and the non-treated cells were found, which contradicts literature. It is described that LX-2 cells can be activated by treatment with TGFβ [40, 107] and expression of, for example, FAP is found to be upregulated after TGFβ treatment [107,117]. A clear cause for the results found in this research being different from the results described in literature is not found. A possible explanation could be the relatively high passage number of the LX-2 cells used here, as cells can change and alter in expression of surface markers after multiple passages [118]. Another option is decreased intensity of the fluorophores conjugated to some of the antibodies. This could have caused the signal to not be detectable by FACS.

5.1.2 Extracellular vesicle characterisation - LX-2 cells

It was shown here that EVs were present in the EV sample using a Calcein staining. However, the presence of other components in the EV sample was not excluded. This could have influenced the results. Size measurements, for example, could have been affected by the presence of proteins in the sample.
Also, about the results of the DLS measurements no reliable conclusions can be drawn, as the standard deviations and PdI were considerably high. Therefore, nothing can be said about potential effects of the size of the EVs on the conjugation results. Furthermore, major changes were observed in measured sizes after one week of storage of the EVs. The same effect is described in literature [110]. This should be taken into account when interpreting results obtained from experiments where EVs had been used that had been stored for a certain period of time.

5.1.3 Dot blot - LX-2 cells

The Dot blot was performed five times here. As described, for the first four Dot blots, the negative control was positive. This was not as expected, since blocking was applied, which is meant to prevent aspecific binding [112,113]. Adjustments in the protocol were made to find out the cause for this. The most important change in the procedure was leaving out the tertiary antibody, as it was thought to bind aspecifically. The fifth Dot blot, with this adjustment, showed no clear spots for the negative control, indicating it was indeed negative. However, quality of the image was low and the experiment needs to be repeated to obtain reliable results and confirm the control being negative. Remarkably, for this Dot blot, CD63 and Vimentin turned out to be positive. In case the control was indeed negative, this is not in line with the FACS results. As dots were visible for these antibodies for both the cells and the EVs, the difference here seems not to originate specifically from possible differences in expression between the cells and EVs. Also, the samples used were the same as used for the cell stainings. Therefore, changes in expression between the experiment could not have had an influence. For the Dot blot, signal is obtained from HRP conjugated to the secondary (and tertiary) antibody, while for the FACS analysis of the cell stainings signal is obtained from the fluorophore conjugated to the primary antibody. It is possible that the fluorescent intensity of the fluorophores conjugated to these antibodies was decreased below detectable levels and that they were therefore not measured as positive in the FACS, as described before. Alternatively, it can be that, due to signal decrease from leaving out the tertiary antibody, the dots on the other membranes (either specific or aspecific) cannot clearly be observed.

5.1.4 Conjugation - LX-2 cells

The conjugation was first performed with LX-2 cells using CD9-antibody. CD9 was chosen, as this is a general EV marker [79, 80]. From the FACS results, it also turned out that the cells expressed CD9. This suggests

that the EVs would be able to bind CD9 antibody too. The low number of events measured for the most samples in this conjugation makes the results less reliable. However, two populations were observed for the full system. This indicates, considering the patterns on the FSC-SSC plot too, the presence of both beads and cells. Despite the procedure including washing steps, which would remove all components not bound to the beads, it cannot directly be concluded from these results that the cells were bound to the beads and that the conjugation was successful, as CD9-APC could not be observed. The second conjugation using CD63 and LX-2 EVs led to even less measured events for the full system. Also, as the cells were not positive for CD63 in the FACS measurement, it was not known whether the EVs could bind to CD63 antibody. Furthermore, CD63 was chosen for this conjugation, because the previous conjugation with CD9 antibody was not successful. However, as CD63 is a general EV marker too [79, 80], this would not lead to the isolation of fibroblast derived EVs exclusively. This specificity is of great importance considering the application of this method in a clinical setting. Using an antibody for a general EV marker would lead to capturing of many different types of EVs. Capturing only one specific type of EVs would provide analysis of, for example, concentration of this type of EVs in the blood of a patient or of the cargo of the EVs.

5.1.5 Cell staining - prostate fibroblasts

Human prostate fibroblasts were stained with FAP-AF647 antibody to test the expression of FAP of these cells. By a FACS measurement, they were found to be strongly positive for FAP. Therefore, these cells were more representative for in vivo activated HSCs in this research than the previously used LX-2 cells. Nevertheless, it should be noticed that, although the cells express FAP, they could have other features different from HSCs that influence the results, such as size and cargo of the EVs, which can be different for different types of EVs [119].

5.1.6 Extracellular vesicle characterisation - prostate fibroblasts

The size of the prostate fibroblast derived EVs was measured with DLS. Similarly to the LX-2 EVs, PdI was very high. Also, no measurements were performed on the day of harvesting for these EVs. As concluded before, measured sizes change over time. Therefore, no conclusions about the actual sizes of the particles in the prostate fibroblast EV sample can be drawn.

5.1.7 Conjugation - prostate fibroblasts

The conjugation was performed twice for human prostate fibroblast derived EVs using FAP-AF647 antibody. Results for adding Tz to the beads-OPSS were consistent with the previous conjugations. Very few events were measured for the other samples. As the beads could be observed in the sample, this was thought to be caused by rapid sedimentation of the beads. Larger volumes of the samples were made in the next conjugation, again using prostate fibroblast derived EVs and FAP-AF647 antibody. Also, concentration of FAP antibody was increased here. In other research, not further discussed here, a higher antibody concentration increased efficiency of the conjugation. In the final results obtained in this research, two populations were observed in the sample containing the full system, possibly one being the conjugated beads and one being unconjugated beads. No signal from the Calcein staining was observed; this could mean that there were no EVs present in the sample or that the Calcein staining was not successful. Also, a relatively low fluorescence of the Calcein compared to other components in the sample is possible, as a similar result in terms of percentages was found in the first conjugation, where the Calcein stained EVs itself were confirmed to be stained succesfully. Remarkably, FAP-AF647 was observed in much lower percentages in the full system, than in the sample without the EVs. Possibly, adding the EVs could have lead to the detectable signal, originating from FAP-AF647, becoming relatively weaker. Another option is the absence of FAP-AF647, which would mean that adding the EVs would in some way cause bonds to break in beads-OPSS-Tz-TCO-FAP.
However, assuming all components that were not bound to the beads were washed away in the procedure, although with low efficiency, the EVs seem to have bound to the beads via OPSS, Tz, TCO and FAP.

5.2 Recommendations

5.2.1 Cell staining

In further research, it is recommended to perform cell stainings multiple times to obtain reliable results. Also, as it was seen that fixation does have an influence, it is advised to analyse both fixed and non-fixed stained cells. As described before, the LX-2 cells used here were negative for all tested surface marker antibodies, except CD9, and it is therefore strongly advised to use a different cell line, like the prostate fibroblasts, or to use LX-2 cells with a lower passage number for research on activated fibroblasts in the context of liver fibrosis, as these would be more representative for in vivo situations. It is also described that the medium of cultured liver cancer

stem-like cells (LCSLCs) activates LX-2 cells and also increases the expression of FAP [120]. In further research, this method can possibly be used to activate the LX-2 cells and can be compared with TGFβ treatment.

5.2.2 Extracellular vesicle characterisation

To characterize the EVs, a size measurement can provide useful information. It was seen in this research that measured sizes for the EV samples changed over time. It is therefore recommended to perform the measurement at the day of EV harvesting. Furthermore, more insight in this topic can be gained by doing multiple measurements over time and analyse the change of the obtained results. Standard deviations for the DLS measurement were considerably high, therefore, another method to measure the size of the EVs could be used. This can, for example, be done by Scanning Electron Microscopy [121]. Imaging the EVs in this way would also provide more insight in the composition of the EV sample. Also, as PdI was high for all EV samples measured here, further purification of the EV sample is recommended. This could also decrease the possible influence of other particles in the sample. Moreover, further characterisation of the EVs can be done by studying the concentration of the EVs in the sample. In this way, the number of EVs can be determined relative to the number of cells they originate from. This can provide useful information about the up- or downregulation of EV release from a certain cell type, which can give insight in progression of diseases [54].

5.2.3 Dot blot

For the Dot blot, it is recommended to repeat the experiment without tertiary antibody, using the protocol as described for the fifth Dot blot. Furthermore, imaging the membranes one by one, so that intensity differences between the membranes do not influence the results, is advised. Also, one control per type of secondary antibody is recommended. Moreover, instead of Dot blot, Western blot could be performed to obtain the desired information about the sample [114].

5.2.4 Conjugation

For further research, it is recommended to optimise the conjugation procedure, so that it will be more efficient. This can be done by testing different concentrations for the added antibodies, Tz, TCO and the beads or different durations of incubation. In the experiments presented here, FAP-AF647 antibody was used. This is useful for visualizing the cells and EVs. However, the presence of the fluorophore could have caused hindrance to binding of the EVs with other components. Therefore, it is suggested to perform the conjugation with an unconjugated FAP antibody.

5.2.5 Future recommendations

To test specificity of the conjugation for EV isolation with FAP antibody, it is recommended to perform experiments with multiple types of EVs, derived from both cells that do express FAP and cells that do not express FAP. Thereafter, it is recommended to test the performance of the sample with FAP in blood samples. Also, further research on EVs of different types of activated fibroblasts (or FAP expressing cells) and how to distinguish between these types is advised. This is important, as capturing other types of EVs is undesired, especially in clinical settings where it could lead to misinterpretations and wrong diagnosis. In addition, it is advised to test influences of the size of the EVs on capturing, to see if the system captures all EVs or mainly either the smaller or the larger EVs, as this could also result in unjustified drawing of generalized conclusions about fibroblast derived EVs.

6 Conclusion

This research was focused on the isolation of fibroblast derived extracellular vesicles using magnetic beads and click chemistry. LX-2 cells, representing activated HSCs, were used. To identify fibroblast specific surface markers, cell stainings and Dot blot were performed. Only CD9 was found to be positive consistently from the cell stainings for these cells. Activation of the cells with TGFβ did not have an influence on the expression of the cells. A high passage number for the cells could have caused these unexpected results. Furthermore, it was seen that fixation of LX-2 cells influences FACS results. As the Dot blots showed aspecific binding, adjustments to the Dot blot protocol were suggested here. Excluding the tertiary antibody seems to prevent the aspecific binding. However, further optimisation is needed to create a functional protocol for the materials used here. The particles in the EV sample originating from the LX-2 cells were confirmed to be EVs by a Calcein staining. Size measurements by DLS to characterize the EVs further resulted in high standard deviations, which made them less reliable. Also, measured sizes increased strongly after one week of storage of the EVs in PBS.
The conjugation was performed for cells and EVs using CD9 and CD63 respectively. However, this was not successful, partly because of low numbers of measured events. Also, CD9 and CD63 both are general EV markers and would not provide the isolation of fibroblast derived EVs specifically.
Human prostate fibroblasts were found to be FAP expressing cells. By cell and EV staining, the EVs were observed and the expression of FAP was confirmed. Conjugation was performed for the EVs using FAP and this eventually led to the presence of two populations in the sample containing the full system, one of which seemed to be both beads and EVs. Hence, fibroblast derived EVs could be isolated using magnetic beads and click chemistry. This can possibly contribute to the development of a novel diagnosing method for liver fibrosis. However, further research is needed to improve efficiency.

References

[1] Sung H, Ferlay J, Siegel RL, Laversanne M, Soerjomataram I, Jemal A, et al. Global Cancer Statistics 2020: GLOBOCAN Estimates of Incidence and Mortality Worldwide for 36 Cancers in 185 Countries. CA: A Cancer Journal for Clinicians. 2021;71(3):209–249. doi:10.3322/caac.21660.

[2] Mauro E, Forner A. Barcelona Clinic Liver Cancer 2022 update: Linking prognosis prediction and evidence-based treatment recommendation with multidisciplinary clinical decision-making. Liver International. 2022;42(3):488–491. doi:10.1111/liv.15180.

[3] Llovet JM BJ Brú C. Prognosis of hepatocellular carcinoma: the BCLC staging classification. Semin Liver Dis. 1999;19(3):329–38. doi:10.1055/s-2007-1007122.

[4] Singal AG, Zhang E, Narasimman M, Rich NE, Waljee AK, Hoshida Y, et al. HCC surveillance improves early detection, curative treatment receipt, and survival in patients with cirrhosis: A meta-analysis. Journal of Hepatology. 2022;77(1):128–139. doi:10.1016/j.jhep.2022.01.023.

[5] Chen L, Chen R, Kemper S, Charrier A, Brigstock DR. Suppression of fibrogenic signaling in hepatic stellate cells by Twist1-dependent microRNA-214 expression: Role of exosomes in horizontal transfer of Twist1. American Journal of Physiology-Gastrointestinal and Liver Physiology. 2015;309(6):G491–G499. doi:10.1152/ajpgi.00140.2015.

[6] Macek Jilkova Z, Kurma K, Decaens T. Animal Models of Hepatocellular Carcinoma: The Role of Immune System and Tumor Microenvironment. Cancers. 2019;11(10). doi:10.3390/cancers11101487.

[7] Ginès P, Krag A, Abraldes JG, Solà E, Fabrellas N, Kamath PS. Liver cirrhosis. The Lancet. 2021;398(10308):1359–1376. doi:10.1016/S0140-6736(21)01374-X.

[8] Tsuchida T, Friedman S. Mechanisms of hepatic stellate cell activation. Nature reviews Gastroenterology hepatology. 2017;14. doi:10.1038/nrgastro.2017.38.

[9] Simonetti RG, Cammà C, Fiorello F, Politi F, D'Amico G, Pagliaro L. Hepatocellular carcinoma - A worldwide problem and the major risk factors. Digestive Diseases and Sciences. 1991;36(7):962 – 972. doi:10.1007/BF01297149.

[10] Ningarhari M, Caruso S, Hirsch T, Bayard Q, Franconi A, Védie AL, et al. Telomere length is key to hepatocellular carcinoma diversity and telomerase addiction is an actionable therapeutic target. Journal of Hepatology. 2021;74. doi:10.1016/j.jhep.2020.11.052.

[11] Li B, Wang JHC. Fibroblasts and myofibroblasts in wound healing: Force generation and measurement. Journal of Tissue Viability. 2011;20(4):108–120. doi:10.1016/j.jtv.2009.11.004.

[12] Schmitt-Graff A, Kruger S, Bochard F, Gabbiani G, Denk H. Modulation of alpha smooth muscle actin and desmin expression in perisinusoidal cells of normal and diseased human livers. American Journal of Pathology. 1991;138(5):1233 – 1242.

[13] Ramadori G, Veit T, Schwögler S, Dienes HP, Knittel T, Rieder H, et al. Expression of the gene of the α-smooth muscle-actin isoform in rat liver and in rat fat-storing (ITO) cells. Virchows Archiv B Cell Pathology Including Molecular Pathology. 1990;59(1):349 – 357. doi:10.1007/BF02899424.

[14] Urushima H, Yuasa H, Matsubara T, Kuroda N, Hara Y, Inoue K, et al. Activation of Hepatic Stellate Cells Requires Dissociation of E-Cadherin–Containing Adherens Junctions with Hepatocytes. The American Journal of Pathology. 2021;191(3):438–453. doi:10.1016/j.ajpath.2020.12.007.

[15] Borkham-Kamphorst E, van Roeyen CRC, Ostendorf T, Floege J, Gressner AM, Weiskirchen R. Pro-fibrogenic potential of PDGF-D in liver fibrosis. Journal of Hepatology. 2007;46(6):1064–1074. doi:10.1016/j.jhep.2007.01.029.

[16] Yoshiji H, Kuriyama S, Yoshii J, Ikenaka Y, Noguchi R, Hicklin DJ, et al. Vascular endothelial growth factor and receptor interaction is a prerequisite for murine hepatic fibrogenesis. Gut. 2003;52(9):1347–1354. doi:10.1136/gut.52.9.1347.

[17] George J, Roulot D, Koteliansky VE, Bissell DM. In vivo inhibition of rat stellate cell activation by soluble transforming growth factor β type II receptor: A potential new therapy for hepatic fibrosis. Proceedings of the National Academy of Sciences of the United States of America. 1999;96(22):12719 – 12724. doi:10.1073/pnas.96.22.12719.

[18] Mu M, Zuo S, Wu RM, Deng KS, Lu S, Zhu JJ, et al. Ferulic acid attenuates liver fibrosis and hepatic stellate cell activation via inhibition of TGF-β/Smad signaling pathway. Drug Design, Development and Therapy. 2019;Volume 13:1819–1820. doi:10.2147/DDDT.S186726.

[19] Liu Z, Li C, Kang N, Malhi H, Shah VH, Maiers JL. Transforming growth factor β (TGFβ) cross-talk with the unfolded protein response is critical for hepatic stellate cell activation. Journal of Biological Chemistry. 2019;294(9):3137–3151. doi:10.1074/jbc.RA118.005761.

[20] Yamamoto M, Sumiyoshi H, Nakagami K, Tahara E. Distribution of Collagen types I, III, and V in fibrotic and neoplastic human liver. Pathology International. 1984;34(1):77–86. doi:10.1111/j.1440-1827.1984.tb02184.x.

[21] Glabman RA, Choyke PL, Sato N. Cancer-Associated Fibroblasts: Tumorigenicity and Targeting for Cancer Therapy. Cancers. 2022;14(16):3906. doi:10.3390/cancers14163906.

[22] Xing F, Saidou J, Watabe K. Cancer associated fibroblasts (CAFs) in tumor microenvironment. Frontiers in bioscience : a journal and virtual library. 2010;15:166–79. doi:10.2741/3613.

[23] Simon T, Salhia B. Cancer-Associated Fibroblast Subpopulations With Diverse and Dynamic Roles in the Tumor Microenvironment. Molecular Cancer Research. 2021;20. doi:10.1158/1541-7786.MCR-21-0282.

[24] Song M, He J, Pan QZ, Yang J, Zhao J, Zhang YJ, et al. Cancer-Associated Fibroblast-Mediated Cellular Crosstalk Supports Hepatocellular Carcinoma Progression. Hepatology. 2021;73(5):1717–1735. doi:10.1002/hep.31792.

[25] Sukowati C, Beatrice A, Croce S, Tiribelli C. The role of multipotent cancer associated fibroblasts in hepatocarcinogenesis. BMC cancer. 2015;15:188. doi:10.1186/s12885-015-1196-y.

[26] Amann T, Bataille F, Spruss T, Mühlbauer M, Gäbele E, Schölmerich J, et al. Activated hepatic stellate cells promote tumorigenicity of hepatocellular carcinoma. Cancer Science. 2009;100(4):646–653. doi:10.1111/j.1349-7006.2009.01087.x.

[27] Yu L, Shen N, Shi Y, Shi X, Fu X, Li S, et al. Characterization of cancer-related fibroblasts (CAF) in hepatocellular carcinoma and construction of CAF-based risk signature based on single-cell RNA-seq and bulk RNA-seq data. Frontiers in Immunology. 2022;13:1009789. doi:10.3389/fimmu.2022.1009789.

[28] Akanda M, Ahn E, Kim Y, Salam S, Noh M, Kim S, et al. Different Expression and Clinical Implications of Cancer-Associated Fibroblast (CAF) Markers in Brain Metastases. J Cancer. 2023;14(3):464–479. doi:10.7150/jca.80115.

[29] Paauwe M, Schoonderwoerd M, Helderman R, Harryvan T, Groenewoud A, Van Pelt G, et al. Endoglin Expression on Cancer-Associated Fibroblasts Regulates Invasion and Stimulates Colorectal Cancer Metastasis. Clinical Cancer Research. 2018;24:6331–6344. doi:10.1158/1078-0432.CCR-18-0329.

[30] Cremasco V, Astarita J, Grauel A, Keerthivasan S, MacIsaac K, Woodruff M, et al. FAP Delineates Heterogeneous and Functionally Divergent Stromal Cells in Immune-Excluded Breast Tumors. Cancer Immunology Research. 2018;6:1472–1485. doi:10.1158/2326-6066.CIR-18-0098.

[31] Pelon F, Bourachot B, Kieffer Y, Magagna I, Mermet-Meillon F, Bonnet I, et al. Cancer-associated fibroblast heterogeneity in axillary lymph nodes drives metastases in breast cancer through complementary mechanisms. 2020;11(1):404. doi:10.1038/s41467-019-14134-w.

[32] Costa A, Kieffer Y, Scholer-Dahirel A, Pelon F, Bourachot B, Cardon M, et al. Fibroblast Heterogeneity and Immunosuppressive Environment in Human Breast Cancer. Cancer Cell. 2018;33(3):463–479.e10. doi:10.1016/j.ccell.2018.01.011.

[33] Primac I, Maquoi E, Blacher S, Heljasvaara R, Deun JV, Smeland HYH, et al. Stromal integrin α11 regulates PDGFRβ signaling and promotes breast cancer progression. The Journal of Clinical Investigation. 2019;129(11):4609–4628. doi:10.1172/JCI125890.

[34] Kobayashi H, Gieniec K, Lannagan T, Wang T, Asai N, Mizutani Y, et al. The Origin and Contribution of Cancer-Associated Fibroblasts in Colorectal Carcinogenesis. Gastroenterology. 2021;162. doi:10.1053/j.gastro.2021.11.037.

[35] Zhu GQ, Tang Z, Huang R, Qu WF, Fang Y, Yang R, et al. CD36+ cancer-associated fibroblasts provide immunosuppressive microenvironment for hepatocellular carcinoma via secretion of macrophage migration inhibitory factor. Cell Discovery. 2023;9. doi:10.1038/s41421-023-00529-z.

[36] Khalifa A, Rockey D. The utility of liver biopsy in 2020. Current Opinion in Gastroenterology. 2020;36:1. doi:10.1097/MOG.0000000000000621.

[37] Regev A, Berho M, Jeffers L, Milikowski C, Molina E, Pyrsopoulos N, et al. Sampling error and intraobserver variation in liver biopsy in patients with chronic HCV infection. The American journal of gastroenterology. 2002;97:2614–8. doi:10.1111/j.1572-0241.2002.06038.x.

[38] Ratziu V, Charlotte F, Heurtier A, Gombert S, Giral P, Bruckert E, et al. Sampling Variability of Liver Biopsy in Nonalcoholic Fatty Liver Disease. Gastroenterology. 2005;128(7):1898–1906. doi:10.1053/j.gastro.2005.03.084.

[39] Sandrin L, Fourquet B, Hasquenoph JM, Yon S, Fournier C, Mal F, et al. Transient elastography: a new noninvasive method for assessment of hepatic fibrosis. Ultrasound in Medicine Biology. 2003;29(12):1705–1713. doi:10.1016/j.ultrasmedbio.2003.07.001.

[40] Lee JE, Shin KS, Cho JS, You SK, Min JH, Kim KH, et al. Non-invasive Assessment of Liver Fibrosis with ElastPQ: Comparison with Transient Elastography and Serologic Fibrosis Marker Tests, and Correlation with Liver Pathology Results. Ultrasound in Medicine Biology. 2017;43(11):2515–2521. doi:10.1016/j.ultrasmedbio.2017.07.008.

[41] Geng XX, Huang RG, Lin JM, Jiang N, Yang XX. Transient Elastography in Clinical Detection of Liver Cirrhosis: A Systematic Review and Meta-analysis. Saudi Journal of Gastroenterology. 2016;22:294. doi:10.4103/1319-3767.187603.

[42] Wai CT, Greenson JK, Fontana RJ, Kalbfleisch JD, Marrero JA, Conjeevaram HS, et al. A simple noninvasive index can predict both significant fibrosis and cirrhosis in patients with chronic hepatitis C. Hepatology. 2003;38(2):518–526. doi:10.1053/jhep.2003.50346.

[43] Lambrecht J, Verhulst S, Mannaerts I, Sowa JP, Best J, Canbay A, et al. A PDGFRβ-based score predicts significant liver fibrosis in patients with chronic alcohol abuse, NAFLD and viral liver disease. EBioMedicine. 2019;43:501–512. doi:10.1016/j.ebiom.2019.04.036.

[44] Vaali Y, Lee J, Boursier J, Spijker R, Verheij J, Brosnan M, et al. FibroTest for Evaluating Fibrosis in Non-Alcoholic Fatty Liver Disease Patients: A Systematic Review and Meta-Analysis. Journal of Clinical Medicine. 2021;10:2415. doi:10.3390/jcm10112415.

[45] Zuo Z, Cui H, Wang M, Huang C, Wu J, Tao C, et al. Diagnostic of FibroTouch and six serological models in assessing the degree of liver fibrosis among patients with chronic hepatic disease: A single-center retrospective study. Plos One. 2022;17:e0270512. doi:10.1371/journal.pone.0270512.

[46] Patel K, Gordon SC, Jacobson I, Hézode C, Oh E, Smith KM, et al. Evaluation of a panel of non-invasive serum markers to differentiate mild from moderate-to-advanced liver fibrosis in chronic hepatitis C patients. Journal of Hepatology. 2004;41(6):935–942. doi:10.1016/j.jhep.2004.08.008.

[47] Chen HJ, Hu MH, Xu FG, Xu HJ, She JJ, Xia HP. Understanding the inflammation-cancer transformation in the development of primary liver cancer. Hepatoma Research. 2018;4:29. doi:10.20517/2394-5079.2018.18.

[48] Stahl Al, Johansson K, Mossberg M, Kahn R, Karpman D. Exosomes and microvesicles in normal physiology, pathophysiology, and renal diseases. Pediatric Nephrology. 2017;34. doi:10.1007/s00467-017-3816-z.

[49] Lachenal G, Pernet-Gallay K, Chivet M, Hemming FJ, Belly A, Bodon G, et al. Release of exosomes from differentiated neurons and its regulation by synaptic glutamatergic activity. Molecular and Cellular Neuroscience. 2011;46(2):409–418. doi:10.1016/j.mcn.2010.11.004.

[50] Jella KK, Yu L, Yue Q, Friedman D, Duke B, Alli A. Exosomal GAPDH from proximal tubule cells regulate ENaC activity. Plos One. 2016;11. doi:10.1371/journal.pone.0165763.

[51] Deng L, Wang Y, Peng Y, Wu Y, Ding Y, Jiang Y, et al. Osteoblast-derived microvesicles: A novel mechanism for communication between osteoblasts and osteoclasts. Bone. 2015;79:37–42. doi:10.1016/j.bone.2015.05.022.

[52] Jiang F, Chen Q, Wang W, Ling Y, Yan Y, Xia P. Hepatocyte-derived extracellular vesicles promote endothelial inflammation and atherogenesis via microRNA-1. Journal of Hepatology. 2020;72(1):156–166. doi:10.1016/j.jhep.2019.09.014.

[53] Zhou Y, Ren H, Dai B, Li J, Shang L, Huang J, et al. Hepatocellular carcinoma-derived exosomal miRNA-21 contributes to tumor progression by converting hepatocyte stellate cells to cancer-associated fibroblasts. Journal of Experimental Clinical Cancer Research. 2018;37:324. doi:10.1186/s13046-018-0965-2.

[54] Li, Chen X, Kemper, Brigstock D. Dynamic Changes in Function and Proteomic Composition of Extracellular Vesicles from Hepatic Stellate Cells during Cellular Activation. Cells. 2020;9:290. doi:10.3390/cells9020290.

[55] Khodayari N, Oshins R, Holliday L, Clark V, Qiang X, Marek G, et al. Alpha-1 antitrypsin deficient individuals have circulating extracellular vesicles with profibrogenic cargo. Cell Communication and Signaling. 2020;18:140. doi:10.1186/s12964-020-00648-0.

[56] Chen L, Huang Y, Duan Z, Huang P, Yao H, Zhou Y, et al. Exosomal miR-500 Derived From Lipopolysaccharide-Treated Macrophage Accelerates Liver Fibrosis by Suppressing MFN2. Frontiers in cell and developmental biology. 2021;9:716209. doi:10.3389/fcell.2021.716209.

[57] Wang F, Li L, Piontek K, Sakaguchi M, Selaru FM. Exosome miR-335 as a novel therapeutic strategy in hepatocellular carcinoma. Hepatology. 2018;67(3):940–954. doi:10.1002/hep.29586.

[58] Zhang Z, Li X, Sun W, Yue S, Yang J, Li J, et al. Loss of exosomal miR-320a from cancer-associated fibroblasts contributes to HCC proliferation and metastasis. Cancer Letters. 2017;397:33–42. doi:10.1016/j.canlet.2017.03.004.

[59] Yugawa K, Yoshizumi T, Mano Y, Itoh S, Harada N, Ikegami T, et al. Cancer-associated fibroblasts promote hepatocellular carcinoma progression through downregulation of exosomal miR-150-3p. European Journal of Surgical Oncology. 2021;47(2):384–393. doi:10.1016/j.ejso.2020.08.002.

[60] Wang F, Hongwei T, Li L, Piontek K, Sakaguchi M, Selaru F. Exosome - miR-335 as a novel therapeutic strategy in hepatocellular carcinoma. Hepatology. 2018;67. doi:10.1002/hep.29586.

[61] Kong J, Tian H, Zhang F, Zhang Z, Li J, Liu X, et al. Extracellular vesicles of carcinoma-associated fibroblasts creates a pre-metastatic niche in the lung through activating fibroblasts. Molecular Cancer. 2019;18. doi:10.1186/s12943-019-1101-4.

[62] Dai X, Xie Y, Dong M. Cancer-associated fibroblasts derived extracellular vesicles promote angiogenesis of colorectal adenocarcinoma cells through miR-135b-5p/FOXO1 axis. Cancer Biology & Therapy. 2022;23(1):76–88. doi:10.1080/15384047.2021.2017222.

[63] Leca J, Martinez S, Lac S, Nigri J, Secq V, Rubis M, et al. Cancer-associated fibroblast-derived annexin A6+ extracellular vesicles support pancreatic cancer aggressiveness. The Journal of Clinical Investigation. 2016;126(11):4140–4156. doi:10.1172/JCI87734.

[64] Kostallari E, Hirsova P, Prašnická A, Verma V, Yaqoob U, Wongjarupong N, et al. Hepatic stellate cell-derived PDGFRα-enriched extracellular vesicles promote liver fibrosis in mice through SHP2. Hepatology. 2018;68. doi:10.1002/hep.29803.

[65] Wan L, Xia T, Du Y, Liu J, Xie Y, Zhang Y, et al. Exosomes from activated hepatic stellate cells contain GLUT1 and PKM2: a role for exosomes in metabolic switch of liver nonparenchymal cells. The FASEB Journal. 2019;33(7):8530–8542. doi:10.1096/fj.201802675R.

[66] Chen Qt, Zhang Zy, Huang Ql, Chen H, Hong Wb, Lin T, et al. HK1 from hepatic stellate cell–derived extracellular vesicles promotes progression of hepatocellular carcinoma. Nature Metabolism. 2022;4:1–16. doi:10.1038/s42255-022-00642-5.

[67] Liu L, Liao R, Wu Z, Du C, You Y, Que K, et al. Hepatic stellate cell exosome-derived circWDR25 promotes the progression of hepatocellular carcinoma via the miRNA-4474-3P-ALOX-15 and EMT axes. BioScience Trends. 2022;16(4):267–281. doi:10.5582/bst.2022.01281.

[68] Zhang X, Chen F, Huang P, Wang X, Zhou K, Zhou C, et al. Exosome-depleted MiR-148a-3p derived from Hepatic Stellate Cells Promotes Tumor Progression via ITGA5/PI3K/Akt Axis in Hepatocellular Carcinoma. International Journal of Biological Sciences. 2022;18:2249–2260. doi:10.7150/ijbs.66184.

[69] Benbow JH, Marrero E, McGee RM, Brandon-Warner E, Attal N, Feilen NA, et al. Hepatic stellate cell-derived exosomes modulate macrophage inflammatory response. Experimental Cell Research. 2021;405(1):112663. doi:10.1016/j.yexcr.2021.112663.

[70] Yeung V, Zhang TC, Yuan L, Parekh M, Cortinas JA, Delavogia E, et al. Extracellular Vesicles Secreted by Corneal Myofibroblasts Promote Corneal Epithelial Cell Migration. International Journal of Molecular Sciences. 2022;23(6):3136. doi:10.3390/ijms23063136.

[71] Kato T, Miyaki S, Ishitobi H, Nakamura Y, Nakasa T, Lotz M, et al. Exosomes from IL-1β stimulated synovial fibroblasts induce osteoarthritic changes in articular chondrocytes. Arthritis research & therapy. 2014;16:R163. doi:10.1186/ar4679.

[72] Li J, Yan Y, Ang L, Li X, Liu C, Sun B, et al. Extracellular Vesicles-Derived OncomiRs Mediate Communication between Cancer Cells and Cancer-Associated Hepatic Stellate Cells in Hepatocellular Carcinoma Microenvironment. Carcinogenesis. 2019;41. doi:10.1093/carcin/bgz096.

[73] Extracellular vesicles derived from fat-laden hepatocytes undergoing chemical hypoxia promote a profibrotic phenotype in hepatic stellate cells. Biochimica et Biophysica Acta (BBA) - Molecular Basis of Disease. 2020;1866(10):165857. doi:10.1016/j.bbadis.2020.165857.

[74] Devhare PB, Sasaki R, Shrivastava S, Bisceglie AMD, Ray R, Ray RB. Exosome-Mediated Intercellular Communication between Hepatitis C Virus-Infected Hepatocytes and Hepatic Stellate Cells. Journal of Virology. 2017;91(6):e02225–16. doi:10.1128/jvi.02225-16.

[75] Lee YS, Kim S, Ko E, Lee JH, Yi HS, Yoo Y, et al. Exosomes derived from palmitic acid-treated hepatocytes induce fibrotic activation of hepatic stellate cells. Scientific Reports. 2017;7. doi:10.1038/s41598-017-03389-2.

[76] Li X, Chen R, Kemper S, Brigstock DR. Dynamic Changes in Function and Proteomic Composition of Extracellular Vesicles from Hepatic Stellate Cells during Cellular Activation. Cells. 2020;9(2):290. doi:10.3390/cells9020290.

[77] Vinaiphat A, Sze SK. Chapter Three - Advances in extracellular vesicles analysis. vol. 97 of Advances in Clinical Chemistry. Elsevier; 2020. p. 73–116. doi:10.1016/bs.acc.2019.12.003.

[78] Phillips W, Willms E, Hill A. Understanding extracellular vesicle and nanoparticle heterogeneity: Novel methods and considerations. Proteomics. 2021;21:e2000118. doi:10.1002/pmic.202000118.

[79] Andreu Z, Yáñez-Mó M. Tetraspanins in Extracellular Vesicle Formation and Function. Frontiers in immunology. 2014;5:442. doi:10.3389/fimmu.2014.00442.

[80] Kowal J, Arras G, Colombo M, Jouve M, Morath JP, Primdal-Bengtson B, et al. Proteomic comparison defines novel markers to characterize heterogeneous populations of extracellular vesicle subtypes. Proceedings of the National Academy of Sciences. 2016;113(8):E968–E977. doi:10.1073/pnas.1521230113.

[81] Levy MT, McCaughan GW, Abbott CA, Park JE, Cunningham AM, Müller E, et al. Fibroblast activation protein: A cell surface dipeptidyl peptidase and gelatinase expressed by stellate cells at the tissue remodelling interface in human cirrhosis. Hepatology. 1999;29(6):1768–1778. doi:10.1002/hep.510290631.

[82] Wang XM, Yu DMT, McCaughan GW, Gorrell MD. Fibroblast activation protein increases apoptosis, cell adhesion, and migration by the LX-2 human stellate cell line. Hepatology. 2005;42(4):935–945. doi:10.1002/hep.20853.

[83] Levy M, McCaughan G, Marinos G, Gorrell M. Intrahepatic expression of the hepatic stellate cell marker fibroblast activation protein correlates with the degree of fibrosis in hepatitis C virus infection. Liver. 2002;22(2):93–101. doi:10.1034/j.1600-0676.2002.01503.x.

[84] Milner J, Kevorkian L, Young D, Jones D, Wait R, Donell S, et al. Fibroblast activation protein αis expressed by chondrocytes following a pro-inflammatory stimulus and is elevated in osteoarthritis. Arthritis research therapy. 2006;8:R23. doi:10.1186/ar1877.

[85] Bauer S, Jendro M, Wadle A, Kleber S, Stenner-Liewen F, Dinser R, et al. Fibroblast activation protein is expressed by rheumatoid myofibroblast-like synoviocytes. Arthritis research therapy. 2006;8:R171. doi:10.1186/ar2080.

[86] Darby I, Skalli O, Gabbiani G. Alpha-smooth muscle actin is transiently expressed by myofibroblasts during experimental wound healing. Laboratory investigation; a journal of technical methods and pathology. 1990;63:21–9.

[87] Hansen JF, Nielsen MJ, Nyström K, Leeming DJ, Lagging M, Norkrans G, et al. PRO-C3: a new and more precise collagen marker for liver fibrosis in patients with chronic hepatitis C. Scandinavian Journal of Gastroenterology. 2018;53(1):83–87. doi:10.1080/00365521.2017.1392596.

[88] Eckes B, Dogic D, Colucci-Guyon E, Wang N, Maniotis A, Ingber D, et al. Impaired mechanical stability, migration and contractile capacity in vimentin-deficient fibroblasts. Journal of cell science. 1998;111:1897–907. doi:10.1242/jcs.111.13.1897.

[89] Eckes B, Colucci-Guyon E, Smola H, Nodder S, Babinet C, Krieg TM, et al. Impaired wound healing in embryonic and adult mice lacking vimentin. Journal of cell science. 2000;113:2455–62.

[90] Pinzani M, Milani S, Herbst H, DeFranco R, Grappone C, Gentilini A, et al. Expression of platelet-derived growth factor and its receptors in normal human liver and during active fibrogenesis. The American journal of pathology. 1996;148:785–800.

[91] Sasikala M, Surya P, Gaddipati R, Kumar P, Mekala SR, Mukherjee R, et al. Identification of circulating CD90 CD73 cells in cirrhosis of liver. World journal of stem cells. 2011;3:63–9. doi:10.4252/wjsc.v3.i7.63.

[92] Xu L, Hui AY, Albanis E, Arthur MJ, O'Byrne SM, Blaner WS, et al. Human hepatic stellate cell lines, LX-1 and LX-2: new tools for analysis of hepatic fibrosis. 2005;54(1):142–151. doi:10.1136/gut.2004.042127.

[93] Castilho-Fernandes A, Almeida D, Melo F, Picanco V, Freitas M, Orellana M, et al. Human hepatic stellate cell line (LX2) exhibits characteristics of bone marrow-derived mesenchymal stem cells. Experimental and Molecular Pathology. 2011;91:664–672.

[94] Weiskirchen R, Weimer J, Meurer S, Kron A, Seipel B, Vater I, et al. Genetic Characteristics of the Human Hepatic Stellate Cell Line LX-2. Plos One. 2013;8:e75692. doi:10.1371/journal.pone.0075692.

[95] Joeh E, O'Leary T, Li W, Hawkins R, Hung J, Parker C, et al. Mapping glycan-mediated galectin-3 interactions by live cell proximity labeling. Proceedings of the National Academy of Sciences of the United States of America. 2020;117:27329–27338. doi:10.1073/pnas.2009206117.

[96] Ramezani-Moghadam M, Wang J, Ho V, Iseli TJ, Alzahrani B, Xu A, et al. Adiponectin Reduces Hepatic Stellate Cell Migration by Promoting Tissue Inhibitor of Metalloproteinase-1 (TIMP-1) Secretion. Journal of Biological Chemistry. 2015;290(9):5533–5542. doi:10.1074/jbc.M114.598011.

[97] Kolb HC, Finn MG, Sharpless KB. Click Chemistry: Diverse Chemical Function from a Few Good Reactions. Angewandte Chemie International Edition. 2001;40(11):2004–2021. doi:10.1002/1521-3773(20010601)40:11¡2004::AID-ANIE2004¿3.0.CO;2-5.

[98] Sun N, Lee YT, Zhang R, Kao R, Teng PC, Yang Y, et al. Purification of HCC-specific extracellular vesicles on nanosubstrates for early HCC detection by digital scoring. Nature Communications. 2020;11. doi:10.1038/s41467-020-18311-0.

[99] Sun N, Zhang C, Lee YT, Tran BV, Wang J, Kim H, et al. HCC EV ECG score: An extracellular vesicle-based protein assay for detection of early-stage hepatocellular carcinoma. Hepatology. 2023;77(3):774–788. doi:10.1002/hep.32692.

[100] Sharma P, Ludwig S, Muller L, Hong CS, Kirkwood JM, Ferrone S, et al. Immunoaffinity-based isolation of melanoma cell-derived exosomes from plasma of patients with melanoma. Journal of Extracellular Vesicles. 2018;7(1). doi:10.1080/20013078.2018.1435138.

[101] Sun N, Tran B, Peng Z, Wang J, Zhang C, Yang P, et al. Coupling Lipid Labeling and Click Chemistry Enables Isolation of Extracellular Vesicles for Noninvasive Detection of Oncogenic Gene Alterations. Advanced Science. 2022;9:2105853. doi:10.1002/advs.202105853.

[102] Schinagl M, Tomin T, Gindlhuber J, Honeder S, Pfleger R, Schittmayer M, et al. Proteomic Changes of Activated Hepatic Stellate Cells. International Journal of Molecular Sciences. 2021;22:12782. doi:10.3390/ijms222312782.

[103] Pan J, Ma Z, Liu B, Qian H, Shao X, Liu J, et al. Identification of cancer-associated fibroblasts subtypes in prostate cancer. Frontiers in immunology. 2023;14:1133160. doi:10.3389/fimmu.2023.1133160.

[104] van der Loos C. A focus on fixation. Biotechnic & Histochemistry. 2007;82(3):141–154. doi:10.1080/10520290701375302.

[105] Stewart JC, Villasmil ML, Frampton MW. Changes in fluorescence intensity of selected leukocyte surface markers following fixation. Cytometry Part A. 2007;71A(6):379–385. doi:10.1002/cyto.a.20392.

[106] Kingston J, Bayly W, Sellon D, Meyers K, Wardrop J. Effects of formaldehyde fixation on equine platelets using flow cytometric methods to evaluate markers of platelet activation. American journal of veterinary research. 2002;63:840–4. doi:10.2460/ajvr.2002.63.840.

[107] Carson J, Robinson M, Ramm G, Gobert G. RNA Sequencing of LX-2 Cells Treated with TGF-β1 Identifies Genes Associated with Early Hepatic Stellate Cell Activation. 2021. doi:10.21203/rs.3.rs-385581/v1.

[108] Gray WD, Mitchell AJ, Searles CD. An accurate, precise method for general labeling of extracellular vesicles. MethodsX. 2015;2:360–367. doi:10.1016/j.mex.2015.08.002.

[109] Safran M, Masoud R, Sultan M, Tachlytski I, Chai Gadot C, Pery R, et al. Extracellular Vesicular Transmission of miR-423-5p from HepG2 Cells Inhibits the Differentiation of Hepatic Stellate Cells. Cells. 2022;11(10):1715. doi:10.3390/cells11101715.

[110] Görgens A, Corso G, Hagey D, Wiklander R, Gustafsson M, Felldin U, et al. Identification of storage conditions stabilizing extracellular vesicles preparations. Journal of Extracellular Vesicles. 2022;11. doi:10.1002/jev2.12238.

[111] Zivko C, Fuhrmann K, Fuhrmann G, Luciani P. Tracking matricellular protein SPARC in extracellular vesicles as a non-destructive method to evaluate lipid-based antifibrotic treatments. Communications Biology. 2022;5:1155. doi:10.1038/s42003-022-04123-z.

[112] Johnson DA, Gautsch JW, Sportsman JR, Elder JH. Improved technique utilizing nonfat dry milk for analysis of proteins and nucleic acids transferred to nitrocellulose. Gene Analysis Techniques. 1984;1(1):3–8. doi:10.1016/0735-0651(84)90049-9.

[113] Burry RW. Controls for Immunocytochemistry: An Update. Journal of Histochemistry & Cytochemistry. 2011;59(1):6–12. doi:10.1369/jhc.2010.956920.

[114] Mahmood T, Yang PC. Western Blot: Technique, Theory and Trouble Shooting. North American journal of medical sciences. 2012;4:429–34. doi:10.4103/1947-2714.100998.

[115] Zhang Y, Zhao J, Ding M, Su Y, Cui D, Jiang C, et al. Loss of exosomal miR-146a-5p from cancer-associated fibroblasts after androgen deprivation therapy contributes to prostate cancer metastasis. Journal of Experimental Clinical Cancer Research. 2020;39. doi:10.1186/s13046-020-01761-1.

[116] Leischner U, Schierloh A, Zieglgänsberger W, Dodt HU. Formalin-Induced Fluorescence Reveals Cell Shape and Morphology in Biological Tissue Samples. Plos one. 2010;5:e10391. doi:10.1371/journal.pone.0010391.

[117] Lee J, Byun J, Shim G, Oh YK. Fibroblast activation protein activated antifibrotic peptide delivery attenuates fibrosis in mouse models of liver fibrosis. Nature Communications. 2022;13:1516. doi:10.1038/s41467-022-29186-8.

[118] Farsani M, Motevaseli E, Neyazi N, Khorramizadeh M, Zafarvahedian E, Ghahremani M. Effect of Passage Number and Culture Time on the Expression and Activity of Insulin-Degrading Enzyme in Caco-2 Cells. Iranian biomedical journal. 2017;22. doi:10.22034/ibj.22.1.70.

[119] Vanderboom PM, Dasari S, Ruegsegger GN, Pataky MW, Lucien F, Heppelmann CJ, et al. A size-exclusion-based approach for purifying extracellular vesicles from human plasma. Cell Reports Methods. 2021;1(3):100055. doi:10.1016/j.crmeth.2021.100055.

[120] Cui Y, Sun S, Ren K, Quan M, Song Z, Zou H, et al. Reversal of liver cancer-associated stellate cell-induced stem-like characteristics in SMMC-7721 cells by 8-bromo-7-methoxychrysin via inhibiting STAT3 activation. Oncology reports. 2016;35. doi:10.3892/or.2016.4637.

[121] Chuo S, Chien J, Lai C. Imaging extracellular vesicles: Current and emerging methods. Journal of Biomedical Science. 2018;25:91. doi:10.1186/s12929-018-0494-5.

7 Appendix

7.1 Conjugation 1 - prostate fibroblasts

The results of the first conjugation for hPrF EVs using FAP antibody are shown in figure 34.
25% of the beads is positive for Tz. Due to the very few measured events for the other samples, no direct conclusions can be drawn. However, compared to the Beads-OPSS-TZ+TCO-FAP sample, the full system (Beads-OPSS-TZ+TCO-FAP-EV) contains particles that are positive for P2, suggesting the presence of EVs. As everything that has not bound to the beads theoretically would have been removed from the sample by washing, this indicates the EVs were bound to the Beads via FAP, TCO, TZ and OPSS.

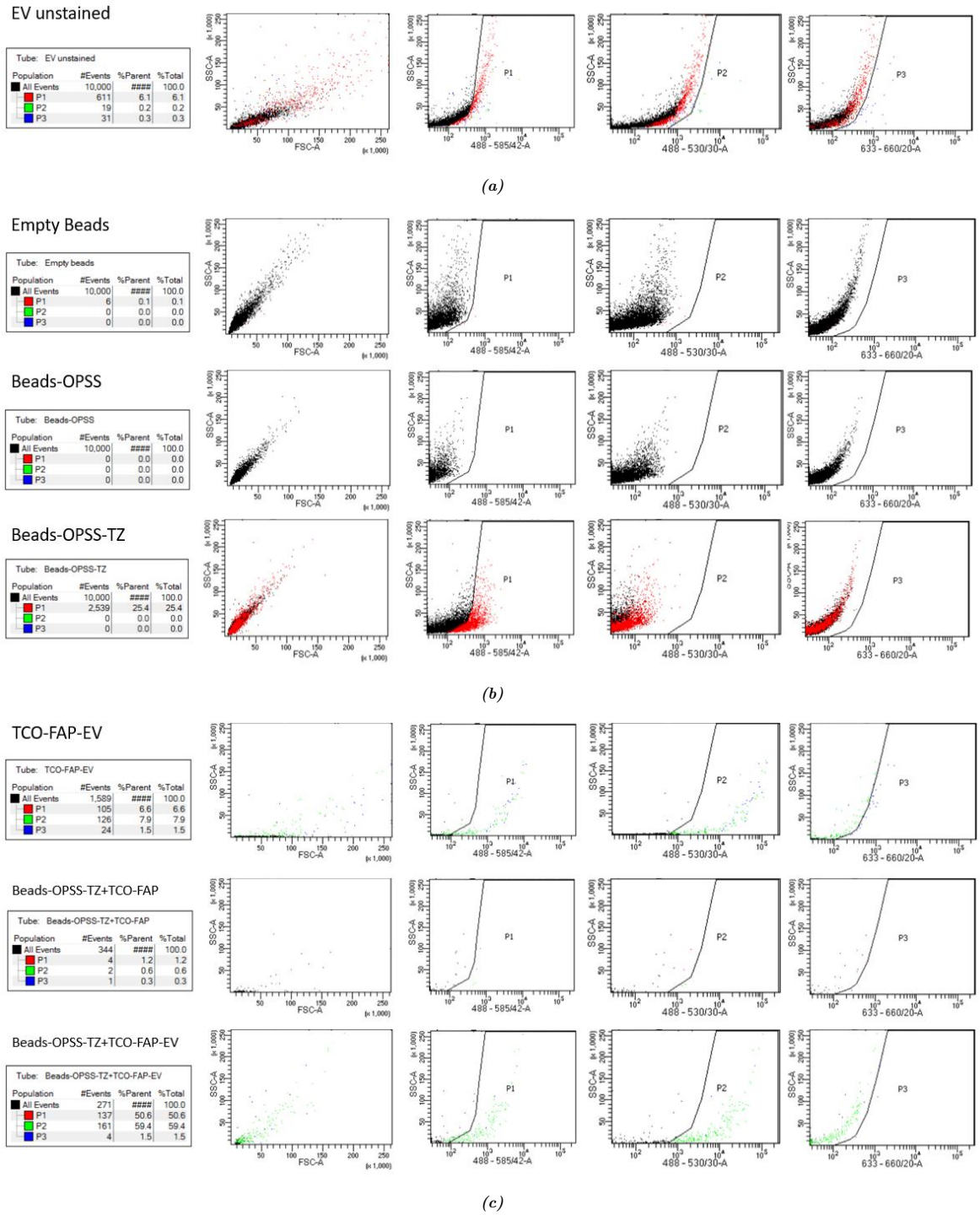

(a)

(b)

(c)

Figure 34: *First conjugation for human prostate fibroblast derived EVs with FAP antibody. The TCO-FAP sample was excluded from the results as the measurement was not performed correctly. Very few events were measured for TCO-FAP-EV, Beads-OPSS-TZ+TCO-FAP and Beads-OPSS-TZ+TCO-FAP-EV.*